RSC Advances

ROYAL SOCIETY OF CHEMISTRY

REVIEW

View Article Online
View Journal | View Issue

Check for updates

Cite this: *RSC Adv.*, 2024, **14**, 26995

Advancements in MAX phase materials: structure, properties, and novel applications

Md. Shahinoor Alam, *[a] Mohammad Asaduzzaman Chowdhury,[a] Tasmina Khandaker,[b] Muhammad Sarwar Hossain, [c] Md. Saiful Islam, *[b] Md. Moynul Islam[b] and Md. Kamrul Hasan[c]

The MAX phase represents a diverse class of nanolaminate materials with intriguing properties that have received incredible global research attention because they bridge the divide separating metals and ceramics. Despite the numerous potential applications of MAX phases, their complex structure leads to a scarcity of readily accessible pure MAX phases. As a result, in-depth research on synthesis methods, characteristics, and structure is frequently needed for appropriate application. This review provides a comprehensive understanding of the recent advancements and growth in MAX phases, focusing on their complex crystal structures, unique mechanical, thermal, electrical, crack healing, corrosion-resistant properties, as well as their synthesis methods and applications. The structure of MAX phases including single metal MAX, i-MAX and o-MAX was discussed. Moreover, recent advancements in understanding MAX phase behaviour under extreme conditions and their potential novel applications across various fields, including high-temperature coatings, energy storage, and electrical and thermal conductors, biomedical, nanocomposites, *etc.* were discussed. Moreover, the synthesis techniques, ranging from bottom-up to top-down methods are scrutinized for their efficacy in tailoring MAX phase properties. Furthermore, the review explores the challenges and opportunities associated with optimizing MAX phase materials for specific applications, such as enhancing their oxidation resistance, tuning their mechanical properties, and exploring their functionality in emerging technologies. Overall, this review aims to provide researchers and engineers with a comprehensive understanding of MAX phase materials and inspire further exploration into their versatile applications in materials science and engineering.

Received 20th May 2024
Accepted 9th August 2024

DOI: 10.1039/d4ra03714f

rsc.li/rsc-advances

Open Access Article. Published on 27 August 2024. Downloaded on 11/30/2024 6:12:35 AM.
This article is licensed under a Creative Commons Attribution-NonCommercial 3.0 Unported Licence.

1. Introduction

In the ever-evolving landscape of material science and engineering, a class of compounds has captured the imagination of scientist's worldwide, propelling research into uncharted territories. Among these compounds, MAX phases have emerged as a captivating category, drawing the attention and concentration of researchers across the globe. MAX phases represent an intriguing group of materials, serving as a link between ceramics and metals, boasting a distinctive blend of characteristics that render them as prospective options for diverse applications.[1–5] MAX phases have emerged as a fascinating and versatile family of materials, renowned for their exceptional combination of properties, thus rendering them a subject of extensive research and exploration. This intriguing class of materials has traversed a dynamic trajectory, experiencing both peaks and troughs in its relatively short history, marked by shifts in nomenclature and periods of relative obscurity. Notably, MXenes, advanced materials with superior efficacy in numerous applications, are derived from MAX phases as precursors. Consequently, the precise synthesis and characterization of MAX phases become crucial processes for producing high-quality MXenes.

The foundational work in the early 1960s, spearheaded by Wolfgang Jeitschko and Hans Nowotny in Vienna, Austria, stands as a pivotal chapter in the MAX phase's saga. Their groundbreaking efforts resulted in the discovery of over 100 new carbides and nitrides,[5,6] including a novel class of ternary systems characterized by a composition involving a transition metal (M), a metalloid (Me), and carbon (C). Among these, the "Hagg phases" or H-phases, named for their hexagonal crystal structure, reminiscent of the carbon-stabilized β-manganese phase seen in Mo_3Al_2C, garnered significant attention. The compositions within this classification, such as the system of Ti–Al–C, V–Al–C, Nb–Al–C, Cr–Al–C, Ti–Sn–C, and V–Ga–C, opened new avenues for exploration.[7] Despite these early breakthroughs, the H-phases experienced a period of relative neglect in subsequent decades. The earliest instances, Ti_2SC

[a]*Department of Mechanical Engineering, Dhaka University of Engineering and Technology, Gazipur-1707, Dhaka, Bangladesh. E-mail: majshahin4282@gmail.com*
[b]*Department of Chemistry, Bangladesh Army University of Engineering and Technology, Qadirabad Cantonment, Natore-6431, Bangladesh*
[c]*Chemistry Discipline, Khulna University, Khulna-9208, Bangladesh*

© 2024 The Author(s). Published by the Royal Society of Chemistry

Open Access Article. Published on 27 August 2024. Downloaded on 11/30/2024 6:12:35 AM.
This article is licensed under a Creative Commons Attribution-NonCommercial 3.0 Unported Licence.

and Zr_2SC, were documented in 1960 by Helga Rohde and Hans Kudielka.[8] This family expanded with discoveries like Ti_3SiC_2 and Ti_3GeC_2, leading to the formulation $M_{n+1}AX_n$, where n could equal 1 or 2.[9,10] Schuster, a protege of Nowotny, uncovered Ti_3AlC_2 in 1994.[11]

In 1988, The IUPAC, which stands for the International Union of Pure and Applied Chemistry took action to clarify the organization of the periodic table, providing a numbering system for the columns that would eliminate previous ambiguities. This universal standard simplified scientific discussions and helped students navigate the elements and their characteristics without the inconsistency of earlier labeling conventions. As time progressed, MAX phases underwent significant changes with more compositions being both predicted and synthesized. This contributed to the development of a wide array of materials that could be categorized under the general formula $M_{n+1}AX_n$ and advanced the use of the $M_{n+1}AX_n$ notation used to describe their chemical composition shown in Fig. 1a. In this formula, "M" stands for a transition metal, "A" represents an A-group element (primarily IIIA or IVA), "X" encompasses C and/or N, and "n" can vary from 1 to 3. This nomenclature, later simplified to "MAX," has since become synonymous with this group of materials. Examples of popular MAX phases include Ti_3SiC_2, Ti_3AlC_2, Ti_2AlC, V_2AlC, Ti_2AlN, *etc.*, each possessing a distinct combination of attributes that make them suitable for a wide array of applications.[12–15] The M_2AX, M_3AX_2, and M_4AX_3 phases are commonly denoted as 211, 312, and 413 phases, respectively, reflecting the value of "n". The key distinction among these phases lies in the count of M layers sandwiched between the A layers. In the crystal lattice of MAX phases, M atoms are densely arranged, while X atoms occupy octahedral sites, resulting in $M_{n+1}AX_n$ layers that display ceramic characteristics. These layers are interspersed with A layers that possess metallic properties. Consequently, MAX phases seamlessly integrate the advantageous characteristics of both ceramics and metallic materials. Similar to metals, they demonstrate efficient thermal and electrical conductivity, can be easily machined using conventional tools, and exhibit resilience against thermal shocks. On the other hand, akin to ceramics, MAX phases showcase remarkable strength, excellent high-temperature resilience, and thermal stability.

Barsoum's influential research, notably his groundbreaking work in 1996, drew considerable focus to MAX phases, initiating a deeper investigation into their characteristics. Subsequently, there has been notable enthusiasm surrounding this material due to its unique blend of physical properties. The resurgence

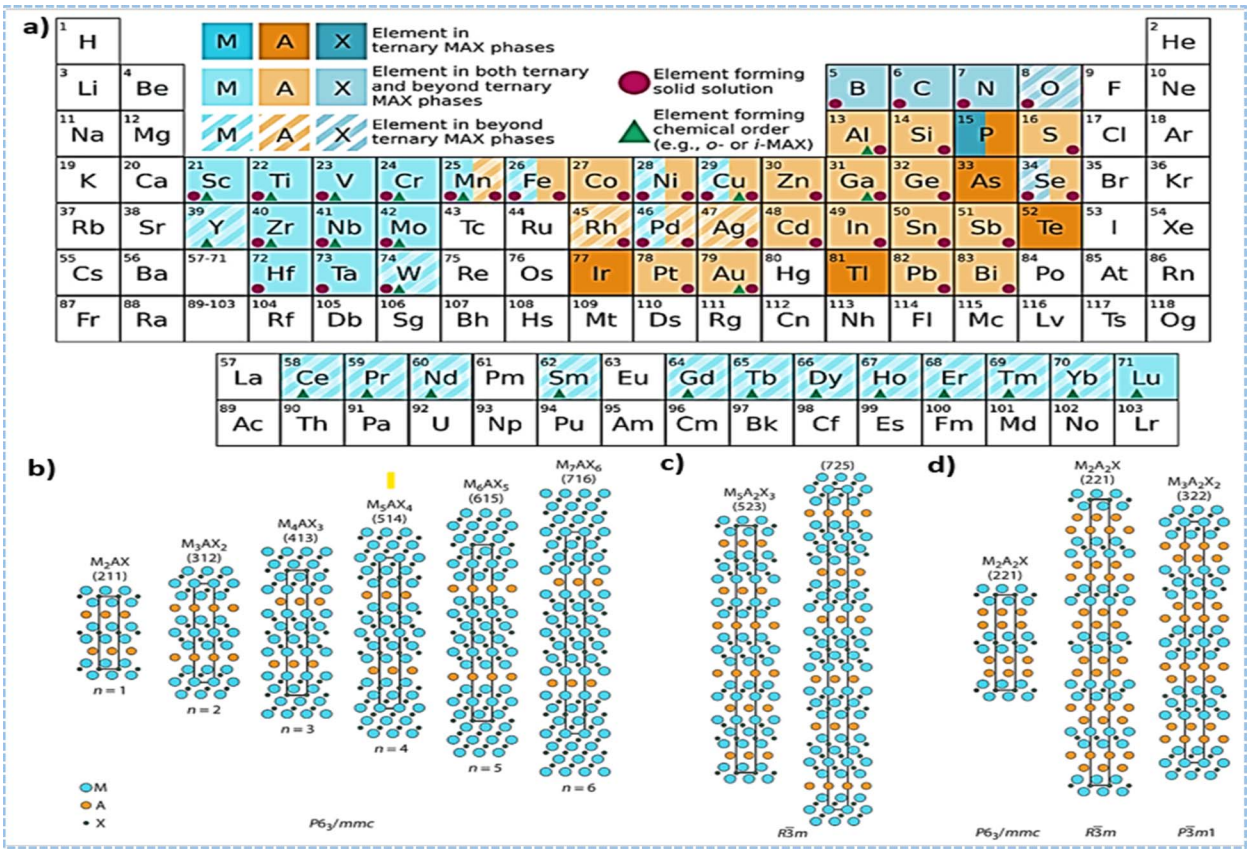

Fig. 1 (a) The periodic table displays M-elements highlighted in blue, A-elements in orange, and X-elements in grey. In ternary MAX phases, the shading is intensified, whereas in those present in both ternary and post-ternary phases, the shading is lighter. Elements contributing to solid solutions or chemical order at M-, A-, or X-sites are represented by purple circles or dark blue triangles, respectively. (b) Conventional MAX phases possessing a general $M_{n+1}AX_n$ configuration crystallize within the $P6_3/mmc$ symmetry group. (c) Intergrown MAX phases, exhibiting alternating $M_{n+1}X_n$ layer thicknesses, crystallize in the $R\bar{3}m$ space group. (d) Phases featuring dual A-layers can crystallize in one of three space groups: $P6_3/mmc$, $R\bar{3}m$, or $P\bar{3}m1$. (Reproduced from ref. 11 with permission from Elsevier, copyright 2023).[11]

© 2024 The Author(s). Published by the Royal Society of Chemistry

Open Access Article. Published on 27 August 2024. Downloaded on 11/30/2024 6:12:35 AM.
This article is licensed under a Creative Commons Attribution-NonCommercial 3.0 Unported Licence.

of interest in this family of materials transpired in 1996 with the publication of "Synthesis and characterization of a remarkable ceramic: Ti_3SiC_2" by Michel W. Barsoum and collaborators. Barsoum and colleagues accomplished the synthesis of predominantly single-phase Ti_3SiC_2 by reactive hot-pressing $TiSi_2$, SiC, and graphite powders, resulting in fully dense material.[13,14] This work not only highlighted the material's distinct blend of ceramic and metallic characteristics but also acted as a catalyst for renewed attention towards the H-phases. The practical creation of compounds within the 211 phases and 312 phases, such as Ti_2AlC and Ti_3SiC_2, marked a turning point in MAX phases research.

In 2000, M. W. Barsoum's review article titled "MAX phases on new ternary transition metal carbide or nitride materials" provided a comprehensive overview. Describing MAX phases as possessing elastic rigidity, excellent thermal and electrical conductivity, lightweight, thermal shock-resistant, machinable, and resistant to oxidation, the review marked a milestone in the understanding and appreciation of these materials.[5,16–19]

Currently, a comprehensive inventory reveals the existence of 155 unique compositions, and this number is consistently expanding. It is crucial to emphasize that not all potential combinations display thermodynamic stability. By 2019, Sokol *et al.* cataloged 155 MAX phases,[15] a figure that has since more than doubled within a brief span, reaching a current count of 342 distinct compositions, with ongoing discoveries fueling continuous expansion.[11] For example, within the Ti–Al–C system, Ti_2AlC and Ti_3AlC_2 demonstrate stability over a wide temperature range. In contrast, systems like Cr_2AlC and Ti_3SiC_2 only maintain stability with a single phase such as Cr–Al–C and Ti–Si–C. The absence of a standardized definition for formulations of solid solutions that are thermodynamically stable, coupled with limited insights into maximal solubility within each system, presents significant challenges due to the multitude of potential permutations involved.[20,21]

Crucially, all MAX phases exhibit a hexagonal crystal lattice (space group $P6_3/mmc$), comprising layers of M_6X-octahedra interconnected by shared edges, alongside layers of "A" elements positioned at the center of trigonal prisms. The M–X bonds exhibit strength due to their combined metallic-covalent character, contrasting with the relatively weaker M–A bonds. This distinctive crystal lattice, along with MAX phases' elements' position on the periodic table, contributes to their characteristic layered arrangement and imparts them with a distinctive blend of characteristics that bridge the traditional gap between ceramics and metals.

Prior to delving deeper, it is essential to precisely define the term "MAX phase". This is a task that has proven to be more complex than initially anticipated due to the existence of numerous layered compounds with three or four components featuring transition metals, A-group elements, and X atoms, as delineated in our set parameters. A fundamental representation of a MAX phase is a layered, hexagonal, nanolaminate compound adhering to $M_{n+1}AX_n$ chemistry, where alternating layers of $M_{n+1}AX_n$ and layers solely comprised of the A-group element are present. A visual depiction of this crystalline structure is presented in Fig. 1a. Though it is generally accepted that many traditional MAX phases are inherently machinable, it is still under debate whether this characteristic can be uniformly applied to all the MAX phases that have been reported thus far. Another family of compounds, the MAB phases, also warrants mention as they bear some similarities to MAX phases. MAB phases, too, are comprised of layered borides with transition metals (M), A-group elements (A), and boron (B). Yet, the most notable difference between MAX and MAB phases lies in their structural differences. While MAX phases strictly maintain the hexagonal $P6_3/mmc$ structure, MAB phases demonstrate a much broader spectrum of both structural and compositional variations. These include orthorhombic (M_2AB_2, M_3AB_4, M_4AB_6, M_4AB_4, $M_2A_2B_2$),[22–25] tetragonal (M_5AB_2),[26] and hexagonal (M_2AB_2, M_3AB_4)[27,28] symmetries. It is worth noting that the B-layers within hexagonal MAB phases create a flat honeycomb lattice—a stark contrast to the hexagonal lattice formation observed in B-based MAX phases.

Although MAX phases have integrated beneficial traits from both metals and ceramics, they are predominantly acknowledged as a class of structural ceramics renowned for their distinctive properties and applications. In contrast to conventional structural ceramics like SiC and Si_3N_4, MAX phases exhibit machinability and electrical conductivity, positioning them as viable alternatives in applications requiring intricate shapes. The integration of features from both ceramics and metals enhances their appeal, paving the way for a wide range of potential uses. Beyond their role as structural ceramics, MAX phases find utility as heating elements, nuclear materials, electrical contact materials and components such as pantograph slide plates for high-speed trains.[29–33] Additionally, MAX phases have shown promise in the field of energy storage and conversion due to their inherent conductivity and electrochemical stability. Recent research has concentrated on customizing the properties of MAX phases through alloying and surface modifications to enhance their performance in specific applications. The creation and analysis of MAX phases have emerged as critical research areas, holding the key to unlocking the full potential of these materials. A comprehensive understanding of their synthesis processes, crystal structures, microstructural properties, and performance under varying conditions is essential to effectively harness their capabilities and explore their applications in diverse fields.

Understanding MAX phases from a chemical perspective and their synthesis methods is a multifaceted issue. We've classified MAX phases into two broad groups, which correspond to the different elemental compositions observed in phases produced through bottom-up or top-down approaches. The first category, dubbed "classic" MAX phases are classified under space group $P6_3/mmc$. In this context, M stands for an early transition metal, while A signifies an A-group element, typically from groups 12 to 16 and X comprises elements such as C, N, B, and/or P. The term "classic" isn't a reflection of age but refers to Nowotny's findings where $n = 1, 2, 3$, later extended to include 4, 5, or 6. A recent discovery of B-containing MAX phases still fits the "classic" definition and thus belongs to this category.[34] Additionally, bottom-up synthesized MAX phases, this includes ternary MAX phases and alloys, which can also encompass multielement

Open Access Article. Published on 27 August 2024. Downloaded on 11/30/2024 6:12:35 AM.
This article is licensed under a Creative Commons Attribution-NonCommercial 3.0 Unported Licence.

solids with significant disorder within the M-sites,[35–38] conforming to hexagonal $P6_3/mmc$ space group symmetry, and may be synthesized in a single step shown in Fig. 1b. This group includes o-MAX phases with ordered out-of-plane structures and i-MAX phases with ordered in-plane structures, typically realized through powder synthesis.[39–46] The i-MAX phase crystallizes in either orthorhombic *Cmcm* or monoclinic *C*2/*c* and *C*2/*m* symmetry, with minor differences in stacking configurations.[42,46,47] On the other hand, top-down synthesis, building upon the first category, introduces beyond groups 12 to 16, A-site elements are introduced. In top-down synthesized MAX phases, the distinctive feature is not their chemistry but rather the modified A-group layers. These phases usually originate from a bottom-up MAX phase precursor, where the A-layer is subsequently partially or entirely replaced after synthesis.

Additional information about various methods of synthesis like the high-temperature reaction of powder mixtures in a furnace,[48,49] hot isostatic pressing,[50,51] self-propagating high-temperature synthesis,[52,53] molten metal synthesis,[54–56] spark-plasma sintering,[57–59] microwave synthesis,[60,61] magnetron sputtering, and alternative methods.[62–68] However, these methods are often associated with significant drawbacks, notably in terms of time and cost, rendering them inefficient. A potential remedy to this challenge lies in Self-propagating High-temperature Synthesis (SHS). SHS stands out as a technique capable of generating over a thousand different materials, including carbides, borides, nitrides, oxides, intermetallic, and composite materials.[69] While high-temperature synthesis is commonly employed, certain instances exist where MAX phases can only be effectively produced through alternative methods.[66,70,71]

Intergrown MAX phases, a unique subgroup, are distinguished by their alternating $M_{n+1}AX_n$ layers, each with distinct n values and thicknesses, as represented in Fig. 1c. Two prominent combinations have been noted 523 (a fusion of 211 and 312) and 725 (consisting of 312 and 413).[72–74] To date, five intertwined MAX phases have been identified. In the case of Ti_3SiC_2, $Ti_5Si_2C_3$ and $Ti_7Si_2C_5$ emerge as secondary components.[72] The formation of $Ti_5Al_2C_3$ is reported following the annealing of Ti_2–AlC.[73] Additionally, $Ti_5Ge_2C_3$ and $Ti_7Ge_2C_5$ have been observed in $Ti_{n+1}GeC_n$ thin films, showcasing intergrown structures.[74] It is crucial to recognize that hybrid MAX phases, distinct from classical $M_{n+1}AX_n$ phases, adopt the *R*3*m* space group due to the altered symmetry arising from the varying thickness and alternating stacking sequence of $M_{n+1}AX_n$ layers. Mo_2Ga_2C ($P6_3/mmc$) stands as the sole representation among the five identified double A-layer MAX phases that fits within the bottom-up synthesis category, depicted in Fig. 1d.[75,76] Illustrated in Fig. 1a is a summary of the elements comprising MAX phases span across a broad spectrum of the Periodic Table, this encompasses 28 variations of M-site elements, 28 A-site elements, and 6 X-site elements.

The distinctive attributes of MAX phases originate from their layered crystal structure, characterized by alternating $M_{n+1}X_n$ layers and A layers. The M–X bonds within the $M_{n+1}X_n$ layers are robust and can be ionic or covalent, contributing to the material's overall strength. Meanwhile, the M–A bonds between the $M_{n+1}X_n$ layers and A layers are metallic bonds, rendering MAX phases as layered materials akin to graphite. This structural resemblance to graphite prompted researchers to explore the possibility of exfoliating MAX phases to obtain two-dimensional (2D) materials. In 2004, the mechanical exfoliation of graphite led to the discovery of graphene, a remarkable 2D material with distinct properties compared to its three-dimensional counterpart.[77] This breakthrough ignited significant interest in the realm of 2D materials, with subsequent discoveries including transition metal dichalcogenides (TMDs) such as MoS_2, hexagonal boron nitride (h-BN), and black phosphorus or phosphorene. Inspired by the success of graphene, researchers sought to exfoliate MAX phases to unlock their 2D potential.

Despite being weaker than intralayer bonds yet stronger than the van der Waals bonds that bind graphite layers, the metallic bonds acting as interlayer bonds in MAX phases have posed a challenge. Prior to 2011, mechanical exfoliation of MAX phases had been unsuccessful. However, a breakthrough occurred when Ti_3AlC_2, a typical MAX phase, was successfully exfoliated by specifically dissolving aluminum atoms in an HF solution, leading to the creation of 2D Ti_3C_2.[78] This significant achievement laid the groundwork for subsequent endeavors by research teams at Drexel University, under the leadership of Prof. Barsoum and Prof. Gogotsi, to exfoliate a range of aluminum-containing MAX phases, producing a family of 2D materials named MXenes.[79–83] These MXenes are created by selectively eliminating A layers from MAX phases, thereby leaving behind MX layers with a graphene-like 2D structure. This novel approach has opened up new paths for investigating the characteristics and diverse applications of MXenes in numerous domains. While several recent reviews have explored the synthesis, properties, and applications of MAX phases, they often fall short in offering a systematic evaluation of the latest developments, synthesis processes, characterization techniques and applications.[83,84] The existing literature lacks an in-depth examination of cutting-edge methodologies employed in the synthesis and characterization of MAX phases, leaving a gap in understanding the full spectrum of advancements in this field. Recognizing this void, our review manuscript aims to bridge the gap by providing a detailed and up-to-date exploration of the synthesis, properties, characteristics, and applications of MAX phases. By addressing the limitations of previous publications and delving into the advantages and challenges of various synthesis methods and characterization techniques, our review manuscript seeks to offer a unique and valuable contribution to the current body of knowledge on MAX phases. Through this comprehensive examination, we aim to provide researchers and practitioners with a nuanced understanding of the latest advancements in this fascinating field, fostering further innovation and progress in the synthesis and application of MAX phases.

2. Structure of MAX phase

2.1 Composition and architecture of MAX phase materials

The broad range of ternary MAX phases, denoted by the general formula $M_{n+1}AX_n$, showcases a remarkable spectrum of

© 2024 The Author(s). Published by the Royal Society of Chemistry

Open Access Article. Published on 27 August 2024. Downloaded on 11/30/2024 6:12:35 AM.
This article is licensed under a Creative Commons Attribution-NonCommercial 3.0 Unported Licence.

structural and compositional variations. These MAX phases share a common space group ($P6_3/mmc$) and possess a hexagonal crystalline structure. Within their unit cells, one encounters edge-sharing M_6X octahedra interspersed with layers of A elements. Remarkably, the MX layers exhibit a twinning phenomenon, where the A layer serves as a mirror plane, leading to distinctive "zig-zag" arrangements along the *c*-axis. The distinguishing feature among the distinguishing factor among these MAX phases is the quantity of M layers that divide the A layers with the 211, 312, 413, and 514 phases containing two, three, four, and five M layers, respectively. Exploration into quaternary MAX phases, attained by replacing elements within the M, A, or X sites reveals numerous disordered solid solutions, exhibiting unit cell and crystal structures resembling those of ternary MAX phases ($P6_3/mmc$) in Fig. 2.[72] Remarkably, two separate ordered quaternary MAX solid solutions arise: MAX phases with out-of-plane ordering (o-MAX) and those with in-plane ordering (i-MAX), contributing to the complex structural diversity within this captivating class of materials.

2.1.1 Solid solutions in MAX phases-single and double site variations single metal MAX (S-MAX). Solid solutions of MAX phases involving single and double sites offer extensive compositional flexibility, enabling the synthesis of novel materials with tailored properties. These solutions open avenues for incorporating unconventional elements and enhancing phase purity, advancing the versatility and applicability of MAX phase ceramics. Initial studies by Tunca *et al.* documented 34 systems exhibiting substitutional solid solutions across M, A, and X sites, with subsequent investigations revealing an expanding inventory, including 29 $(M', M'')_{n+1}AX_n$ and 15 single-site solution MAX phases of the form $M_{n+1}(A', A'')X_n$.[85,86] These solutions offer the potential to incorporate unconventional elements like W or Fe and enhance phase purity by introducing a fourth element, as seen in the addition of Al to Ti_3SiC_2.[87,88] Recent research has focused on the production of nearly pure MAX phase ceramics through fifth element additions, resulting in the creation of double solid solutions $(M', M'')_{n+1}(A', A'')X_n$. Strategic alloying on both M and A sites has enabled the production of near-phase pure ceramics, such as $(Zr, Nb)_2(Al, Sn)C$ and $(Zr, Ti)_2(Al, Sn)C$.[89–91] Additionally, introducing alloying into ternary MAX phases enables the adjustment of several properties, including the coefficient of thermal expansion, high-temperature stability, hardness, toughness, and magnetic properties. Crystallographically, alloying influences lattice parameters *a* and *c*, altering the unit cell's anisotropy and distortion factors od and pd. The evolution of ZM in the 211 type varies with the partially replaced element, as observed in $(Ti, Nb)_2AlC$ and $Cr_2(Al, Ge)C$.[92,93] Overall, these findings underscore the profound impact of alloying on MAX phase properties, supported by a statistical dispersion of host and solute atoms across all listed structures.

2.1.2 Out-of-plane direction MAX phases (o-MAX). This review manuscript focuses on a comprehensive examination of out-of-plane (o-MAX) phase structures, providing an insightful exploration into their unique properties and practical applications. The MAX-phase family has expanded, leading to the discovery of novel microstructures, with the out-of-plane ordered microstructure standing out as a defining subgroup known as o-MAX phases. Characterized by a general formula of $(M_1, M_2)_{n+1}AlC_n$, with *n* being either 2 or 3, o-MAX phases exhibit a distinctive ordering of M layers. Within these structures, two M_1 layers enclose either one or two M_2 layers in each M layer, forming a characteristic arrangement. The pioneering discovery of the first o-MAX phase, $(Cr_{2/3}Ti_{1/3})_3AlC_2$, arose from a solid-state reaction between Cr_2AlC and TiC.[43] The ordered arrangement of Cr and Ti atoms in $(Cr_{2/3}Ti_{1/3})_3AlC_2$ was revealed through diffraction techniques utilizing neutrons and X-rays (XRD) analyses. Rietveld refinement provided more precise localization of Ti and Cr atoms within the 2a and 4f Wyckoff sites, respectively. The emergence of the M site ordered structure was explained by notable variations in electronegativity and covalent radius between Ti and Cr atoms. These differences made the formation of a $(Cr, Ti)_3AlC_2$-type solid solution challenging, while the ordered quaternary $(Cr_{2/3}Ti_{1/3})_3AlC_2$ structure emerged more readily.[94] A similar M site ordering was later discovered in $(Cr_{1/2}V_{1/2})_{n+1}AlC_n$ MAX phases with *n* values of two and three. Refinements using neutron diffraction showcased the distinct occupancy of V atoms in the 2a and 4f Wyckoff sites in $(Cr_{1/2}V_{1/2})_3AlC_2$ and $(Cr_{1/2}V_{1/2})_4AlC_3$, revealing varying occupancies in the 4e and 4f Wyckoff sites.[95]

Additionally, out-of-plane ordering was observed in $(MoTi)_{n+1}AlC_n$ ($n = 2$ or 3) MAX phases. Diagrams illustrating the 312- and 413-unit cells depicted outer M layers "sandwiching" middle M layers, with the ordering influenced by the ratio of M elements. However, incomplete ordering was observed due to partial intermixing, as evidenced by neutron diffraction analysis. The out-of-plane chemical order in M_3AX_2 and M_4AX_3 o-MAX phases displayed M element specificity. In M_3AX_2, the first M element (Mo, Ti, Cr) occupied the 4f Wyckoff site, adjacent to the Al layer, while the second M element (Ti, Sc, Zr, V) occupied the 2a Wyckoff site shown in Fig. 3a.[95,96] The emergence of o-MAX phases is suggested to arise from the introduction of a second M element, which disrupts the energetically unfavorable stacking of the first M element. This is particularly relevant for M elements like Mo and Cr, whose binary carbides do not form crystals with the rock salt structure,

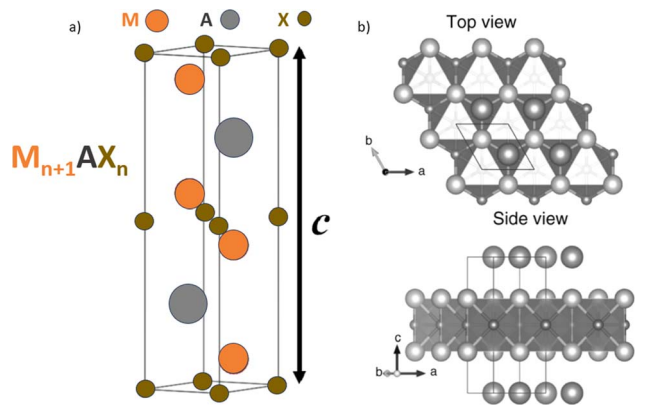

Fig. 2 (a) Unit cell and (b) crystal structure of MAX-phases. (Reproduced from ref. 72 with permission from American Physical Society, copyright 2004).[72]

Open Access Article. Published on 27 August 2024. Downloaded on 11/30/2024 6:12:35 AM.
This article is licensed under a Creative Commons Attribution-NonCommercial 3.0 Unported Licence.

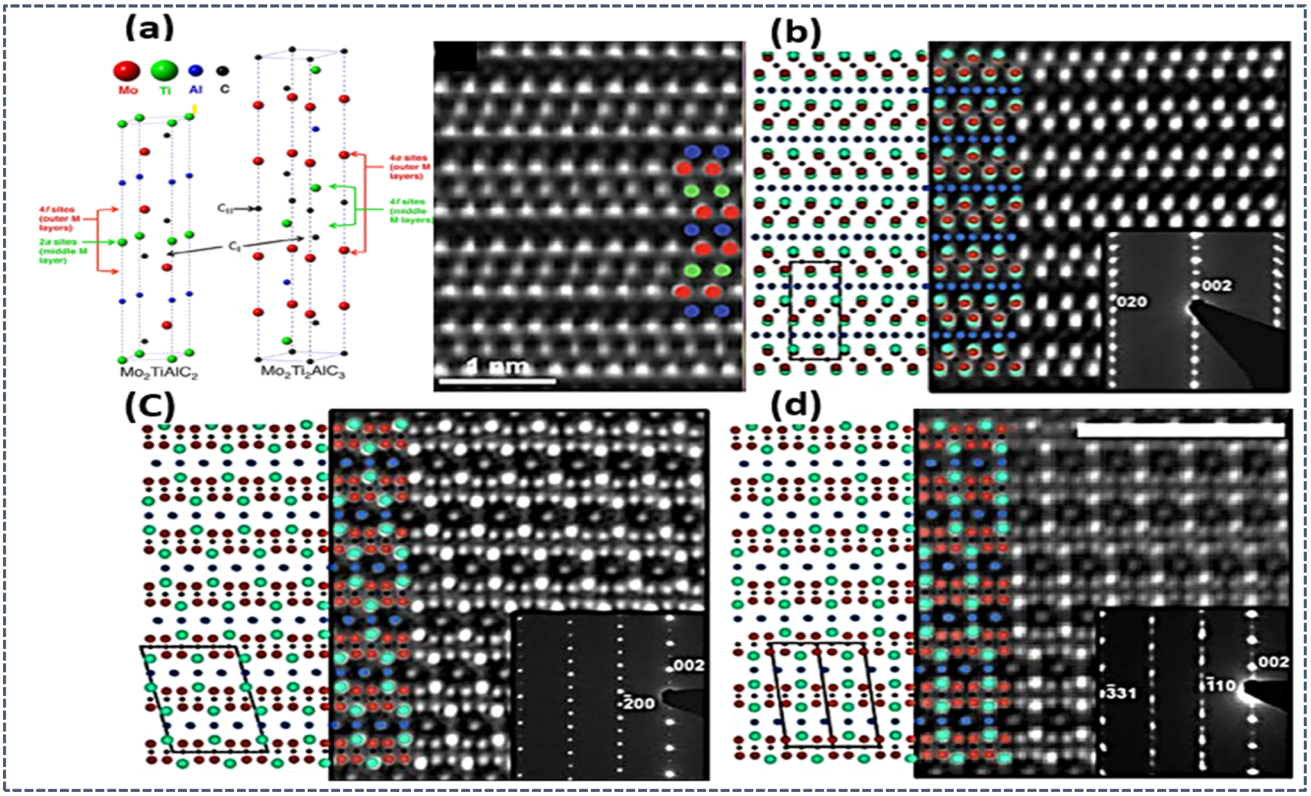

Fig. 3 (a) o-MAX phase microstructure STEM analyses of $(MoTi)_{n+1}AlC_n$ (n = 2 or 3) MAX phases, with HAADF-STEM images and EDS maps. HRSTEM of Mo_2ScAlC_2 and $Mo_2Ti_2AlC_3$ o-MAX. Reprinted with permission[95,96] and microstructures of traditional and i-MAX phases are depicted, featuring schematic illustrations and HAADF-STEM images. Images (b–d) show $(V_{2/3}Zr_{1/3})_2AlC$ i-MAX phase viewed along [010], [110], and [100] zone axes. Reprinted with permission.[101]

thus avoiding the occupation of center layers. Another noteworthy o-MAX phase, $(Mo_2Sc)AlC_2$, demonstrated clear interleaving of Sc layers between two layers of Mo. The stability of this phase was attributed to electronic configurations, with Sc atoms likely donating electrons to C atoms and Mo atoms attracting electrons from the Al layer.[96,98] As of now, only six o-MAX phases, including $(Cr_{2/3}Ti_{1/3})_3AlC_2$, $(Cr_{1/2}V_{1/2})_3AlC_2$, $(Cr_{1/2}V_{1/2})_4AlC_3$, $(MoTi)_3AlC_2$, $(MoTi)_4AlC_3$, and $(Mo_2Sc)AlC_2$, have been synthesized. Notably, Al is consistently found occupying the A site, while C occupies the X site in all o-MAX phases. Interestingly, no o-MAX phases have been experimentally identified within the 211 MAX phase, despite theoretical predictions. This absence may be attributed to the singular Wyckoff site in the 211 phase, and the ordering of which would lead to the formation of a superlattice, thereby decreasing configurational entropy.[99] Finally, they exploration of o-MAX phases continues to unravel their unique structural intricacies and holds promise for further advancements in materials science.

2.1.3 In-plane ordered MAX phases (i-MAX). The i-MAX phase structure represents a captivating realm in materials science, particularly within the domain of in-plane configurations. This phase structure entails a meticulous exploration of its intriguing characteristics, unveiling a complex and intricate framework. Researchers delve into the subtle nuances of i-MAX phases, deciphering their unique properties and behavior. Navigating through fundamental principles to recent advancements, we offer a concise yet thorough overview of the structural nuances and promising functionalities exhibited by i-MAX phases. The seminal discovery of the $(Mo_{2/3}Sc_{1/3})_2AlC$ compound marked the inception of a novel ordering known as the i-MAX phase has emerged, featuring a 211 stoichiometry and an in-plane organization of the M elements. In contrast to the conventional 211-type MAX structures, the i-MAX crystal structure presents a more intricate unit cell that extends in-plane along both a and b axes. Within this structure, non-equivalent M-sites demonstrate comparable stability under both monoclinic (space group 15 – $C2/c$) and orthorhombic (space group 6_3 – $Cmcm$) descriptions. The structural exploration extends beyond $(Mo_{2/3}Sc_{1/3})_2AlC$ to encompass other i-MAX phases such as $(V_{2/3}, Zr_{1/3})_2AlC$, $(Mo_{2/3}, Y_{1/3})_2AlC$, and $(Cr_{2/3}, Zr_{1/3})_2AlC$.[100,101] HAADF-STEM images expose the in-plane chemical arrangement within these i-MAX phases, emphasizing the unique atomic arrangements and the Kagomé-like pattern formed by Al atom columns shown in Fig. 3b–d.[97] The crystallographic diversity of i-MAX phases manifests in two structures: $C2/c$ monoclinic and $Cmcm$ orthorhombic, elucidated through a close interplay of experimental synthesis, characterization, and computational stability assessment using density functional theory (DFT).[43,102] Anticipating the potential to derive

© 2024 The Author(s). Published by the Royal Society of Chemistry

Open Access Article. Published on 27 August 2024. Downloaded on 11/30/2024 6:12:35 AM.
This article is licensed under a Creative Commons Attribution-NonCommercial 3.0 Unported Licence.

attractive MXene 2D-derivatives, theoretical predictions on ordered MAX phases encompassing 24 structures.[103,104] These predictions hinge on key parameters, including the formation enthalpy (ΔH_{cp}) and the temperature at which the transition from order to disorder occurs (T_disorder).[100,105] The latter parameter underscores the necessity for Tdisorder to exceed the synthesis temperature for the experimental realization of ordered structures.[106] Sokol *et al.* offer an overview of around 30 i-MAX phases, revealing the discovery of rare-earth-containing phases for the first time.[15] Notably, all known i-MAX phases thus far have been synthesized using Al or Ga as A-elements and C as X-element, emphasizing the need for further exploration into other A-elements and X-elements. Despite the wealth of discovered (i-MAX) phases, the absence of high phase purity bulk i-MAX ceramics precludes a comprehensive understanding of their intrinsic material properties. Theoretical and empirical analyses have laid the foundation for formulating rules governing i-MAX formation, encompassing criteria such as a ratio of 2 : 1 for $M_1 : M_2$, substantial differences in the sizes of the two metals, with M_2 being larger, an electron population favoring bonding orbitals, and a small-sized A element.[100,107,108] The first three criteria are deemed particularly crucial, while intermixing of M elements can be anticipated. However, further investigations are required to elucidate the impact of deviations from the ideal 2 : 1 ratio on stability and the implications for the transformation of i-MAX into i-MXene structures. It is noteworthy that despite the diverse crystal structures observed in Intermediate (i-MAX) phases i-MAX phases, the resulting i-MXene structures remain identical, highlighting the intriguing consistency in the transformation process.

Also, this manuscript explores the intriguing domain of MAX phases, with a particular emphasis on their rare-earth (RE) variations, often referred to as RE-i-MAX phases. The structural attributes of these RE-i-MAX phases have been extensively scrutinized, owing to their distinctive and auspicious characteristics. Inspired by the recent revelation of RE-i-MAX phases and the possibility of employing, these magnetic phases serve as precursor materials in layered compounds to synthesize 2D magnetic MXenes, the investigation focused on the $(Mo_{2/3}RE_{1/3})_2AlC$ unit cell, comprising 48 atoms – 16 Mo, 8 RE (Nd, Sm, Gd, Tb, Dy, Ho, Er, Tm, or Lu), 12 Al, and 12 C atoms – and crystallizing in the *C*2/*c* (#15) space group.[109,110] Owing to their analogous structures, a schematic representation valid for any RE element is depicted in Fig. 4a. Additionally, the quality and structure of monocrystalline samples were scrutinized *via* scanning transmission electron microscopy (STEM) shown in Fig. 4b.[111] The precise arrangement of atoms in the samples affirmed the *C*2/*c* crystalline structure. Furthermore, the alternation of one bright RE atom and two less bright Mo atoms is discernible from the line profile in the inset of the second panel. Most of the regions under study were devoid of faults, with only a few stacking faults being observed, such as the one highlighted by the red arrows in the third panel of Fig. 4b. The inclusion of rare-earth elements introduces a layer of complexity, ushering in distinct electronic and magnetic properties that augment their utility. For instance, the integration of RE elements can alter the electronic and magnetic traits of MAX phases, thereby widening their potential applications in domains such as spintronics, energy storage, and catalysis. Additionally, the varying sizes and electronegativities of RE elements compared to other MAX phase constituents contribute to the emergence of unique crystal structures, which have been thoroughly explored through both computational and experimental studies.

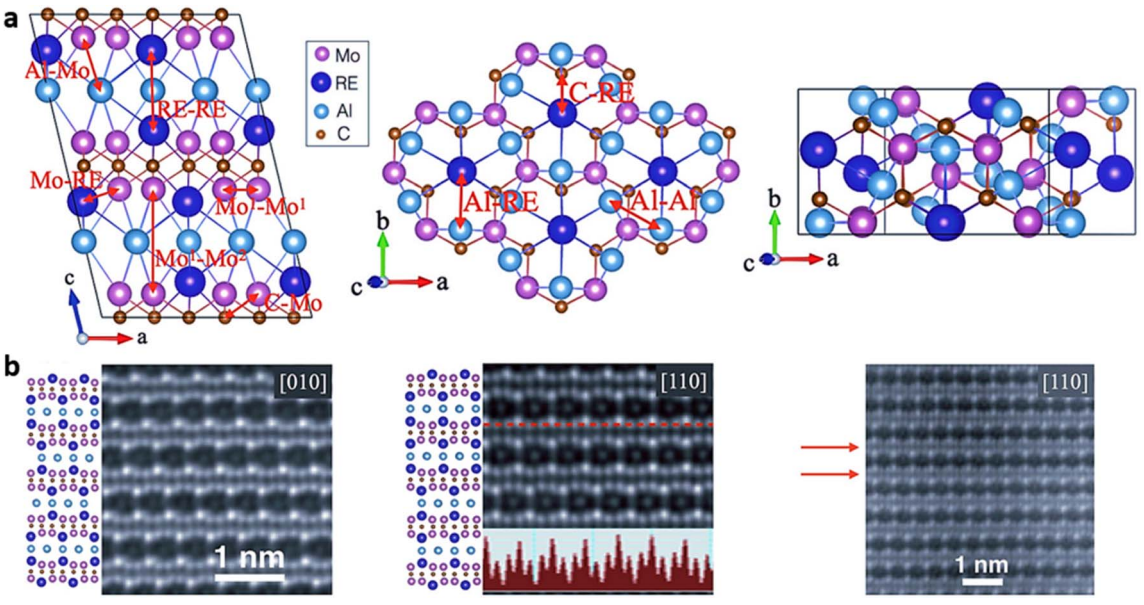

Fig. 4 (a) Schematic depiction of the conventional monoclinic *C*2/*c* unit cell for $(Mo_{2/3}RE_{1/3})_2AlC$, with specific interatomic bonds highlighted by red arrows. (b) High-resolution STEM images of $(Mo_{2/3}Dy_{1/3})_2AlC$ single crystals along [010] and [110] zone axes, accompanied by corresponding schematics for the *C*2/*c* monoclinic structure. Inset exhibits the line-profile of Z contrast along the red dashed line, and the area with a stacking fault is indicated by red arrows. (Reproduced from ref. 109 and 111 with permission from American Physical Society, copyright 2019).[109,111]

Open Access Article. Published on 27 August 2024. Downloaded on 11/30/2024 6:12:35 AM.
This article is licensed under a Creative Commons Attribution-NonCommercial 3.0 Unported Licence.

Table 1 presents a list of synthesized MAX phases. It is observed that the number of single metal MAX phases surpasses that of o-MAX and i-MAX phases (Table 1). The structures of i-MAX and o-MAX are notably more intricate compared to single metal MAX phases. The synthesized single metal MAX, o-MAX, and i-MAX phases are outlined in Table 1.

3. Properties of MAX phases

MAX phases are a unique class of layered ternary carbides and nitrides with the general formula $M_{n+1}AX_n$ (where M is an early transition metal, A is an A-group element, and X is carbon and/or nitrogen). These materials combine the best properties of metals and ceramics, making them highly desirable for various applications. They exhibit high strength and hardness, excellent damage tolerance, and remarkable fracture toughness, allowing them to withstand mechanical stresses without cracking. The unique properties of MAX phases arise from their layered structure, where 'M' layers (metallic) alternate with 'A' layers (group elements) and 'X' layers (carbon/nitrogen). This structure enables a combination of metallic and ceramic characteristics. MAX phases can deform plastically at relatively low temperatures due to the presence of basal slip systems, which facilitate dislocation movement. This is unusual for ceramics and contributes to their damage tolerance. The strong covalent bonding in the 'M–X' layers provides thermal stability, while the metallic bonding in the 'M' layers ensures good electrical and thermal conductivity. Their high thermal conductivity and stability enable them to maintain performance at elevated temperatures, while their good electrical conductivity makes them suitable for electromagnetic shielding. MAX phases are also known for their corrosion and oxidation resistance, ensuring long-term stability in harsh environments. Additionally, they offer excellent thermal shock resistance and are machinable using conventional tools, unlike most ceramics. Below Fig. 5 provides a comprehensive summary of the properties of MAX phases, which are a class of layered ternary carbides and nitrides. The unique layered structure of MAX phases contributes to their distinctive combination of properties, making them ideal for use in coatings, high-temperature components, electrical contacts, and other demanding applications.

The future of MAX phases depends on substantial research and development efforts. One key area is exploring new combinations of M, A, and X elements to discover MAX phases with enhanced properties. Additionally, developing nanostructured MAX phases can further improve their mechanical and thermal properties. Another promising direction is creating hybrid materials by combining MAX phases with other materials to produce composites with tailored properties for specific applications. These advancements will likely expand the potential uses of MAX phases across various industries, driving innovation and improving performance in numerous high-demand areas.

3.1 Electrical and thermal properties

Electronic and thermal properties play a crucial role in understanding the behavior of MAX phases. These materials exhibit good electrical conductivity, with variations observed among different compositions. Variations in electronic conductivity are evident across different MAX compositions, with Ti_4AlN_3 exhibiting notably lower conductivity attributed to reduced charge carrier mobility resulting from scattering by vacancies. Moreover, the microstructure plays a pivotal role in determining electronic conductivity, as demonstrated by the stark contrast in conductivity between Ti_2AlC samples synthesized *via* different methods. Lattice defects such as vacancies, dislocations, stacking faults, and grain boundaries in self-propagating high-temperature synthesis (SHS)/pressurized by hot isostatic pressing (PHIP)-synthesized Ti_2AlC lead to increased electron-scattering and higher electrical resistivity. Similar to metals, the electronic resistivity of MAX phases shows a linear increase with temperature, described by a characteristic temperature coefficient of resistivity. For instance, the electronic resistivity of Ti_2AlC rises from 0.36×10^{-6} Ω m at 300 K to approximately 1.0×10^{-6} Ω m at 1200 K shown in Fig. 6a and b. Conversely, the electrical conductivity of MAX phases generally decreases as temperature rises, reflecting their thermally dependent behavior.[159]

Thermal properties of MAX phases, encompassing thermal expansion coefficients, heat capacity, and conductivity, provide insights into their behavior under varying temperature conditions. While most MAX phases exhibit thermal expansion coefficients within the range of $7–10 \times 10^{-6}$ K, exceptions such as Cr_2AlC display significantly higher values. Notably, Cr_2AlC and Ti_2AlC demonstrate lower heat capacities at room temperature compared to other MAX phases, indicating distinctive thermal behavior. Regarding thermal conductivity at room temperature, Ta_4AlC_3 stands out as the highest among the mentioned MAX phases. Similar to electronic attributes, the thermal behavior of MAX phases alters with temperature, as demonstrated by the temperature-dependent heat capacity and thermal conductivity of Ti_2AlC.The linear increase in thermal conductivity with temperature mirrors the trend observed in electronic resistivity. Furthermore, the contribution of electrons and phonons to total thermal conductivity varies with temperature, with electrons dominating at room temperature. Phonon contributions become more significant in Al-containing MAX phases due to the strong binding of aluminum atoms facilitating coherent vibrations with neighboring atoms. The relationship between thermal conductivity and temperature differs among various MAX phases, with some demonstrating a decrease in thermal conductivity as temperature rises, while others display slight increases, underscoring the complex interplay of factors influencing thermal behavior in Table 2.

3.2 Mechanical properties in ambient temperature condition

MAX phases possess a distinctive microstructure and chemical bonding that contribute to their impressive mechanical properties at ambient temperatures. These materials typically exhibit elevated Young's modulus, flexural and compressive strength, as well as fracture toughness, although they tend to have relatively low hardness and shear modulus. The robust

© 2024 The Author(s). Published by the Royal Society of Chemistry

Open Access Article. Published on 27 August 2024. Downloaded on 11/30/2024 6:12:35 AM.
This article is licensed under a Creative Commons Attribution-NonCommercial 3.0 Unported Licence.

Table 1 Summary of various MAX phase types and their corresponding structural properties

Types	Single metal MAX	Structure
211	Ti_2AlC,[112] Ti_2GaC,[113] Ti_2GeC,[114] Ti_2SiC, Zr_2SiC, Hf_2AlC,[115] Hf_2GaC, Hf_2GeC, Hf_2InC, Hf_2SiC, V_2AlC,[112] V_2AuC, V_2CdC, V_2ZnC, V_2GaC, Nb_2AlC, Nb_2AuC,[116] Nb_2CdC, Nb_2GaC,[113] Nb_2InC,[117] Nb_2IrC, Nb_2TlC, Nb_2ZnC, Ta_2AlC, Ta_2AuC, Ta_2GaC, Ta_2InC, Ta_2ZnC, Cr_2AuC,[118] Cr_2GaC, Cr_2ZnC, Mo_2AlC, Mo_2ZnC, Ti_2AlN, Ti_2GaN, Hf_2AlN, V_2ZnN	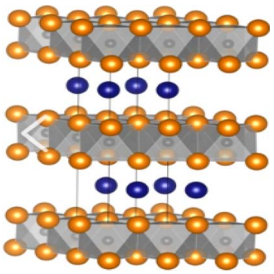
312	Ti_3AlC_2, Ti_3AuC_2, Ti_3CdC_2, Ti_3GaC_2, Ti_3GeC_2, Ti_3InC_2, Ti_3IrC_2,[119] Ti_3SiC_2,[120] Ti_3TlC_2, Ti_3ZnC_2, Zr_3AlC_2,[121] Hf_3AlC_2,[115] Hf_3AuC_2, Hf_3CdC_2, Hf_3CuC_2, Hf_3GaC_2, Hf_3GeC_2, Hf_3InC_2,[122] Hf_3IrC_2, Hf_3PbC_2,[123] Hf_3SiC_2, Hf_3SnC_2,[104] Hf_3TlC_2, Hf_3ZnC_2, V_3AlC_2, V_3AuC_2, V_3CdC_2, V_3GaC_2, V_3ZnC_2, Nb_3AlC_2, Nb_3AuC_2, Nb_3CdC_2, Nb_3GaC_2, Nb_3GeC_2, Nb_3InC_2, Nb_3IrC_2, Nb_3TlC_2, Nb_3ZnC_2, Ta_3AlC_2,[124] Ta_3AuC_2, Ta_3CdC_2, Ta_3GaC_2, Ta_3IrC_2, Ta_3ZnC_2, Ti_3AlN_2, Ti_3ZnN_2, Hf_3AlN_2	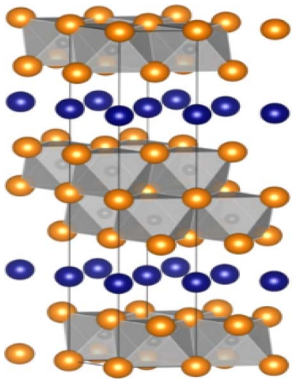
413	Ti_4AlC_3, Ti_4AsC_3, Ti_4AuC_3, Ti_4CdC_3, Ti_4GaC_3,[125] Ti_4GeC_3,[126] Ti_4InC_3, Ti_4IrC_3, Ti_4SiC_3,[127] Ti_4TlC_3, Ti_4ZnC_3, Zr_4AlC_3, Zr_4CdC_3, Zr_4GaC_3, Zr_4InC_3, Zr_4IrC_3, Zr_4SiC_3, Zr_4ZnC_3, Hf_4AlC_3, Hf_4AuC_3, Hf_4BiC_3, Hf_4CdC_3, Hf_4GaC_3, Hf_4GeC_3, Hf_4InC_3, Hf_4IrC_3, Hf_4PbC_3, Hf_4SiC_3, Hf_4SnC_3, Hf_4TlC_3, Hf_4ZnC_3 V_4AlC_3,[128] V_4GaC_3, V_4ZnC_3 Nb_4AlC_3,[129] Nb_4AuC_3, Nb_4CdC_3, Nb_4GaC_3, Nb_4GeC_3, Nb_4InC_3, Nb_4IrC_3, Nb_4SnC_3, Nb_4TlC_3 Ta_4AlC_3,[130] Ta_4AuC_3, Ta_4CdC_3, Ta_4GaC_3, Ta_4InC_3, Ta_4IrC_3, Ta_4TlC_3, Ta_4ZnC_3 Ti_4AlN_3,[131] Ti_4GaN_3	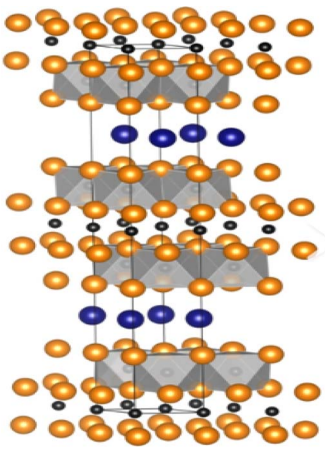
212, 314, 211, 222	Hf_2InB_2, Hf_2SnB_2, Zr_2TlB_2, Zr_2PbB_2, Zr_2InB_2, Ti_2InB_2, Hf_3PB_4, Zr_3CdB_4, Hf_2BiB, Hf_2PbB, $Hf_2B_2F_2$, $Hf_2B_2CI_2$, $Zr_2B_2F_2$, $Zr_2B_2FCI_2$	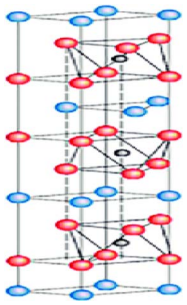

Open Access Article. Published on 27 August 2024. Downloaded on 11/30/2024 6:12:35 AM.
This article is licensed under a Creative Commons Attribution-NonCommercial 3.0 Unported Licence.

Table 1 (*Contd.*)

Types o-MAX		Structure
312	$(Cr_{2/3}V_{1/3})_3AlC_2$,[132] $(Cr_{2/3}Ti_{1/3})_3AlC_2$,[133] $(Mo_2Ti)AlC_2$,[134,135] Cr_2TiAlC_2,[136] $(Cr_{0.75}V_{0.25})_2VAlC_2$,[a137] $(Mo_2Sc)AlC_2$ (ref. 138)	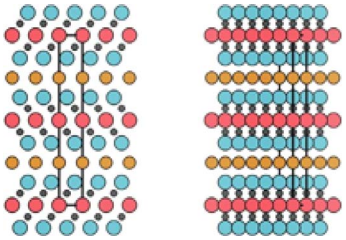
413	$(Cr_2V_2)AlC_3$,[132] $(Mo_2Ti_2)AlC_3$,[134] $Cr_{2+x}Ti_{2-x}AlC_3$ ($x = 0.5$),[a139] $(Cr_{0.7}V_{0.3})_2(Cr_{0.2}V_{0.8})_2AlC_3$,[a137] $Mo_2Nb_2AlC_3$[a] (ref. 140)	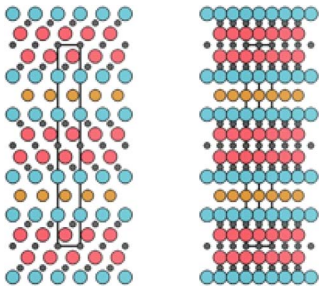

Types i-MAX		Structure
211	$(Mo_{2/3}Sm_{1/3})_2AlC$, $(Mo_{2/3}Nd_{1/3})_2AlC$, $(Mo_{2/3}Gd_{1/3})_2AlC$, $(Mo_{2/3}Tb_{1/3})_2AlC$, $(Mo_{2/3}Ho_{1/3})_2AlC$, $(Mo_{2/3}Dy_{1/3})_2AlC$,$(Mo_{2/3}Er_{1/3})_2AlC$, $(Mo_{2/3}Tm_{1/3})_2AlC$, $(Mo_{2/3}Lu_{1/3})_2AlC$, $(Mn_{2/3}Sc_{1/3})_2GaC$, $(Cr_{2/3}Sc_{1/3})_2GaC$, $(Mo_{2/3}Ce_{1/3})_2AlC$, $(Mo_{2/3}Pr_{1/3})_2AlC$,[141] $(Mo_{2/3}Gd_{1/3})_2GaC$, $(Mo_{2/3}Tb_{1/3})_2GaC$, $(Mo_{2/3}Dy_{1/3})_2GaC$, $(Mo_{2/3}Er_{1/3})_2GaC$, $(Mo_{2/3}Ho_{1/3})_2GaC$, $(Mo_{2/3}Tm_{1/3})_2GaC$, $(Mo_{2/3}Lu_{1/3})_2GaC$, $(Mo_{2/3}Yb_{1/3})_2GaC$, $W_{4/3}Er_{2/3}AlC$, $V_{2/3}Zr_{1/3})_2AlC$, $(Mo_{2/3}Sc_{1/3})_2AlC$, $(W_{2/3}Sc_{1/3})_2AlC$, $(Mo_{2/3}Y_{1/3})_2AlC$, $(W_{2/3}Y_{1/3})_2AlC$, $(Cr_{2/3}Sc_{1/3})_2AlC$, $(Mo_{2/3}Y_{1/3})_2GaC$, $(Cr_{2/3}Y_{1/3})_2AlC$, $(Mo_{2/3}Sc_{1/3})_2GaC$, $(Cr_{2/3}Zr_{1/3})AlC_2$,[142] $W_{4/3}Sc_{2/3}AlC$, $W_{4/3}Y_{2/3}AlC$,[143] $W_{4/3}Gd_{2/3}AlC$, $W_{4/3}Tb_{2/3}AlC$, $W_{4/3}Dy_{2/3}AlC$, $W_{4/3}Ho_{2/3}AlC$, $W_{4/3}Tm_{2/3}AlC$, $W_{4/3}Lu_{2/3}AlC$,[144] $Mo_{4/3}Sc_{2/3}AlC$,[145] $V_{4/3}Zr_{2/3}AlC$,[146] $Mo_{4/3}Y_{2/3}AlC$,[147] $Mo_{4/3}Ce_{2/3}AlC$, $Mo_{4/3}Dy_{2/3}AlC$, $Mo_{4/3}Ho_{2/3}AlC$, $Mo_{4/3}Er_{2/3}AlC$, $Mo_{4/3}Tm_{2/3}AlC$, $Mo_{4/3}Eu_{2/3}AlC$, $Mo_{4/3}Pr_{2/3}AlC$, $Mo_{4/3}Nd_{2/3}AlC$, $Mo_{4/3}Sm_{2/3}AlC$,[148] $Cr_{4/3}Sc_{2/3}GaC$,[149] $V_{4/3}Sc_{2/3}AlC$,[150] $Cr_{4/3}Sc_{2/3}AlC$, $Cr_{4/3}Y_{2/3}AlC$,[151] $Cr_{4/3}Zr_{2/3}AlC$,[152] $Cr_{4/3}Gd_{2/3}AlC$, $Cr_{4/3}Tb_{2/3}AlC$,[153] $Cr_{4/3}Dy_{2/3}AlC$, $Cr_{4/3}Ho_{2/3}AlC$, $Cr_{4/3}Er_{2/3}AlC$, $Cr_{4/3}Tm_{2/3}AlC$, $Cr_{4/3}Lu_{2/3}AlC$, $Mn_{4/3}Sc_{2/3}GaC$,[133] $Mo_{4/3}Sc_{2/3}GaC$, $(Mo_{2/3}Y_{2/3}GaC$,[154] $Mo_{4/3}Gd_{2/3}GaC$, $Mo_{4/3}Tb_{2/3}GaC$, $Mo_{4/3}Dy_{2/3}GaC$, $Mo_{4/3}Ho_{2/3}GaC$, $Mo_{4/3}Er_{2/3}GaC$, $Mo_{4/3}Tm_{2/3}GaC$, $Mo_{4/3}Yb_{2/3}GaC$, $Mo_{4/3}Lu_{2/3}GaC$,[155] $(W_{0.5}Mo_{0.5})_{4/3}Y_{2/3}AlC$,[b] $W_{2/3}Mo_{2/3}Gd_{2/3}AlC$,[b] $(W_{0.5}Mo_{0.5})_{4/3}Tb_{2/3}AlC$,[b] $(W_{0.5}Mo_{0.5})_{4/3}Dy_{2/3}AlC$,[b] $(W_{0.5}Mo_{0.5})_{4/3}Ho_{2/3}AlC$,[b] $(W_{0.5}Mo_{0.5})_{4/3}Er_{2/3}AlC$,[b156] $Nb_2(Al_{0.2}Au_{0.8})C$,[b157] $Ti_3(AI_{1/3}Cu_{2/3})C_2$ (ref. 158)	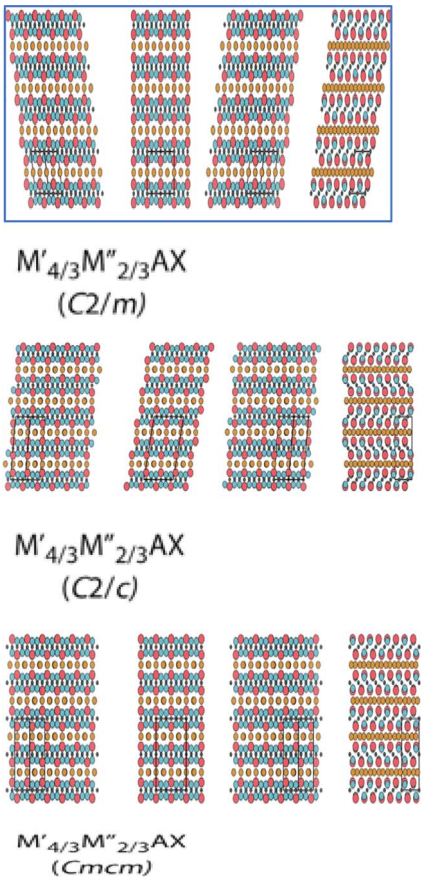

[a] Partial mixing or off-stoichiometry in contrast to the ideal o-MAX phase. [b] Solid solution i-MAX (in-plane metal ordering).

© 2024 The Author(s). Published by the Royal Society of Chemistry

Open Access Article. Published on 27 August 2024. Downloaded on 11/30/2024 6:12:35 AM.
This article is licensed under a Creative Commons Attribution-NonCommercial 3.0 Unported Licence.

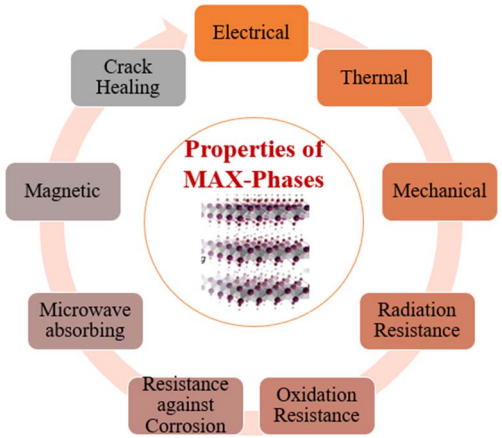

Fig. 5 Overview of MAX-phase properties.

covalent bonds formed between M-site and A-site elements largely contribute to their high Young's modulus, strength, and fracture toughness. Conversely, the weaker bonds between the MX layer and A layer lead to a lower shear modulus. Despite their robust mechanical characteristics, MAX phases maintain a relatively low density, ranging from 4.1 to 5 g cm^{-3}, rendering them elastically stiff. Consequently, their specific stiffness values, notably high when calculated as the ratio of Young's modulus to density. For instance, Ti_2AlC MAX phases exhibit Specific stiffness values marginally below those of Si_3N_4 ceramics but roughly three times higher than Ti metal.[166] Notably, Ta-containing MAX phases go against the low-density trend, with Ta_2AlC and Ta_4AlC_3 boasting densities reaching up to 11.64 g cm^{-3} and 13.18 g cm^{-3}, respectively. Despite their high stiffness, MAX phases exhibit relatively lower hardness compared to other ceramic materials like ZrO_2-based or ZrO_2 toughened Al_2O_3, having hardness values within the limited range of 2–5 GPa.[167,168] Their Young's modulus, ranging from 282 GPa to 340 GPa, positions them between ZrO_2 and Al_2O_3 ceramics but significantly higher than most metals like Ti_6Al_4V alloy.[167] While MAX phases exhibit lower flexural strength compared to some structural ceramics, they demonstrate excellent crack propagation resistance, as evidenced by their high fracture toughness values. These properties are similar to those observed in structural Si_3N_4 ceramics, which exhibit an interlocking microstructure.[169] While MAX phases generally exhibit favorable mechanical properties at room temperature, there is still potential for enhancement in certain aspects such as hardness and flexural strength. Drawing from strategies commonly employed in ceramic materials, various strengthening and toughening mechanisms have been explored for MAX phases. Notably, a novel MAX phase solid solution, $Ti_3(Al_{0.8}Si_{0.2}Sn_{0.2})C_2$, incorporating three A-site elements, has been synthesized. This solid solution exhibits improved flexural strength and Vickers hardness, measuring 649 ± 27 MPa and 6.4 ± 0.12 GPa, respectively, surpassing those of single-phase counterparts like Ti_3AlC_2 or $Ti_3(AlSn_{0.2})C_2$. The observed enhancement is credited to solid solution reinforcement.[170]

Particle toughening techniques have been employed to enhance fracture toughness, exemplified by ZrC particles-reinforced Ti_3AlC_2 composites. The incorporation of 20 vol% ZrC resulted in a notable enhanced fracture toughness, rising from 7.8 ± 0.4 MPa $m^{-1/2}$ for monolithic Ti_3AlC_2 to 11.5 ± 1.0 MPa $m^{-1/2}$ for the composite.[171] Similarly, ZrO_2 particles were utilized to improve fracture toughness in ZrO_2/Ti_3AlC_2 composites, attributed to transformation toughening effects.[172] Moreover, the addition of ZrO_2 led to enhancements in flexural strength and Vickers hardness, further underscoring the influence of composition on mechanical behavior. Notably, in ternary MAX phases with similar microstructures, the substitution of Ti with V or Cr has been shown to significantly enhance bulk modulus by up to 36%.[173] These findings highlight the multifaceted approaches and the pivotal role of composition in tailoring mechanical properties of MAX phases. MAX phases with their distinctive layered nanolaminate structure exhibit remarkable mechanical properties characterized by kinking nonlinear elastic (KNE) behavior. Recent investigations, exemplified by the work of Bei *et al.*, have elucidated the intricate deformation mechanisms of Ti_3AlC_2 MAX phase under compression.[160] The observed microstructures near critical cracks unveil a range of mechanisms for energy dissipation, such as grain bending, pull-out, push-in, *trans*-granular fracture, grain decohesion, crack deflection along grain boundaries, and the creation of kink bands (KBs) and delamination. These KBs, arising from dislocation glide, demonstrate continuous propagation within the lamella, indicative of the complex nature of mechanical responses in MAX phases. Additionally, studies on Nb_2AlC MAX phase by Zhang *et al.* reveal shear deformation in laminated grains alongside *trans*-granular fracture, with crack propagation aligned parallel to the layer orientation.[174] These findings underscore the recurring nature of KBs and shear deformation across various MAX phases such as Ti_2AlC, Cr_2AlC, and Ta_4AlC_3, underscoring their pivotal role in governing mechanical deformation processes.[159,175,176] Table 3 presents an overview of ambient-temperature mechanical characteristics across selected MAX phases.

3.3 Mechanical properties in elevated temperature condition

Outstanding mechanical performance at elevated temperatures is a defining characteristic of MAX materials, garnering considerable attention in research endeavors. These materials commonly exhibit a brittle-plastic transition temperature (BPTT), delineating their behavior. Below this threshold, which varies among MAX phases, temperature fluctuations have negligible effects on strength, and brittle fracture akin to traditional ceramics is observed. Conversely, above the BPTT, MAX phases display pronounced plastic deformation resembling conventional metals.[180] Bai *et al.* conducted comprehensive flexural and compressive assessments on Ti_3AlC_2 MAX phase across a temperature gradient, revealing distinct behaviors.[159] At room temperature (RT) through 900 °C, Ti_3AlC_2 exhibited typical brittle fracture, transitioning to plastic deformation at 950 °C without a discernible yield point. The BPTT, determined through flexural testing, fell between 900 and 950 °C, while in compression testing, it ranged from 800 to 900 °C,

Open Access Article. Published on 27 August 2024. Downloaded on 11/30/2024 6:12:35 AM.
This article is licensed under a Creative Commons Attribution-NonCommercial 3.0 Unported Licence.

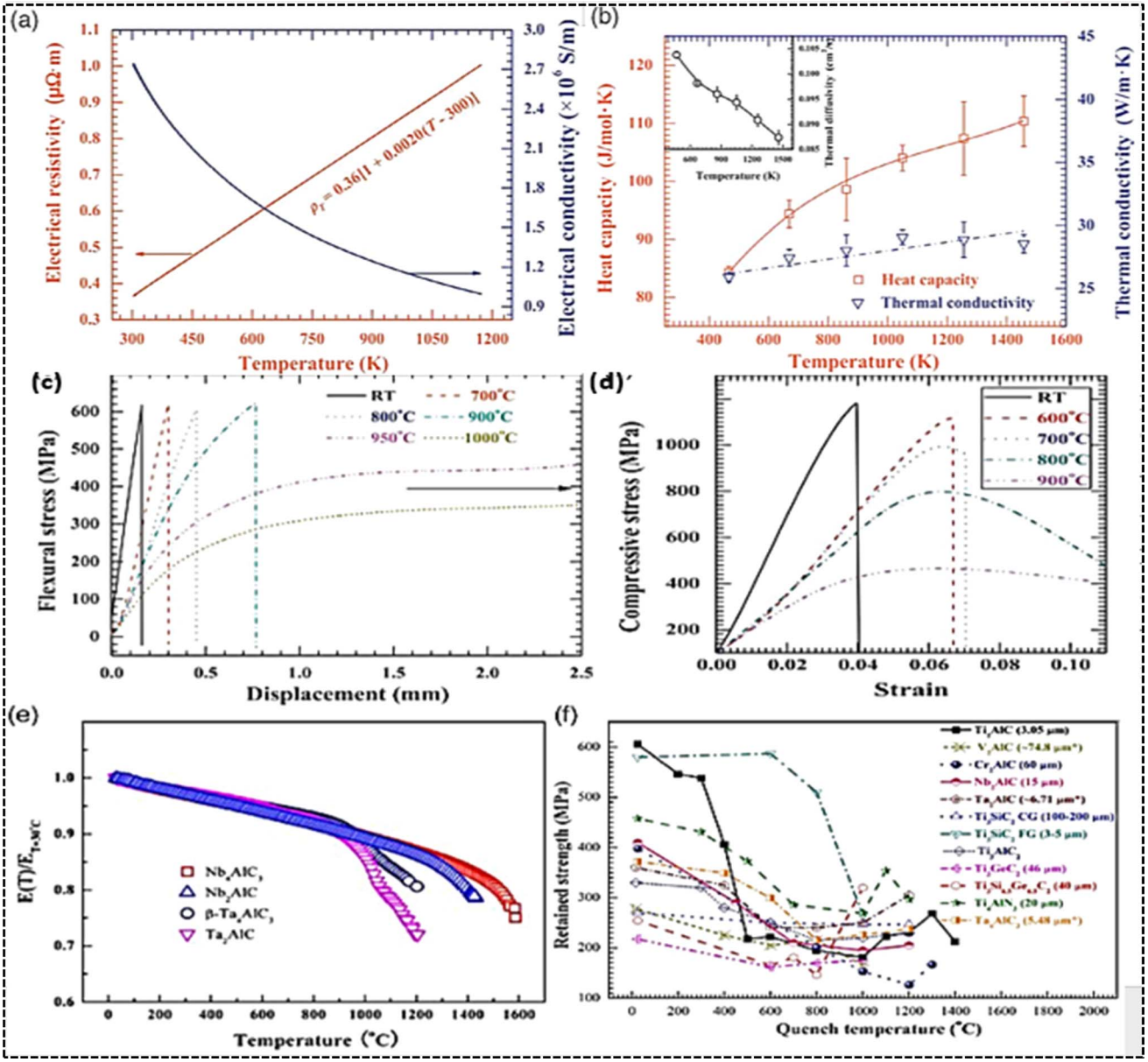

Fig. 6 MAX phases electrical and thermal characteristics: (a) Ti_2AlC's electronic conductivity and resistivity as a function of temperature. (b) Thermal conductivity, heat capacity, and diffusivity variations in Ti_2AlC across temperatures. Mechanical properties of MAX phases: graphs illustrating deformation characteristics under flexural and compressive stress of Ti_2AlC from ambient conditions to increased temperatures are shown. (c and d). Mechanical behaviours of MAX phases (e and f). (Reproduced from ref. 159 with permission from Elsevier, copyright 2013).[159] (Reproduced from ref. 160 with permission from American Ceramic Society, copyright 2012).[160]

indicating phase-specific variability shown in Fig. 6c and d. Furthermore, it was evident that temperature increments below the BPTT did not significantly affect flexural or compressive strength, whereas beyond this threshold, a rapid strength decline ensued. Variations in BPTT were also observed among different MAX phases, exemplified by Nb_4AlC_3's remarkable retention of ambient strength up to 1400 °C, contrasting with the lower BPTT of Cr_2AlC, situated between 800 and 900 °C.[161,181] Moreover, the decline in Young's modulus with rising temperatures shown in Fig. 6e mirrored the trend observed in strength, underscoring the interplay between mechanical properties and temperature in MAX materials.[159,161,176]

Evaluation of mechanical properties at elevated temperatures is crucial for assessing the viability of MAX phases as high-temperature materials. Thermal shock behavior, in particular, is a key aspect in this regard, wherein samples are rapidly quenched from elevated temperatures to room temperature to measure retained strength. Bai *et al.* conducted a study on Ti_2Al_C and compared its thermal shock behavior with other MAX phases.[182] Their findings delineate four distinct regions: There's a fragile damage zone up to 300 °C, a robust damage zone between 300 °C and 500 °C, a steady damage zone from 500 °C to 1000 °C, and an area where strength unexpectedly rebounds above 1000 °C shown in Fig. 6f. Similar trends were

© 2024 The Author(s). Published by the Royal Society of Chemistry

Open Access Article. Published on 27 August 2024. Downloaded on 11/30/2024 6:12:35 AM.
This article is licensed under a Creative Commons Attribution-NonCommercial 3.0 Unported Licence.

Table 2 Electrical and thermal characteristics of certain representative MAX phases

	Properties						
MAX phases	Electrical conductivity at RT ($\times 10^6\ \Omega^{-1}\ m^{-1}$)	Electrical resistivity ($\times 10^{-6}\ \Omega$ m)	Temperature resistivity coefficient (K^{-1})	Thermal expansion coefficient ($\times 10^{-6}$ K)	Heat capacity at room temp. ($J\ mol^{-1}\ K^{-1}$)	Thermal conductivity at room temp, ($W\ m^{-1}\ K^{-1}$)	Ref.
Nb_4AlC_3	1.33	0.75	0.0025	7.2	158	13.5	161
Ta_4AlC_3	2.59	0.39	0.0035	8.2 ± 0.3	185	38.4	162
Ti_4AlN_3	0.5	2	0.0075	9.7 ± 0.2	150	12	161
Ti_3AlC_2	3.48	0.29	0.0031	9	—	—	162 and 163
Ti_2AlC	2.5	0.4	0.002	8.2	87.2	27.0	164
Ti_2AlC	4.42	0.23	0.00295	—	—	—	164
Cr_2AlC	3.45	0.29	0.0028	13.3	84.4	17.9	165

observed in other MAX phases, highlighting the significance of grain size. Coarse-grained MAX phases exhibit superior thermal shock resistance compared to fine-grained counterparts. Notably, coarse-grained Ti_3SiC_2 retained its strength even at 1400 °C quenching temperature, whereas fine-grained samples experienced significant strength loss at lower temperatures.[183] MAX phases demonstrate enhanced thermal shock resistance compared to traditional ceramics due to their micro-scale ductility and exceptional tolerance to damage similar to metals, attributed to the generation of kink bands and delamination during quenching processes.[182]

3.4 Property of radiation resistance

Several MAX phases, such as Ti_3AlC_2 and Ti_3SiC_2, exhibit promising potential for applications in nuclear settings, serving as either fuel matrices or protective coatings due to their resilience to high temperatures and radiation damage.[184,185] Various types of radiation sources, methods such as heavy ions, neutrons, and protons are frequently utilized to evaluate the radiation resilience of MAX phases. The interaction between these radiation sources and MAX phases can trigger various microstructural changes, including lattice distortions, phase shifts, micro-strain, amorphization, as well as the creation of vacancies and dislocations. Both the direct impact of incident radiation beams and secondary effects stemming from displaced atoms can contribute to radiation-induced damage, disrupting electronic interactions or bonds within MAX phases. For instance, Bowden *et al.* conducted experiments on Zr_3AlC_2, Nb_4AlC_3, and $(Zr_{0.5}, Ti_{0.5})_3AlC_2$, revealing an expansion in the *c* lattice parameter following proton irradiation at elevated temperatures.[186] Deng *et al.* investigated the impact of C^{4+} ions on Ti_3AlC_2, observing an increase in micro-strain with higher irradiation fluence and a sequential transformation from the α phase to the β and γ-fcc phases. Transmission electron microscopy studies by Deng *et al.* also demonstrated the formation of defect clusters or loops in irradiated Ti_2AlC and Ti_3AlC_2 MAX phases.[187] Notably, Nappé *et al.* documented partial amorphization of Ti_3SiC_2 MAX phase upon irradiation with Xe ions, as evidenced by decreased X-ray diffraction peak intensities.[188] Similarly, Whittle *et al.* observed amorphization in Ti_3AlC_2 and Ti_3SiC_2 through diffuse scattering halos in selected-area electron diffraction patterns following irradiation with Kr cations.[185] These findings collectively underscore the

Table 3 Mechanical characteristics of selected typical MAX phases at ambient temperature

MAX phase	Density ($g\ cm^{-3}$)	Young's modulus (GPa)	Vickers hardness (GPa)	Compressive strength (MPa)	Flexural strength (MPa)	Fracture toughness ($MPa\ m^{-1/2}$)	Reference
211 phase							
Ti_2AlC	~4.1	—	5.8 ± 0.5	952 ± 6	432 ± 12	6.5 ± 0.2	164
V_2AlC	~4.0	—	2.2 ± 0.1	527 ± 12	270 ± 12	5.7 ± 0.2	176
Cr_2AlC	5.17	~282	~4.9	949 ± 22	469 ± 27	6.2 ± 0.3	175
Nb_2AlC	6.44	~294	4.5 ± 0.3	—	481 ± 42	5.9 ± 0.3	174
Ta_2AlC	11.46	292	4.4 ± 0.1	~804	360 ± 19	7.7 ± 0.2	177
312 phase							
Ti_3SiC_2	~4.5	~320	~4.0	~600	260 ± 20	—	178
Ti_3AlC_2	4.21	297	2.7–3.2	760	340	6.9–7.2	179
Ti_3GeC_2	5.22	340	5.0	1277	—	—	180
413 phase							
Ti_4AlN_3	4.6	310 ± 2	2.5	475 ± 15	350 ± 15	—	161
Nb_4AlC_3	6.97	306	2.6 ± 0.2	515 ± 44	346 ± 38	7.1 ± 0.3	162
Ta_4AlC_3	13.18	324	5.1 ± 0.1	821 ± 97	372 ± 20	7.7 ± 0.5	162

Open Access Article. Published on 27 August 2024. Downloaded on 11/30/2024 6:12:35 AM.
This article is licensed under a Creative Commons Attribution-NonCommercial 3.0 Unported Licence.

intricate responses of MAX phases to radiation exposure, emphasizing the need for further exploration to harness their full potential in nuclear applications.

In exploring the radiation resistance mechanisms of MAX phases, numerous factors contribute to their ability to endure radiation damage. One such exemplar is Ti_3AlC_2, where researchers have observed a sequential phase transformation during irradiation, transitioning successively through α, β, γ, and finally to an fcc phase shown in Fig. 7. Particularly noteworthy is the reversibility of this phase evolution, demonstrated at elevated temperatures between 500 °C to 800 °C. Higher irradiation temperatures are found to support more thorough phase recovery. Additionally, Ti_3AlC_2 can maintain its lattice structure even when subjected to irradiation-induced defects, thanks to the low formation energy of Ti–Al antisite defects and carbon interstitials, allowing it to accommodate such defects effectively prevents amorphization. Moreover, the saturation of vacancy intensity beyond 5×10^{15} fluence, rather than exhibiting a linear increase, further fortifies Ti_3AlC_2's resistance to amorphization and radiation damage. This suite of inherent traits collectively endows Ti_3AlC_2 with exceptional resilience against irradiation and amorphization. Exploring how variations in irradiation temperature, ranging from 350 to 600 °C, affect the crystallographic stability of Ti_3AlC_2, through exposure

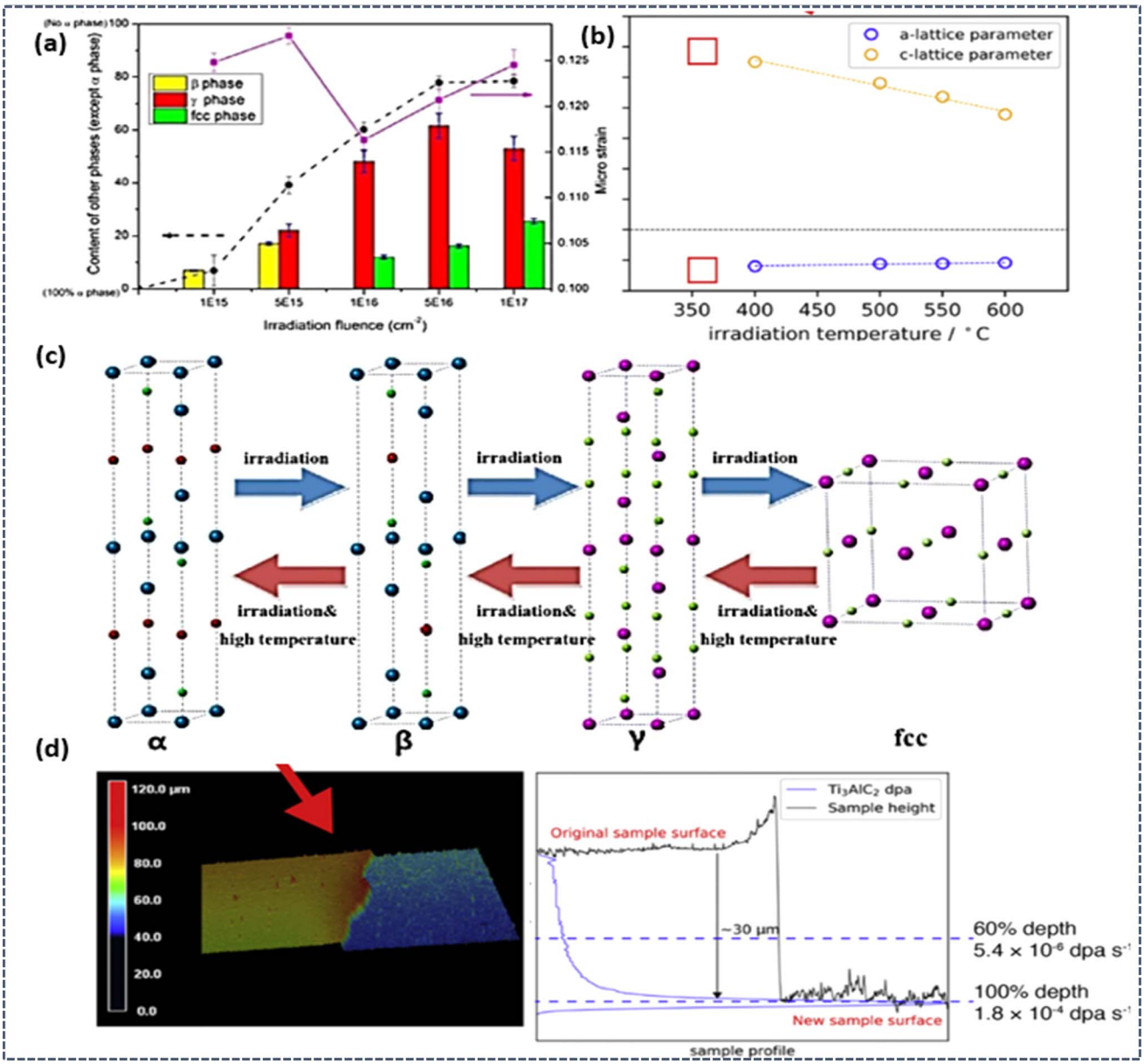

Fig. 7 Behavior of MAX phases under irradiation: (a) micro strain and phase component shifts in Ti_3AlC_2 upon C^{4+} ion irradiation at room temperature across various fluences. (b) Proton irradiation induced defects cause lattice strain in MAX phase materials. (c) Phase transformation sequences and recovery in Ti_3AlC_2 post-irradiation at high temperature. (d) Ti_3AlC_2 has low defect recovery rate, causing the irradiated surface to exfoliate at low irradiation temperature. (Reproduced from ref. 187 with permission from Elsevier, copyright 2020).[187] (Reproduced from ref. 189 with permission from Elsevier, copyright 2019).[189]

© 2024 The Author(s). Published by the Royal Society of Chemistry

Open Access Article. Published on 27 August 2024. Downloaded on 11/30/2024 6:12:35 AM.
This article is licensed under a Creative Commons Attribution-NonCommercial 3.0 Unported Licence.

to 2 MeV protons at a fluence of 2.25×10^{18} protons cm^{-2}, shows that as the irradiation temperature increases, the recovery of defects reduces the extent of anisotropic lattice alterations. However, diminished recovery at lower temperatures results in surface exfoliation and heightened damage rates. Consequently, these findings suggest that the practical application of these compositions in reactor environments may be chiefly suitable for high-temperature conditions.[189]

3.5 Property of oxidation resistance

The outstanding ability to resist high-temperature oxidation displayed by Al-containing MAX phases, like Ti_2AlC, Ti_3AlC_2, V_2AlC, and Cr_2AlC, underscores their promising applications in elevated temperature environments.[190–193] The resistance arises because of the tendency of loosely bonded aluminum components to migrate towards the surface under high temperatures. This migration facilitates the creation of a dense and uninterrupted layer of Al_2O_3, effectively blocking the inward diffusion of O^{2-}.[194,195] Several factors, such as particle size, composition of the solid solution, and oxidation temperature, greatly impact the oxidation characteristics of MAX phases. For instance, increase in weight per unit of surface area initially with oxidation time at lower temperatures like 800 °C and 900 °C before reaching a plateau, while at higher temperatures like 1000 °C and 1100 °C, weight gain continues to increase as oxygen atoms penetrate deeply, establishing an advanced oxidation front shown in Fig. 8. Cubic and parabolic oxidation kinetics are observed, characterized by $(\Delta W/S)^3 = k_{ct}$ and $(\Delta W/S)^2 = k_{pt}$, respectively, with cubic kinetics associated with the formation of a dense and continuous Al_2O_3 layer indicative of excellent oxidation resistance. Conversely, discontinuous Al_2O_3 layer formation, often accompanied by a TiO_2 layer, leads to parabolic kinetics and weaker oxidation resistance.[195,196] Cross-sectional observations *via* SEM reveal an increase in oxide layer thickness from ~7 μm at 24 hours to ~200 μm at 500 hours of oxidation at 800 °C for Ti_3AlC_2, highlighting compositional

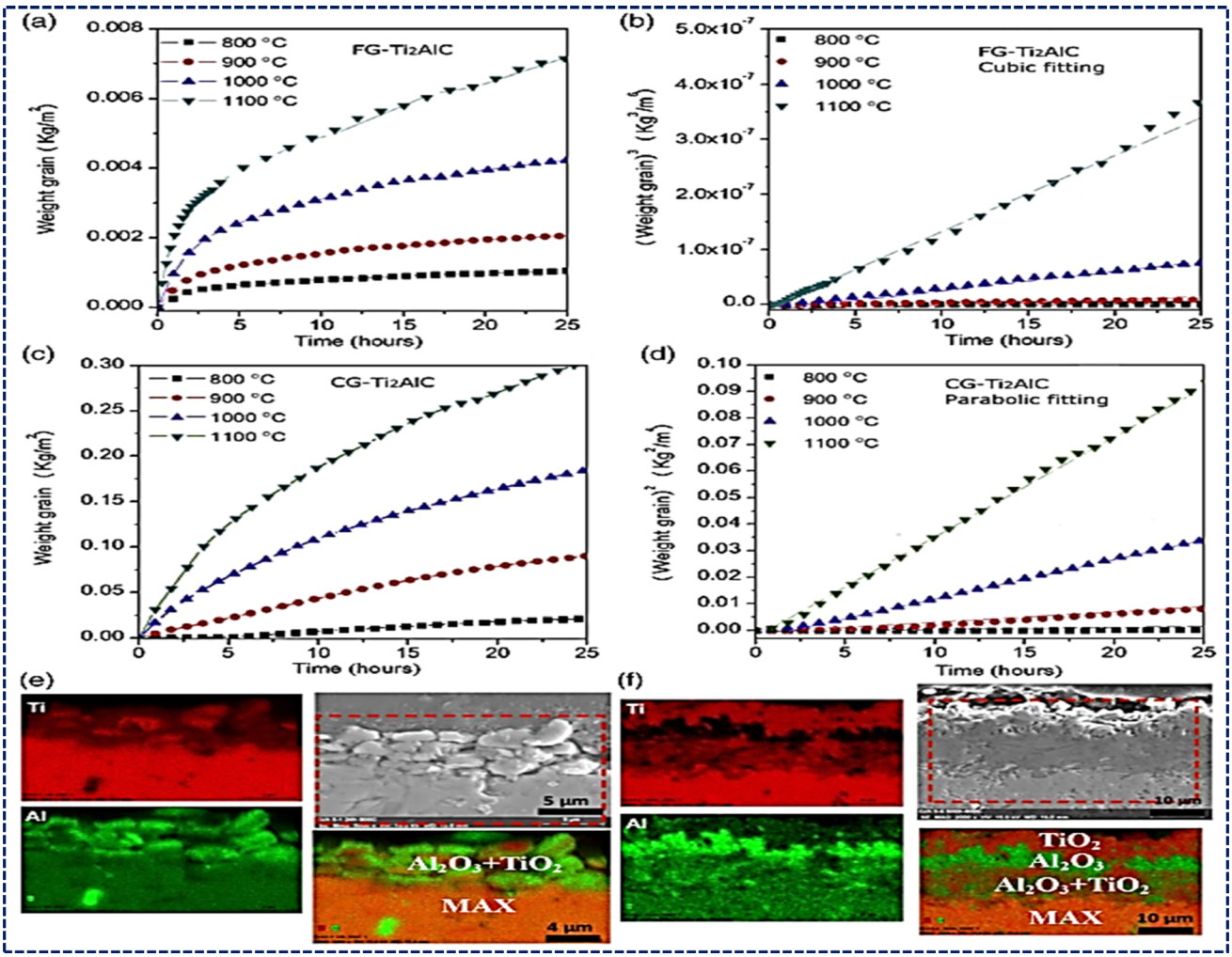

Fig. 8 MAX phases' oxidation behavior: (a and c) increase in weight per unit surface area over time due to oxidation for fine-grained (FG) and coarse-grained (CG) Ti_2AlC MAX phases at elevated temperatures. (b and d) Fitting of corresponding oxidation kinetics. (Reproduced from ref. 195 with permission from Elsevier, copyright 2020).[195] (e and f) SEM cross-section views of the oxide layer on Ti_3AlC_2 MAX phase oxidized for 24 h (e) and 500 h (f) at 800 °C. (Reproduced from ref. 194 with permission from John Wiley and Sons, copyright 2019).[194]

Open Access Article. Published on 27 August 2024. Downloaded on 11/30/2024 6:12:35 AM.
This article is licensed under a Creative Commons Attribution-NonCommercial 3.0 Unported Licence.

changes driven by inward O^{2-} diffusion and outward Ti^{4+} and Al^{3+} diffusion during oxidation shown in Fig. 8.

Grain size plays a pivotal role in modifying the oxidation resistance of MAX phases, with coarse-grained structures exhibiting significantly enhanced resistance compared to their fine-grained counterparts. For instance, fine-grained Ti_2AlC displays cubic oxidation kinetics, with a cubic rate constant of 8.3×10^{-13} kg^3 m^{-6} s^{-1} at 1000 °C, while coarse-grained Ti_2AlC follows parabolic oxidation kinetics shown in Fig. 6d, with a rate constant of 4.0×10^{-7} kg^2 m^{-4} s^{-1} under the same conditions.[191,195] This disparity results from fine-grained Ti_2AlC having a higher density of grain boundaries and more Al diffusion pathways, which promote the creation of a protective Al_2O_3 layer. Conversely, in coarse-grained Ti_2AlC, Al diffusion and the formation of the protective Al_2O_3 layer are constrained. Drouelle *et al.* conducted a comparative study on the oxidation resistance of Ti_3AlC_2 and $Ti_3(Al_{0.8}Sn_{0.2})C_2$ solid solution, revealing that the oxidation kinetics of $Ti_3(Al_{0.8}Sn_{0.2})C_2$ are notably higher than those of Ti_3AlC_2.[194] This disparity is attributed to the facile diffusion of Sn atoms in $Ti_3(Al_{0.8}Sn_{0.2})C_2$, leading to the formation of nonprotective and rapidly growing SnO_2 oxide at approximately 460 °C. Bei *et al.* have also obtained similar results, supporting the important impact of solid solution composition and grain size on the oxidation behavior of MAX phases.[197]

3.6 Crack healing properties

The scientific community has shown considerable interest in the crack healing capabilities of MAX phase materials because of their distinct blend of metallic and ceramic characteristics. These materials, which form a class of layered ceramics, demonstrate exceptional high-temperature mechanical strength, thermal stability, and outstanding oxidation resistance. This review endeavors to provide a thorough summary of the fundamental mechanisms accountable for the crack healing characteristics observed in MAX phase materials. Our focus will encompass a detailed examination of various contributing factors such as microstructural evolution, interfacial chemistry, and mechanical characteristics.

The crack propagates along the basal planes of the hexagonal Ti_2AlC's randomly oriented lamellar grains, creating a zigzag pattern and leaving smooth cleavage fracture surfaces locally. When the crack deflects perpendicular to the basal planes, it produces a stair-like fracture surface. Features such as local crack branching, crack bridging, and grain pull-out are characteristic of this material. The high toughness of Ti_2AlC is attributed to the simultaneous operation of multiple deformation and cracking mechanisms. The local variations in crack opening are influenced by the differences in grain orientations along the crack path, affecting the local deformation and failure processes. This Fig. 9 illustrates the progression of crack growth and healing steps in Ti_2AlC at 1500 K in air from 1st to 8th cycle and provides an SEM image of the healed-damage zone, obtained using electron backscatter diffraction, highlighting the microstructural changes associated with the healing process.[198]

Previous research within the Ti–Al–C system has revealed the capacity of MAX phases to "heal" cracks. This self-healing process entails subjecting Ti_2AlC or Ti_3AlC_2 to heat treatment in an oxidative environment, resulting in the deposition of TiO_2 and Al_2O_3 oxidation products within the cracks. This in turn (partially) restores the strength of the material.[199] Similar observations have been reported for Cr_2AlC, thus indicating

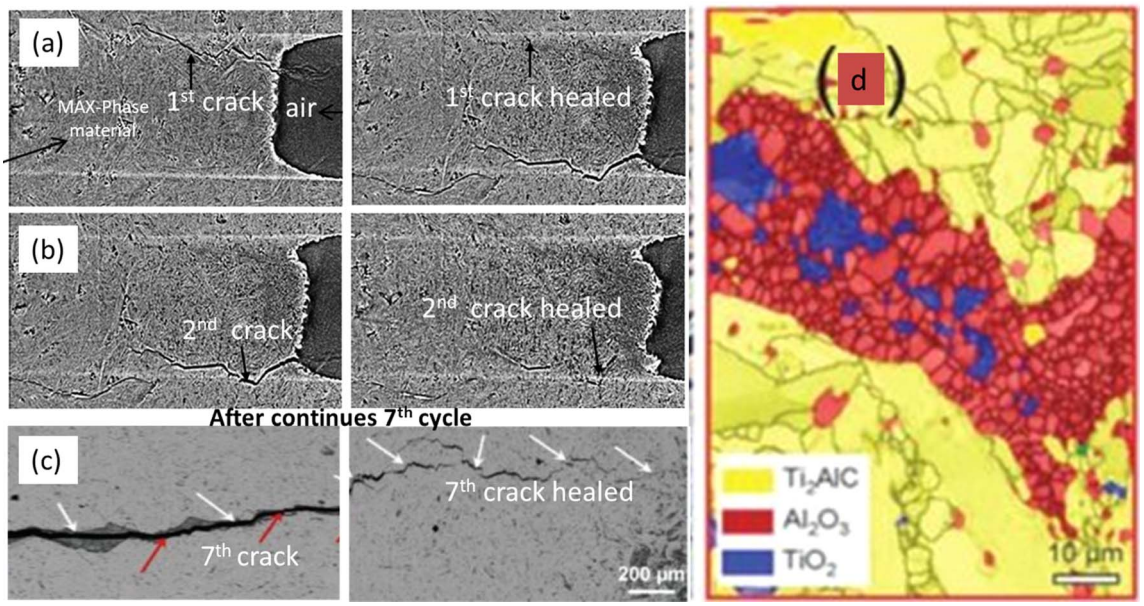

Fig. 9 Images depict the fracture and crack healing process in Ti_2AlC from the 1st to the 8th cycle. (a) Shows the first crack and its healed state. (b) Illustrates the second crack and its healed state. (c) Displays the crack path after seven healing cycles and subsequent fracture, with red arrows pointing to the remnants of the crack. (d) Presents an SEM image of the healed-damage zone captured using electron backscatter diffraction. (Reproduced from ref. 198 with permission from Springer Nature, copyright 2016).[198]

© 2024 The Author(s). Published by the Royal Society of Chemistry

Open Access Article. Published on 27 August 2024. Downloaded on 11/30/2024 6:12:35 AM.
This article is licensed under a Creative Commons Attribution-NonCommercial 3.0 Unported Licence.

a wider applicability of the crack healing phenomenon within the MAX phase family.[200] In an attempt to identify additional MAX phases that could exhibit this self-healing behavior, Farle *et al.* highlighted several thermodynamic and mechanical requirements. As a result, V_2AlC, Ti_3SiC_2, and Zr_2AlC were identified as promising candidates for further investigation.[201] A more recent study showcased the crack healing abilities of Ti_2SnC, specifically in response to thermal shock-induced cracks.[202,203] Treatment of these materials in air led to the formation of TiO_2, SnO_2, and metallic Sn, which effectively filled the cracks and restored the material's strength. This example serves to underscore the broader application of crack healing beyond commonly studied elements such as Al and Si. A thorough exploration of the crack healing capabilities in MAX phase materials could lead to the development of highly resilient, durable materials with numerous potential applications in high-temperature environments.

3.7 Magnetic properties

Since the pioneering synthesis of the first magnetic MAX phase, characterized by a heteroepitaxial single-crystal thin film comprising $(Cr_{0.75}Mn_{0.25})_2GeC$,[204] the exploration of magnetic MAX materials has flourished. Subsequent investigations have unveiled a diverse array of magnetic MAX phases, such as $(V, Mn)_3GaC_2$, Cr_2AlC, Cr_2GeC, and Mn_2GaC; and $(Cr, Mn)_2AlC$, Cr_2GeC, and $(Cr, Mn)_2GaC$; and $(Mo, Mn)_2GaC$, predominantly centered around chromium and manganese substitutions.[205] A significant breakthrough occurred when Tao and colleagues introduced rare earth (RE) elements into Mo_2AlC-based i-MAX phases, leading to the discovery of a novel class of magnetic i-MAX phases denoted as $(Mo_{2/3}RE_{1/3})_2AlC$, with RE comprising Ce, Pr, Nd, Sm, Gd, Tb, Dy, Ho, Er, Tm, and Lu.[206] These innovative phases exhibited a distinctive microstructure characterized *via* quasi-2D magnetic frustrated triangular lattice bilayers on top of a Mo honeycomb configuration, resulting in complex magnetic orders arising from intricate intra- and in-plane magnetic interactions. More recently, the exploration of magnetic MXenes has emerged, with notable works such as the synthesis of Ti_3C_2 MXene containing a small fraction of silicon carbide, exhibiting a combination of ferromagnetic and diamagnetic properties suitable for potential applications in spintronics devices.[207] Additionally, investigations into the magnetic transitions of MAX phases, exemplified by the transition observed in $Cr_2TiC_2T_x$, have shed light on the complex magnetism inherent in these materials. Theoretical studies have played a pivotal role in elucidating the magnetic properties of MAX phases, offering insights into their stability and electronic structures. For instance, theoretical predictions have highlighted Fe-based MAX phases, particularly Fe_3AlC_2, as promising candidates for ferromagnetic behavior, although experimental confirmation remains elusive.[208] Computational approaches, such as density functional theory (DFT) and DFT + U methods, have enabled researchers to unravel the underlying mechanisms governing magnetism in MAX phases, revealing the dominant contribution in Cr-containing MAX phases of Cr 3d valence electrons to the magnetic moments.[130] Furthermore, theoretical calculations have elucidated the influence of structural factors, such as intercalated nonmagnetic slabs, on the magnetic properties of MAX phases, exemplified by the enhanced magnetic moments observed in $(Cr_2Ti)AlC_2$ compared to Cr_2AlC due to the larger interatomic distances between out-plane Cr atoms. Bulk Mn- and Fe-substituted Cr_2AlC samples were prepared for the study Fig. 10 shows the magnetization data for the Mn (a) and Fe (b) substituted samples, $(Cr_{1-x}Mn_x)_2AlC$ and $(Cr_{1-x}Fe_x)_2AlC$, with nominal compositions ranging from $x = 0$ $x = 0$ $x = 0$ to $x = 0.15$ $x = 0.15$ $x = 0.15$ and $x = 0$ $x = 0$ $x = 0$ to $x = 0.075$ $x = 0.075$ $x = 0.075$, respectively.[209] These multifaceted investigations underscore the intricate interplay between composition, structure, and magnetism in MAX phases, paving the way for the design and exploration of novel magnetic materials with tailored properties and functionalities.

3.8 Resistance against corrosion in liquid metals

The evaluation of MAX phase materials for potential applications in lead-cooled fast reactors (LFRs) of Generation IV necessitates a thorough understanding of their corrosion resistance in contact with heavy liquid metal (HLM) primary coolants such as lead (Pb) and lead-bismuth eutectic (LBE). Unlike conventional stainless steels, which are susceptible to dissolution corrosion when most MAX phases come into contact with liquid LBE, they behave inertly at high temperatures (>450 °C) and low HLM oxygen concentrations (CO < 10–8 mass%).[210] This inherent liquid metal corrosion (LMC) resistance renders MAX phases highly promising for structural components in Gen-IV LFRs. Recent experiments involving commercially available MAX phase ceramics, exposed to liquid Pb and LBE at reactor-relevant temperature ranges, such as Maxthal® 312 and Maxthal® 211, have shown no corrosion effects that would jeopardize their structural integrity. Notably, Ti_3SiC_2 exhibited thin rutile TiO_2 formation, while Ti_2AlC ceramic showed dissolution of the TiAl phase resulting in LBE ingress.[211] Lapauw *et al.* (2019) conducted stability tests on 11 MAX phase ceramics in oxygen-depleted liquid LBE at 500 °C, revealing either intrinsic resistance to LBE attack or passivation *via* nanometric Al_2O_3 or SiO_2 oxide scales.[133,212] The susceptibility of MAX phases to LBE interaction was observed in Ti_2SnC and Zr-rich MAX phases, emphasizing the significance of phase purity on LMC resistance. Despite local LBE interaction with MAX phase grains, surface integrity was maintained, with attacked Zr-rich MAX phase grains transforming into MAX phase solid solutions. Additionally, experiments conducted under fast-flowing LBE conditions resulted in the formation of oxide scales on MAX phase ceramics, while reference structural materials such as solution-annealed 316L stainless steels showed erosion damage shown in Fig. 11, further highlighting the favorable corrosion resistance properties of MAX phases in liquid metal environments (Table 4).[123,133]

3.9 Microwave absorbing properties

In the realm of microwave absorbing materials, while carbon materials have traditionally held sway, their susceptibility to oxidation under high temperatures has constrained their

Open Access Article. Published on 27 August 2024. Downloaded on 11/30/2024 6:12:35 AM.
This article is licensed under a Creative Commons Attribution-NonCommercial 3.0 Unported Licence.

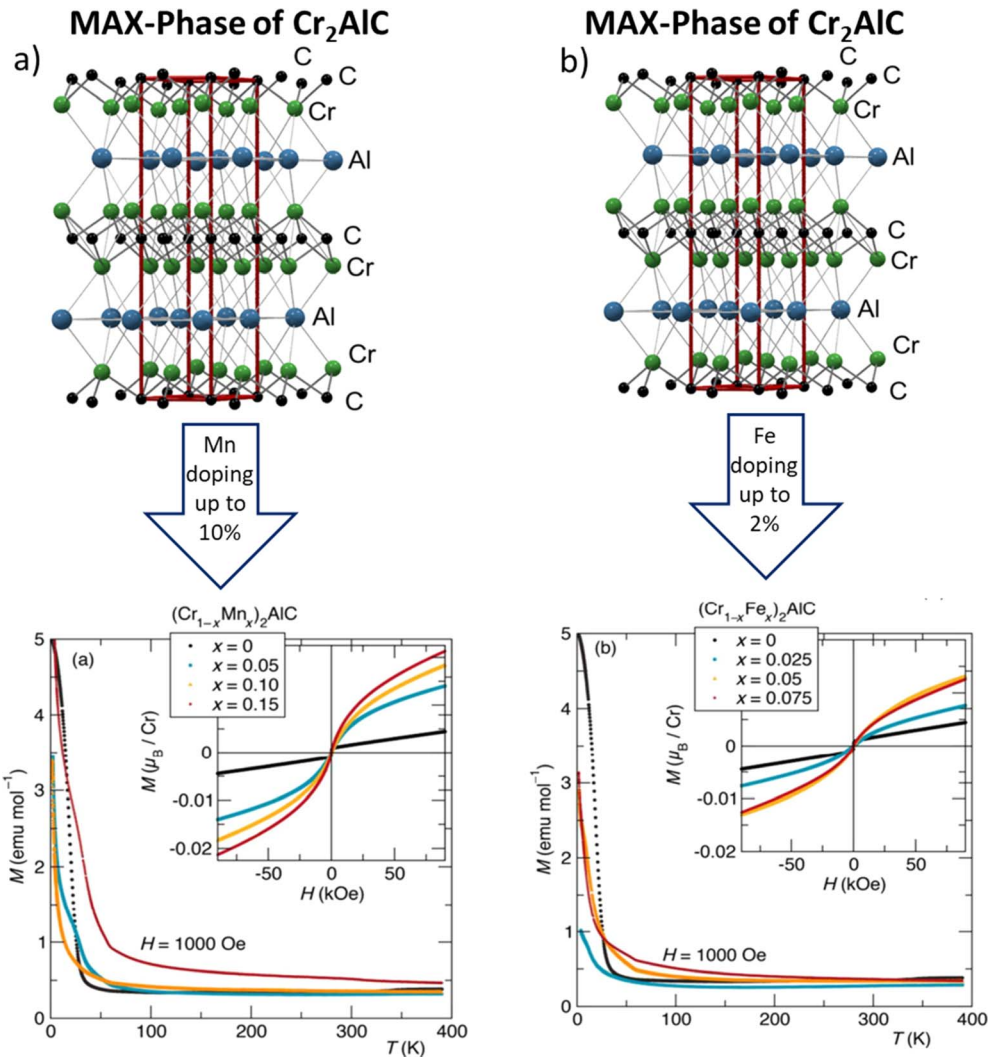

Fig. 10 Magnetization data for the Mn (a) and Fe (b) substituted samples, $(Cr_{1-x}Mn_x)_2AlC$ and $(Cr_{1-x}Fe_x)_2AlC$, with nominal compositions. (Reproduced from ref. 209 with permission from The Royal Society of Chemistry, copyright 2017).[209]

widespread application. However, MAX phases, renowned for their exceptional thermal stability and versatile properties, have emerged as promising contenders for microwave absorption, particularly in elevated temperature settings. Beginning with the investigation of Ti_3SiC_2 MAX phase's microwave dielectric properties, researchers have delved into understanding its potential. Studies by Li *et al.* revealed the influence of Ti_3SiC_2 purity on its microwave absorbing characteristics, with higher purity variants exhibiting superior complex permittivity and dielectric loss.[218] Subsequent research efforts have focused on enhancing Ti_3SiC_2 purity through Al doping, yielding notable improvements in permittivity.[219] Moreover, the incorporation of Ti_3SiC_2 into composite materials has yielded intriguing results. For instance, Ti_3SiC_2/cordierite composites demonstrated effective microwave absorption, achieving significant absorption bandwidths. Additionally, the exploration of other MAX phases, such as $(Cr_{2/3}Ti_{1/3})_3AlC_2$, has unveiled further potential.[220,221] Yao *et al.*'s investigation into $(Cr_{2/3}\ Ti_{1/3})_3AlC_2$'s microwave absorption properties underscored the importance of particle size and matrix thickness in influencing absorption efficacy. Notably, at specific thicknesses and frequencies, $(Cr_{2/3}Ti_{1/3})_3AlC_2$ showcased remarkable microwave absorption capabilities, suggesting its viability for practical applications in the X-band frequency range.[222]

The future path of MAX phases is poised for remarkable advancements in their electrical and thermal properties. As researchers continue to explore these materials, a deeper understanding of the mechanisms underlying their conductivity and thermal behaviors will be achieved. Variations in electronic conductivity, influenced by composition and microstructural factors, will likely be fine-tuned for specific applications, improving performance in various technological fields. For example, minimizing lattice defects such as vacancies and dislocations will reduce electron scattering, thereby enhancing electrical conductivity. The temperature-dependent nature of MAX phases' resistivity and conductivity will be harnessed to develop materials with tailored properties for high-temperature electronics and thermal management systems. Innovations in synthesis methods, such as optimizing self-propagating high-temperature synthesis (SHS) and hot isostatic pressing (PHIP),

© 2024 The Author(s). Published by the Royal Society of Chemistry

Open Access Article. Published on 27 August 2024. Downloaded on 11/30/2024 6:12:35 AM.
This article is licensed under a Creative Commons Attribution-NonCommercial 3.0 Unported Licence.

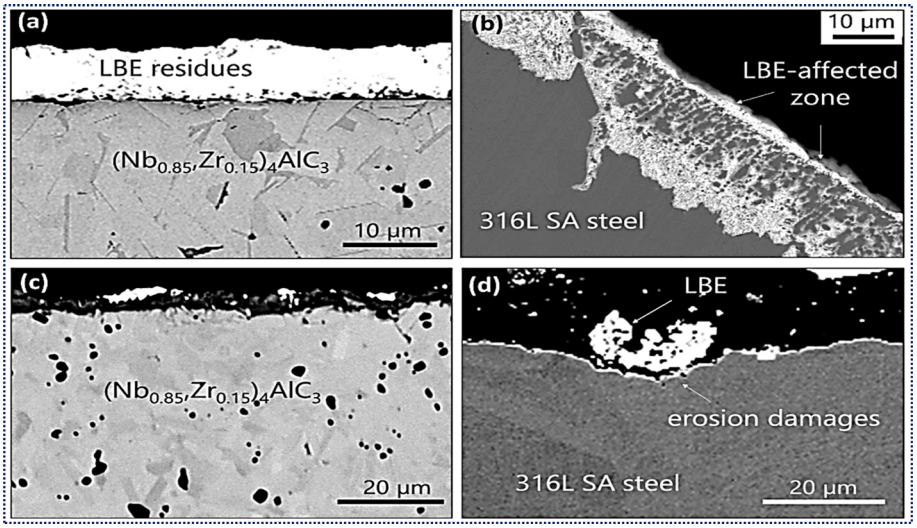

Fig. 11 Materials exposed for 1000 hours at 500 °C to oxygen-deficient, static LBE: (a) solid solution in the MAX phase $(Nb_{0.85}, Zr_{0.15})_4AlC_3$, (b) stainless steel 316L SA. Materials subjected for 1000 hours at 500 °C to fast-slowing, oxygen-deficient LBE: (c) $(Nb_{0.85}, Zr_{0.15})_4AlC_3$ (d) 316L SA stainless steel; $4AlC_3$ MAX phase solid solution. (Reprinted from ref. 213 with permission from Elsevier, copyright 2021).[213]

Table 4 Summary of literature studies on the exposure of MAX phases to liquid Pb and LBE

MAX phase	Pb/LBE	Time (kh)	T (°C)	Flow	Interaction	CO (wt%)	Ref.
Ti_3AlC_2	LBE	3.5	500	Static	Local GB penetration	10^{-10}	133
$(Ti, Nb)_2AlC$	LBE	3.5	500	Static	No interaction	10^{-10}	133
Nb_2AlC	LBE	3.5	500	Static	No interaction	10^{-10}	133
Nb_4AlC_3	LBE	3.5	500	Static	No interaction	10^{-10}	133
$(Nb_{0.85}Zr_{0.15})_4AlC_3$	LBE	1	500	Static	No interaction	$\sim10^{-11}$	133
				$\sim$8 ms^{-1}	3–4 μm Nb_2O_5-based scale	5×10^{-9}	
Ti_3SiC_2	LBE	1	700	Static	No interaction	5×10^{-6}	214
	LBE	3	550/650	Static	TiO_2 (rutile)	$10^{-6}/10^{-8}$	130
	LBE	1/3	550/650	Static	TiO_2 (rutile), local surface disintegration	$10^{-6}/10^{-8}$	211
		5/10	700				
	LBE	3.5	500	Static	No interaction	10^{-10}	133
	Pb	1	650/800	—	No interaction	[a]10^{-12}	215
	Pb	0.5	550/600	Static	TiO_2 (rutile) formation	$10^{-6}/10^{-8}$	216
		2/4	750				
	Pb	2	500	1 ms^{-1}	Thin oxide layer	10^{-6}	217
Zr_2AlC	LBE	1	500	Static	Penetration of LBE into MAX phase resulting in the formation of Zr_2(Al, Bi, Pb)C	$\sim10^{-11}$	133
				$\sim$8 ms^{-1}	Mild ZrO_2 formation	5×10^{-9}	
Zr_3AlC_2	LBE	1	500	Static	Penetration of LBE into MAX phase resulting in the formation of Zr3(Al, Bi, Pb)C	$\sim10^{-11}$	133
				$\sim$8 ms^{-1}	Severe ZrO_2 formation	5×10^{-9}	
Ti_2AlC	LBE	1/3 5/10	550/650 700	Static	TiO_2(rutile) & Al_2O_3 formation (CO = 10^{-6}) dissolution of secondary phases (CO = 10^{-8}, T = 650, 750 °C)	$10^{-6}/10^{-8}$	211
	LBE	3.5	500	Static	No interaction	10^{-10}	133
	Pb	1	650/800	—	No interaction	[a]10^{-12}	215
$(Zr_{0.8}, Ti_{0.2})_2AlC$ & $(Zr_{0.8}\ Ti_{0.2})_3AlC_2$	LBE	1	500	Static	When LBE penetrates the MAX phase, the intermetallic $(Zr_{0.8}, Ti_{0.2})_{n+1}$ (Al, Pb, Bi)Cn production dissolves	10^{-11}	133
Ti_2SnC	LBE	1	500	Static	LBE penetration through grain boundaries with secondary Sn phase attacked at grain boundaries	10^{-11}	133

[a] Denotes a calculated CO value.

Open Access Article. Published on 27 August 2024. Downloaded on 11/30/2024 6:12:35 AM.
This article is licensed under a Creative Commons Attribution-NonCommercial 3.0 Unported Licence.

will lead to more consistent and high-quality MAX phase materials with superior electrical and thermal conductivities. Additionally, the interplay between electrons and phonons in thermal conductivity will be better understood, allowing for the design of MAX phases with enhanced heat dissipation capabilities. As these materials continue to be refined, their applications in fields like aerospace, energy, and electronics will expand, leveraging their unique combination of metallic and ceramic properties.

4. Synthesis of MAX phases

4.1 Synthesis techniques (bottom-up *vs.* top-down approaches)

Synthesis techniques play a pivotal role in defining the characteristics of MAX phases, with bottom-up and top-down approaches offering distinct pathways for material synthesis and customization. The characterization of MAX phases, innovative materials bridging the gap between metals and ceramics with their distinctive layered structure, heavily relies on the synthesis techniques applied. These methods, classified as either bottom-up or top-down approaches, significantly influence the elemental composition and structural attributes of the resultant materials. Traditional MAX phases, adhering to the space group $P6_3/mmc$ and comprising an early transition metal (M), an A-group element (A) from groups 12 to 16, and additional elements like carbon, nitrogen, boron, or phosphorus(x), are commonly synthesized through bottom-up methodologies. While upholding Nowotny's seminal findings, this category has evolved to encompass materials with higher n values and, more recently, boron-containing phases, emphasizing the adaptability of the approach in generating intricate compositions.[223] Bottom-up synthesis encompasses direct techniques such as powder metallurgy and thin film deposition, yielding a wide array of MAX phases, including ternary compositions, alloys, and multi-element solids with significant disorder on the M sites, such as high entropy MAX phases. This method facilitates the inclusion of A-site elements beyond conventional groups, thereby expanding the spectrum of achievable material

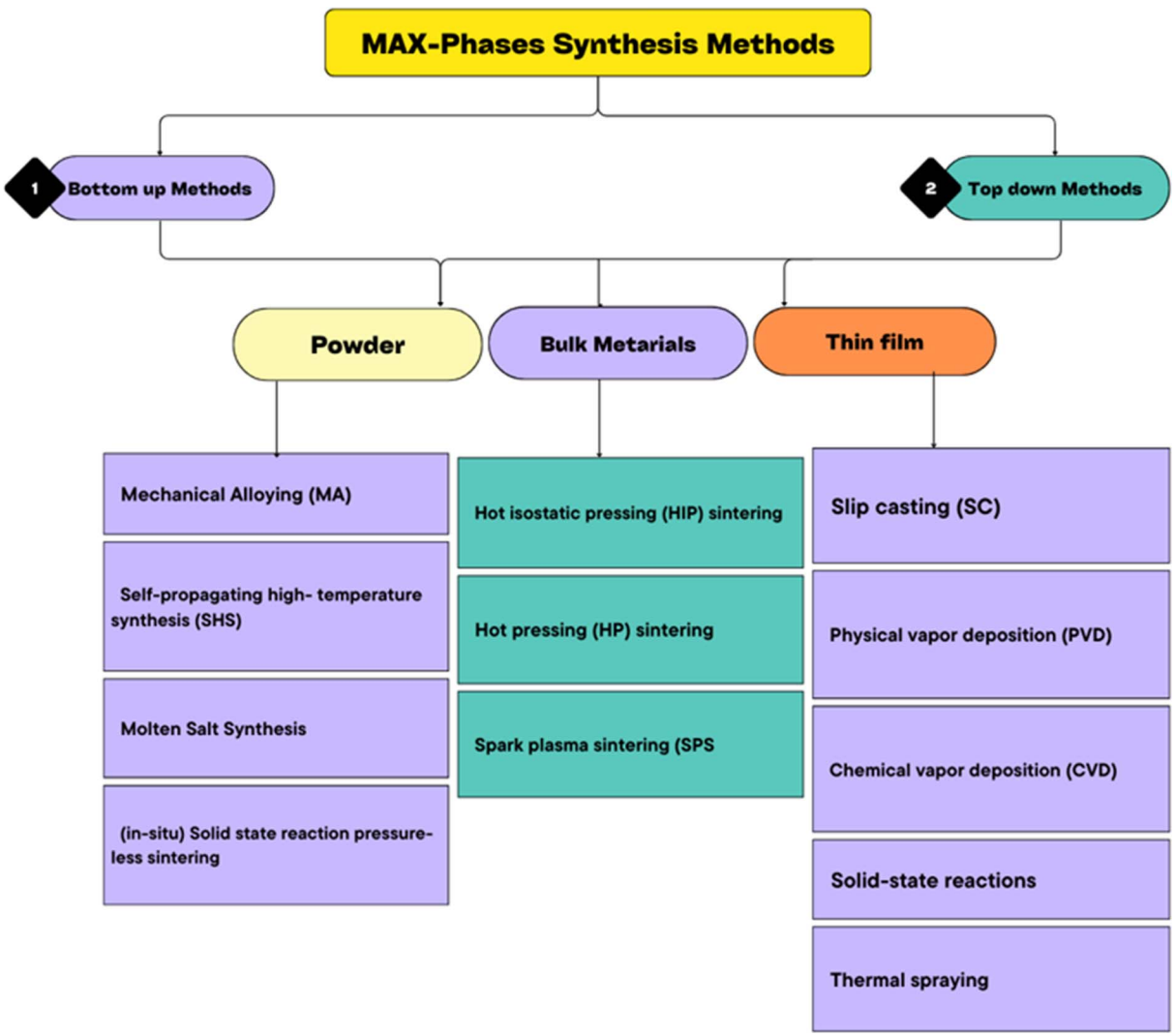

Fig. 12 An illustration of the methods used to synthesize MAX phases presented in a flowchart format.

© 2024 The Author(s). Published by the Royal Society of Chemistry

Open Access Article. Published on 27 August 2024. Downloaded on 11/30/2024 6:12:35 AM.
This article is licensed under a Creative Commons Attribution-NonCommercial 3.0 Unported Licence.

properties.[224,225] Conversely, top-down synthesized MAX phases involve modifying the A-group layers post-synthesis, rather than altering their initial chemical composition.[226] Derived from a bottom-up synthesized precursor, these materials undergo partial or complete replacement of the A-layer through subsequent treatments, demonstrating the method's potential for tailoring material properties. The dichotomy between bottom-up and top-down synthesis of MAX phases underscores the versatility and complexity of these materials, highlighting the crucial role of synthesis techniques in shaping their structure, composition, and ultimately, their properties.[227]

Over the past two decades, significant endeavors have been invested in advancing the synthesis and characterization of MAX phases. Fig. 12 provides a detailed flowchart depicting the various synthesis methods employed to produce MAX-phase materials. Addressing the synthesis of MAX phase ceramics proves to be a noteworthy challenge, with a limited selection of commercially available powder sources in the market, encompassing compositions such as Ti_3SiC_2, Ti_2AlC, Ti_3AlC_2, V_2AlC, and Nb_2AlC. Notably, the absence of commercially available bulk MAX phase ceramics has been conspicuous. The synthesis approaches for MAX phases can be broadly categorized into powder, bulk, and thin film methods, with a comprehensive overview presented in Table 5. It is interesting to note that a majority of observed MAX phases are commonly produced in a highly polycrystalline form, although a few instances report thin single crystalline layers[245] or single-crystalline platelets.[246] The synthesis of bulk single crystals has become a pivotal strategy for exploring the anisotropic physical properties of MAX phases. However, until recently, the synthesis of bulk single crystals presented a considerable challenge, impeding in-depth investigations into their physical properties. A significant breakthrough in 2011, led by the LMGP team, successfully developed a method for producing single crystal MAX phases,[247,248] unlocking new avenues for research in a field that already commands intense international interest and research activity.

4.2 MAX phase powders

In the realm of MAX phase powder synthesis, various production methodologies have been explored, each contributing to the versatility of the field. The self-propagating high-temperature synthesis (SHS) technique has found application in the production of Maxthal 211 and 312, showcasing its efficacy.[229,230] Microwave synthesis and molten salt routes have also been pivotal in MAX phase powder synthesis. Notably, molten salt synthesis from elemental powders has proven successful in obtaining MAX phase powders like Ti_2AlC, Ti_3AlC_2, and Cr_2AlC.[231,249,250] The use of different molten salt compositions, such as KBr, NaCl/KCl mixtures, and NaCl/KCl, allows for the tailored synthesis of specific phases. Moreover, electrosynthesis emerges as a viable approach, enabling the transformation of oxide/carbon precursors into MAX phase powders in molten salt environments. For instance, $TiO_2/Al_2O_3/C$ precursor pellets can be used to produce Ti_3AlC_2 powder at 900 °C and 3.1 V in molten $CaCl_2$, whereas Cr_2AlC precursor pellets can be used to produce Cr_2AlC powder at 700 °C and 3 V in molten NaCl–$CaCl_2$.[251,252] Alternatively, method for producing MAX phase powder is through the comminution of bulk materials that have undergone reactive synthesis, further diversifying the available synthesis routes.

4.3 MAX phase bulk ceramics

In recent years, the development of bulk processing techniques for MAX phase ceramics has seen significant advancements. Powder metallurgy stands out as the predominant method, necessitating a meticulous fusion of the starting powder constituents. Within this domain, various approaches have emerged, ranging from conventional methods like CS or microwave sintering conducted under protective atmospheres to more sophisticated techniques such as hot isostatic pressing (HIP),[233–235] hot pressing (HP),[236,237] spark plasma sintering (SPS),[238,239] single-crystal growth[253] and mechanical alloying (MA). Haemers *et al.* provided a comprehensive review of the

Table 5 Synthesis of various forms of MAX phases

Category	Method	Example	Reference
Powder	Mechanical alloying (MA)	Ti_3SiC_2	228
	Self-propagating high-temperature synthesis (SHS)	Ti_3AlC_2	229
		Ti_2AlC	230
	Molten salt synthesis	Ti_3AlC_2	231
	(*In situ*) solid state reaction pressure-less sintering	Ti_3SiC_2	232
Bulk materials (polycrystalline MAX and its composites)	Hot isostatic pressing (HIP) sintering	Ti_3SnC_2, Ti_2SnC	233
		Hf_2PbC, Zr_2PbC	234
		V_2AlC	235
	Hot pressing (HP) sintering	Cr_2AlC	236
		Nb_2AlC	237
	Spark plasma sintering (SPS	Ti_3SiC_2	238
		Ti_2AlC	239
Thin film	Slip casting (SC)	Ti_3AlC_2	240
	Physical vapor deposition (PVD)	Ti_3GeC_2, Ti_2GeC	241
	Chemical vapor deposition (CVD)	Ti_3SiC_2	242
	Solid-state reactions	Ti_2AlN	243
	Thermal spraying	Ti_2AlC	244

Open Access Article. Published on 27 August 2024. Downloaded on 11/30/2024 6:12:35 AM.
This article is licensed under a Creative Commons Attribution-NonCommercial 3.0 Unported Licence.

synthesis protocols for the most prevalent layered carbide and nitride MAX phases, shedding light on the intricate processes involved,[254,255] Bulk synthesis techniques are often categorized based on their synthesis routes, distinguishing between pressure less methods like CS and SHS, and pressure-assisted techniques like HIP, HP, and SPS. Among these, the latter group has demonstrated greater efficacy in synthesizing various members of the MAX phase family, particularly those of higher orders like Nb_4AlC_3, which have been exclusively reported through HP or SPS synthesis routes.

Notably, the synthesis of MAX phases involves complex thermodynamic considerations, especially regarding the temperature requirements for the formation of different MAX phase compositions. For instance, MAX phases with a higher '*n*' in the $M_{n+1}AX_n$ formula demand elevated formation temperatures compared to those with smaller '*n*' layers in the same ternary system. This nuanced understanding has enabled the targeted synthesis of specific MAX phases like Ti_3AlC_2, Nb_4AlC_3, and Ta_4AlC_3 through annealing processes tailored to their respective ternary systems.[243] However, at elevated temperatures, MAX phase decomposition becomes a competing reaction, leading to the breakdown of $M_{n+1}AX_n$ into $M_{n+1}X_n$ and A components.

The M–A bond, the weakest in MAX phases, tends to break first at high temperatures, leading to outward diffusion of the A-element. Pressure-assisted techniques offer a notable advantage by enclosing the material in a die/punch system or metal capsule, thus reducing A-element loss. This assertion finds support in a study where a ternary powder mixture was embedded in Al_4C_3, resulting in a significant enhancement in Ti_3AlC_2 formation during pressure less sintering.[256] To discuss synthesis routes and process parameters, the ternary Ti–Al–C system is chosen, housing two extensively researched MAX phases: Ti_2AlC and Ti_3AlC_2. Self-propagating high-temperature synthesis (SHS) emerges as the most cost-effective method for MAX phase production, being efficient in time and energy, requiring minimal infrastructure, and scalable for industrial use. Although exothermal, with the powder bed igniting and a reaction front advancing through it, SHS often yields competing phases like TiC.[257] While commonly employing elemental powders, alternative combinations like M-oxides, Al, and Al_4C_3 have been explored, albeit with limited process control and product predictability. Conventional sintering, conducted under protective atmospheres or vacuum, offers better control and scalability. It has been successfully applied to various ternary and quaternary MAX phases. Pressure less sintering can be coupled with mechanical alloying (MA) to introduce elements like Cu into MAX phase structures, as demonstrated by Lyu *et al.*[258]

Furthermore, microwaves offer an alternative heat source. During microwave sintering, grain orientation in the Ti_2AlN MAX phase was shown to be favored during growth, although the underlying mechanism remains incompletely understood.[259] Hot isostatic pressing (HIP) and reactive hot pressing (HP) have been extensively employed in the synthesis of high purity, dense Ti_2AlC and Ti_3AlC_2 on a laboratory scale within the Ti–Al–C system. Key process parameters include the chemistry and stoichiometric ratio of the starting powders, sintering temperature (typically ranging from 1200 °C to 1500 °C), dwell time (0.5 to 16 hours), pressure (30 to 70 MPa), and optionally, a heat treatment at lower temperatures. While elemental powders are commonly used as starting materials, binary compounds like TiC_x, Al_4C_3, and TiH_2 are also utilized.[260] When compared to fine pure Ti powder, TiH_2 is a less pyrophoric and more cost-effective source of Ti,[261] dehydrogenating *in situ* around 600 °C. Although Al_4C_3 is noted for its effectiveness as a source of Al and C in the Ti–Al–C MAX phase synthesis, this carbide's hygroscopic nature causes parasitic phases like Al_2O_3 to exist in the finished product.[262] Processing cycles that are comparatively slow limit HP and HIP and a restricted amount of material per run, rendering these techniques, particularly HIP, costly. Because Spark Plasma Sintering (SPS), sometimes called PDS or FAST, has shorter dwell durations of only a few minutes and higher heating and cooling rates, it can speed up processing. Furthermore, SPS synthesis temperatures have been observed to be normally 50–200 °C lower than those of hot pressing. As an illustration, another research team combined mechanical alloying (MA) with SPS at 1050 °C to synthesize dense Ti_3AlC.[263] It is uncertain whether this inconsistency with traditional methods such as HP or HIP is due to the process's nature, increased diffusion caused by current flow, or simply a result of the temperature measurement technique used.

4.4 MAX phase thin film

In the realm of MAX phase coating synthesis, the exploration of various deposition techniques has been pivotal, particularly from the perspective of thin films. Notably, three primary methods have gained prominence: physical vapor deposition (PVD) utilizing elemental dc sputtering, cathodic arc deposition or magnetron sputtering,[241] and chemical vapor deposition (CVD).[242] Additionally, solid-state reaction synthesis has been employed both between thin films and at film-bulk interfaces. An informative study of MAX phase thin films is given by Eklund *et al.*, with a focus on the synthesis of innovative MAX phase coatings.[243] The thermal substitution reaction of a Ti_3SiC_2 coating with noble metals like Au and Ir is one interesting direction, yielding coatings like Ti_3AuC_2, $Ti_3Au_2C_2$, and Ti_3IrC_2.[264] A comparative analysis between bulk and thin film processing reveals distinct disparities. The primary difference is the synthesis temperature, as MAX phase production occurs at substantially lower temperatures for thin films (*e.g.*, PVD of Cr_2AlC at 450 °C),[243] compared to the 1200–1400 °C range reported for bulk synthesis.[244,265] This temperature contrast is attributed to the additional energetic flux resulting from atomic bombardment during thin film deposition. Another differentiating factor lies in the thermodynamic state of the formed material. Bulk techniques typically aim for a near-equilibrium state, assuming greater stability of the produced MAX phases compared to competing phases. However, certain thin film processes yield MAX phase compounds marked as 'metastable', such as Ti_4SiC_3, Ti_4GeC_3, and Ti_3SnC_2.[266] Although these MAX phases are considered intrinsically stable based on the Cauchy–Born criterion, their synthesis proves challenging in bulk, where specific techniques or additives are required. Notably,

© 2024 The Author(s). Published by the Royal Society of Chemistry

Open Access Article. Published on 27 August 2024. Downloaded on 11/30/2024 6:12:35 AM.
This article is licensed under a Creative Commons Attribution-NonCommercial 3.0 Unported Licence.

Thorsteinsson *et al.* reported the thin film synthesis of the magnetic MAX phase Mn_2GaC, an achievement not replicated in bulk synthesis to date, underscoring the unique capabilities and challenges inherent in thin film MAX phase synthesis.[267]

Additionally, there is another type of MAX phase known as MAX phase composite material, which we discuss in this article. The synthesis of MAX phase composite materials presents an intriguing avenue for material scientists, offering enhanced properties and structural versatility. In this review, we delve into the synthesis methodologies, focusing particularly on the High-Pressure (HP) process as a primary approach. Notably, Zhang *et al.* demonstrated the fabrication of Cu/Ti_3AlC_2 composites *via* HP, shedding light on their structural stability.[268] Through XRD analysis, it was revealed that Cu and Ti_3AlC_2 could coexist below 850 °C, with moderate reactivity observed between 850 and 950 °C, and substantial reaction beyond 950 °C. The diffusion of Al from Ti_3AlC_2 into Cu, initiating the formation of Cu(Al) solid solution, marked the commencement of the process. Moreover, the ability of Ti_3AlC_2 to withstand some Al loss while preserving its structural integrity underscores its robust nature. Additionally, we explore bulk procedures and solid-state reaction techniques, which bear resemblance to each other and differ from Physical Vapor Deposition (PVD). The unique attributes of PVD, such as the capability to supply energy for film growth through methods other than temperature, like energetic growth or ion bombardment, facilitate the deposition of thin-film MAX phases even at low substrate temperatures. This comprehensive examination illuminates the diverse pathways available for the synthesis of MAX phase composites, offering valuable insights for further advancements in material engineering.

5. Advanced application of MAX phases

In recent years, the quest for overcoming the hurdles to MAX phase commercialization has intensified, with researchers and industry players alike focusing on innovative solutions. Notably, advancements in materials synthesis, processing techniques, and characterization methods have propelled the exploration of MAX phases into new realms of possibility. For instance, since the late 1990s, following Kanthal Corp.'s acquisition of the MAX technology, significant progress has been achieved in pushing the boundaries of MAX phases' applications. Particularly noteworthy are the advancements in Ti_2AlC heating elements, which underwent thorough testing, displaying exceptional stability over roughly 8000 cycles between room temperature and 1350 °C, thanks to the development of a protective oxide layer.[269] Furthermore, Ti_2AlC has emerged as a superior alternative to traditional steel nozzles in corrosive environments, demonstrating its versatility and potential. Despite these breakthroughs, the widespread availability of MAX phase products remains limited. However, instances such as the adoption of Cr_2AlC pantographs in electric high-speed trains underscore the incremental progress towards broader commercialization.[270]

Nonetheless, challenges persist, including the scarcity of economically viable high-purity powders, the intricate nature of the vast MAX phase family, and the protracted qualification processes required for critical applications. This review manuscript aims to delve into these recent advancements, offering insights into the evolving landscape of MAX phase utilization and charting a course toward future breakthroughs and commercialization prospects across various industries. Overall, the diverse properties of MAX phases make them promising candidates for a wide range of applications across industries, driving ongoing research and innovation in materials science and engineering is shown in Fig. 13. Here are some notable examples:

5.1 Material for high-temperature structural applications

High-temperature structural materials in MAX phase compounds delves into the fascinating realm of MAX phase materials, highlighting their remarkable properties and potential applications in extreme environments. This succinct review offers insights into the structural stability, thermal conductivity, and oxidation resistance of MAX phases, elucidating their pivotal role in advancing aerospace, energy, and automotive industries. Given the remarkable attributes displayed by Al_2O_3 scale-forming MAX phases, their utilization in extreme conditions and high-temperature environments is becoming increasingly evident. One particularly promising avenue lies in incorporating Ti_2AlC, Ti_3AlC_2, and Cr_2AlC into components utilized within gas turbine engines, with the potential to significantly improve efficiency and performance. These MAX phases offer substantially higher operating temperatures compared to conventional Ni/Co superalloys, potentially enabling operations at temperatures exceeding 1400 °C.[271] This advancement is critical for components like combustor liners, blades, and vanes, which endure temperatures surpassing 1600 °C, along with exposure to oxidizing atmospheres, corrosive particles, and intense thermal and mechanical stresses. Additionally, their compatibility with thermal barrier coatings (TBCs) further enhances their utility by reducing thermal stresses and extending system longevity. Boatemaa *et al.* conducted a study where they incorporated 20 vol% Ti_2AlC into Al_2O_3 and investigated the crack healing shown in Fig. 14a–d behavior of the composite at elevated temperatures.[271,273] They observed that surface cracks induced by Vickers indentation were filled with newly formed Al_2O_3 after annealing above 800 °C, leading to a restoration of bending strength to about 90% of the undamaged composite after annealing at 1000 °C for 15 minutes, with full strength recovery achieved after 1 hour of annealing. Moreover, the abundance of constituent elements such as Ti, Al, and C in MAX phases presents a sustainable and cost-effective alternative to superalloys, which often rely on strategic elements with limited availability and environmental concerns. Recent research has highlighted the exceptional oxidation resistance exhibited by Al-containing MAX phases, illustrated by oxidation-induced crack healing inclusions observed in Ti_2AlC and Ti_3AlC_2 composites. Long-term oxidation studies on Ti_3AlC_2 have further demonstrated the maintenance of structural integrity and protective capabilities even after prolonged exposure to high temperatures. Additionally, the fabrication of Cr_2AlC foams using sacrificial template

Open Access Article. Published on 27 August 2024. Downloaded on 11/30/2024 6:12:35 AM.
This article is licensed under a Creative Commons Attribution-NonCommercial 3.0 Unported Licence.

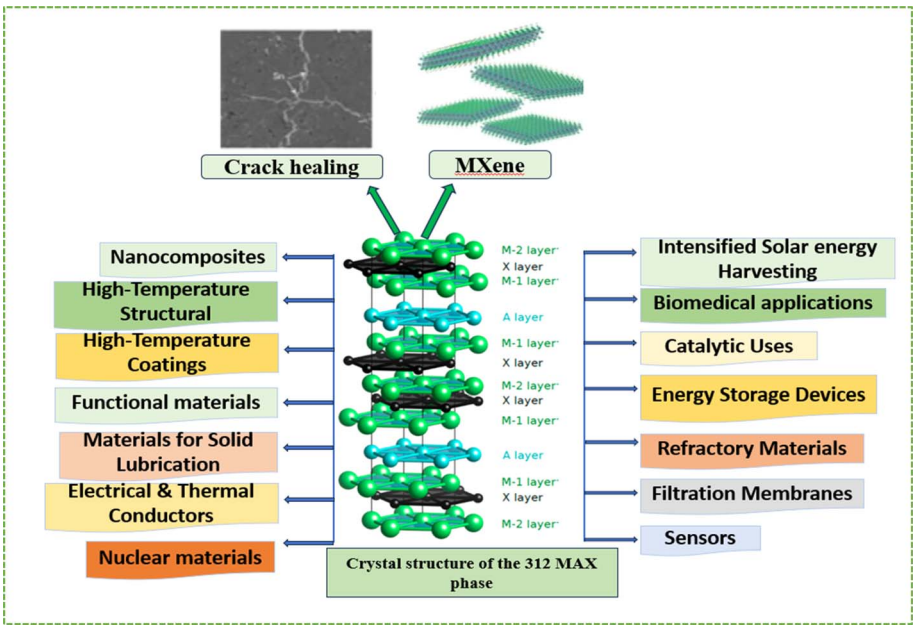

Fig. 13 The overview of multi-applications of MAX-phases.

techniques has demonstrated their potential as robust heat exchangers and catalyst supports, underscoring the versatility and promise of MAX phases in high-temperature applications.[274] These findings collectively emphasize the transformative potential of Al_2O_3 scale-forming MAX phases in driving materials innovation for extreme environments and high-temperature applications.

5.2 High-temperature coatings

In the domain of cutting-edge materials, High-Temperature Coatings (HTCs) applied on MAX phases have emerged as a promising frontier. MAX phases, with their unique combination of metallic and ceramic properties, present a fertile ground for innovative coating technologies. MAX phase coatings have garnered attention as protective layers for refractory alloys and as bond-coat layers within Thermal Barrier Coating (TBC) systems. The Coefficient of Thermal Expansion (CTE) plays a pivotal role in both applications, aiming to mitigate stresses and prevent coating spallation. While Cr_2AlC, with its higher CTE ranging from 12.0 to 13.3 $\times$ 10^{-6} K^{-1}, is deemed more suitable for metallic systems, Ti_2AlC and Ti_3AlC_2 with CTE values between 8.2 and 9.0 $\times$ 10^{-6} K^{-1}, align better with TBC

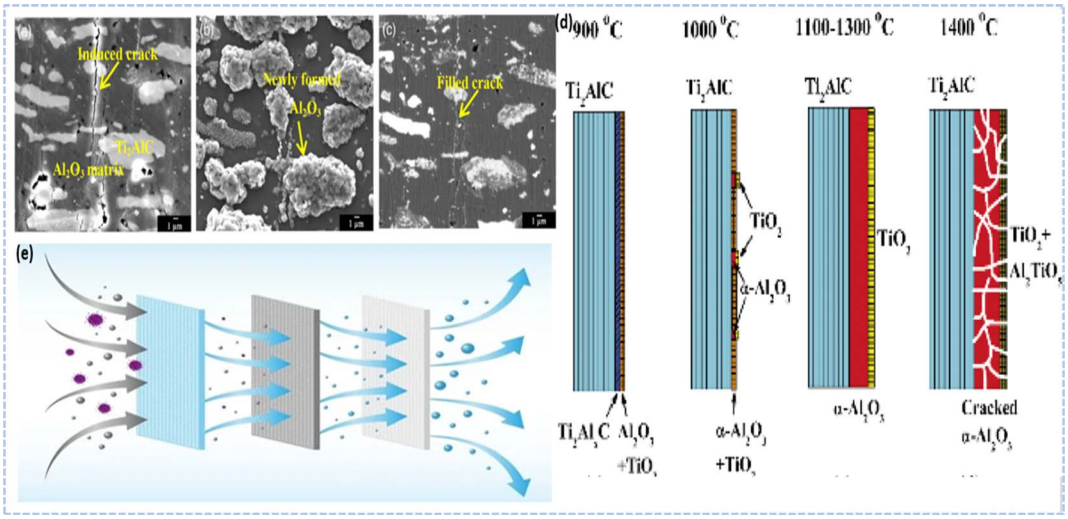

Fig. 14 Examples of MAX phases applications: (a–c) SEM images showcasing Al_2O_3–Ti_2AlC composite before and after 1 hour oxidation at 1000 °C in air. (a) Crack initiation prior to oxidation, (b) post-oxidation with visible cracks, and (c) a polished surface revealing filled cracks. (Reproduced from ref. 271 with permission from John Wiley and Sons, copyright 2018).[271] (d) Schematic illustrating microstructural evolution during Ti_2AlC oxidation. (e) Creating a membrane by combining Ti_2AlN MAX phase with cellulose acetate for the removal of dye, protein, and lead ions. (Reproduced from ref. 272 with permission from Elsevier, copyright 2022).[272]

© 2024 The Author(s). Published by the Royal Society of Chemistry

Open Access Article. Published on 27 August 2024. Downloaded on 11/30/2024 6:12:35 AM.
This article is licensed under a Creative Commons Attribution-NonCommercial 3.0 Unported Licence.

compounds. Notably, advanced turbine disks can be shielded against Type I and II Low Temperature Hot Salt Corrosion (LTHC).[275,276] For instance, Cr_2AlC coatings applied on a low γ' solvus and high refractory content alloy, referred to as LSHR and developed by NASA, effectively prevented hot corrosion pitting and substantially enhanced low cycle fatigue resistance by up to 90%. A novel fabrication technique was employed to produce dense, single-phase Cr_2AlC MAX phase coatings, thereby circumventing columnar structures. These coatings demonstrated exceptional resistance to oxidation, enduring temperatures up to 1100 °C, with the oxidation process manifesting two distinct stages due to the formation of dense Al_2O_3 and $(Cr, Al)_2O_3$ layers shown in Fig. 15.[277] Recent advancements include the deposition of Cr_2AlC bond-coats on Inconel 738 substrates, succeeded by the application of porous yttria-stabilized zirconia as an external TBC. Under conditions akin to a gas turbine environment, the system endured surface and substrate temperatures of 1400 °C and 1050 °C, respectively, albeit failing after 745 cycles, mainly attributed to the open porosity of the Cr_2AlC bond-coat layer, oxidation of secondary phases, and inter-diffusion.[274] Moreover, future endeavors aim to address the challenges in transferring MAX phase coatings as bond-coats, with Ti_2AlC showing promising potential for such applications.

5.3 Filtration membranes

The distinctive layered structure of MAX phases provides a promising framework for developing advanced filtration membranes with superior performance characteristics. These membranes possess the capability to selectively separate molecules based on various attributes such as size, charge, or other properties, rendering them suitable for applications in water purification, gas separation, and industrial processes. The initial phase of the current study involved synthesizing Ti_2AlN MAX phase using the reactive sintering method and subsequently characterizing it shown in Fig. 14e. The hexagonal crystalline structure of the MAX phase was confirmed *via* X-ray diffraction analysis. Incorporating the MAX phase into cellulose acetate membranes enhanced their hydrophilicity and overall performance. An optimal nanocomposite membrane containing 0.75 weight% of MAX phase exhibited a significant three-fold increase in permeability during the filtration of dye solutions and pure water. Furthermore, this optimized membrane demonstrated a remarkable 92.7% improvement in flux recovery ratio, along with high removal efficiencies for various contaminants, including reactive dyes and proteins. The nanocomposite membrane also exhibited substantial rejection rates for common salts like sodium sulfate and sodium chloride, highlighting its potential as an effective membrane material for diverse membrane technology applications.[278]

5.4 Materials for solid lubrication

Exploring the frontier of solid lubricant materials, MAX phases emerge as a promising avenue for enhanced tribological performance. With their unique combination of metallic and ceramic properties, MAX phases offer exceptional resistance to wear and friction, making them ideal candidates for various engineering applications. MAX phases possess remarkable attributes such as high damage tolerance, thermal shock resistance, machinability, and a ductile–brittle transition occurring above 1000 °C, in addition to their layered hexagonal structure. These distinctive characteristics render MAX phases highly promising candidates for solid lubricant materials, with potential applications spanning MAX-based composites, monolithic bulk MAX, and MAX coatings.[15] Among the various MAX phases, Ti_3SiC_2 and Cr_2AlC have garnered significant

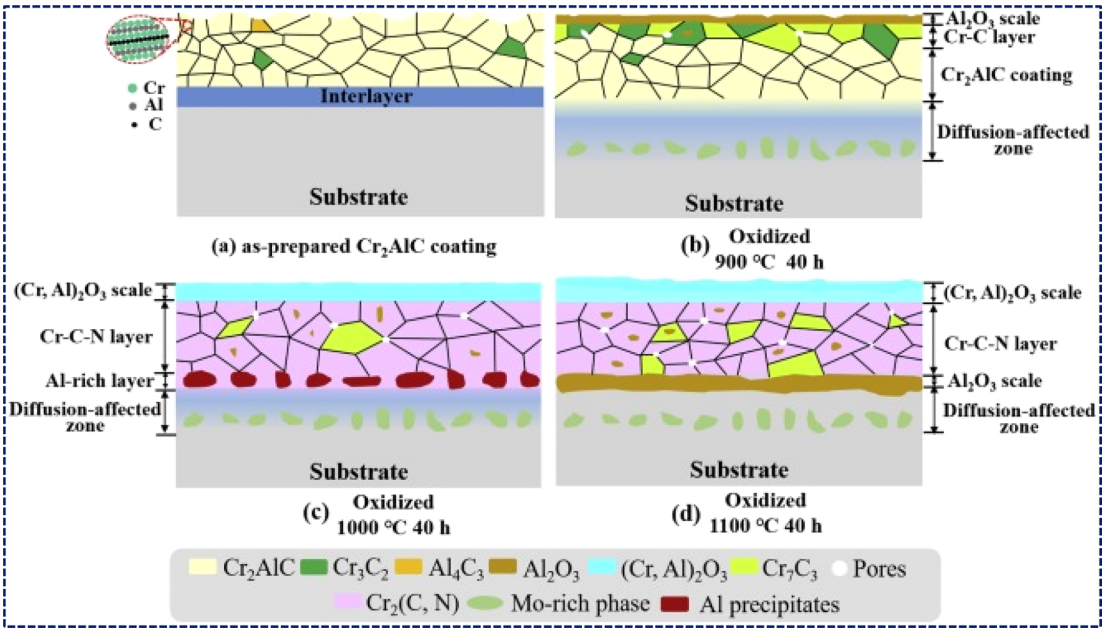

Fig. 15 Oxidation mechanisms of Cr_2AlC MAX phase coatings at 900–1100 °C. (Reproduced from ref. 277 with permission from Elsevier, copyright 2020).[277]

Open Access Article. Published on 27 August 2024. Downloaded on 11/30/2024 6:12:35 AM.
This article is licensed under a Creative Commons Attribution-NonCommercial 3.0 Unported Licence.

attention in research endeavors. For instance, investigations by Shi *et al.* unveiled the pivotal role of Ti_3SiC_2 content in modulating the tribological properties of NiAl matrix, with an optimal Ti_3SiC_2 content of 10 wt% resulting in a composite exhibiting a low friction coefficient of 0.60 and a minimal wear rate of 5.45 $\times 10^{-5}$ mm^3 $(N\ m)^{-1}$, where micro ploughing and delamination were identified as dominant wear mechanisms.[279] Similarly, Shamsipoor *et al.* highlighted the influence of Cr_2AlC purity on wear performance, with a maximum Cr_2AlC phase content of 68.05% showcasing superior wear resistance among all samples. Moreover, the synthesis of a Ti_3SiC_2–$TiSi_2$–TiC composite *via* Spark Plasma Sintering (SPS) demonstrated inherent self-lubricating behavior.[280] Furthermore, the deposition of Ti_2AlC coating onto an Inconel substrate using the cold-spray technique revealed a substantially reduced friction coefficient of 0.603 at 600 °C compared to 0.766 at room temperature, with a corresponding 40% decrease in volume loss at elevated temperatures, underscoring the potential of Ti_2AlC coatings as high-temperature tribological coatings.[281] Insights from Magnus *et al.* elucidated the intrinsic lubricity of Ti_3SiC_2–$TiSi_2$–TiC composites, delineating various wear mechanisms such as graphitization, Tri biofilm spallation, grain pull-out, fracture, and re-graphitization, indicative of the complex interplay of chemical and physical reactions during wear processes.[282] Another study focuses on creating self-lubricating nanocomposite coatings, using Ag-doped Cr_2AlC, exhibiting reduced friction and wear for aerospace and marine applications. Incorporating Ag led to unique structures with enhanced self-lubrication, notably reducing friction below 500 °C and promoting plastic strain accommodation without extensive cracking even at higher temperatures shown in Fig. 16.[283]

5.5 Electrical and thermal conductors

This comprehensive review delves into the captivating domain of MAX phases, examining their distinctive amalgamation of electrical and thermal conductive traits. MAX phases, defined by their stratified crystalline arrangement, showcase compelling attributes in facilitating the flow of both electricity and heat. Their commendable electrical and thermal conductivity renders them apt for diverse applications like electrical connectors and thermal dissipators in electronic apparatuses. The amalgamation of metallic and ceramic attributes in MAX phases enables effective heat dispersion and enhanced electrical functionality.

Ti_3SiC_2 has emerged as a promising candidate for ohmic contacts on 4H–SiC owing to its desirable linear current–voltage characteristics. This material offers the advantage of facile processing through a one-step method involving the sputter-deposition of Ti onto SiC substrates.[284] This innovative approach opens avenues for the direct synthesis of oxygen-barrier capping layers subsequent to the deposition of the primary contact. By circumventing exposure to air, it effectively mitigates risks associated with oxidation, contamination, or the necessity for additional cleaning steps, thereby augmenting the long-term stability of the device. Additionally, Ti_2AlN has garnered attention as an ohmic contact material for GaN-based devices, demonstrating favorable ohmic behavior with a contact resistivity falling within the range of 10^{-4} Ω cm^{-2}.[285]

Beyond electronic applications, MAX phases have been explored for their potential as heat exchangers capable of operating at elevated temperatures (~850 °C), surpassing the capabilities of conventional metallic systems.[286] This niche arises from the fact that ceramics remain the sole alternative for such high-temperature environments. However, the widespread adoption of MAX phases for this purpose has been impeded by inherent limitations, including poor mechanical properties, challenging machinability, low thermal conductivity, and coefficient of thermal expansion (CTE). Despite these drawbacks, MAX phases exhibit a remarkable capacity to withstand high temperatures, reaching up to 1400 °C, coupled with superior thermal shock resistance, mechanical robustness, chemical inertness, and machinability compared to materials like SiC and other advanced ceramics.[287] This research unveils a novel economical method for producing high-purity MAX phases,

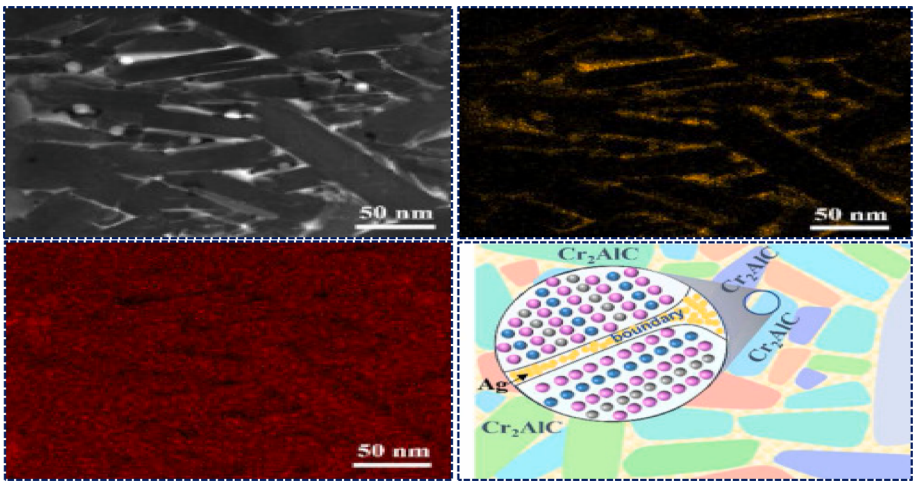

Fig. 16 The cross-sectional images and schematics representation of the Ag doped Cr_2AlC nanocomposite coatings. (Reproduced from ref. 283 with permission from Elsevier, copyright 2024).[283]

© 2024 The Author(s). Published by the Royal Society of Chemistry

Open Access Article. Published on 27 August 2024. Downloaded on 11/30/2024 6:12:35 AM.
This article is licensed under a Creative Commons Attribution-NonCommercial 3.0 Unported Licence.

offering a promising avenue for refining synthesis techniques to yield low-cost, high-conductivity MAX phases in the times ahead. Notably, the Ti_3AlC_2-coated stainless steel 304 exhibits remarkable characteristics, displaying minimal corrosion and interfacial contact resistance. These findings position it as a highly viable option for deployment in simulated Proton Exchange Membrane Fuel Cell (PEMFC) environments, holding significant potential for advancing clean energy technologies shown in Fig. 17.[288,289]

Nevertheless, the primary drawback hindering their broader application remains their intermediate thermal conductivity, typically ranging between 12 and 60 W m^{-1} K^{-1}. While this level of thermal conductivity is deemed acceptable for many applications, it falls short when compared to the thermal conductivity of SiC compounds, which can reach up to 125 W m^{-1} K^{-1}.[287] This thermal disparity underscores a key area for further research and development aimed at enhancing the thermal transport properties of MAX phases, potentially through the exploration of novel synthesis techniques or compositional modifications, to unlock their full potential in high-temperature heat exchange applications and beyond.

5.6 Nuclear materials

MAX phases, a class of materials characterized by a unique combination of metallic and ceramic properties, have emerged as promising candidates for various nuclear applications. Their exceptional thermal and mechanical properties, coupled with good radiation tolerance, make them suitable for reactor structural components, fuel cladding, and even as matrix materials for nuclear waste immobilization. MAX phases including Ti_3SiC_2, Ti_2AlC, Ti_3AlC_2, Cr_2AlC, V_2AlC, Zr_2AlC, Zr_3AlC_2, and Nb_4AlC_3 have attracted considerable attention due to their remarkable radiation tolerance, resistance to oxidation and corrosion, mechanical strength, and chemical stability. These characteristics position them as promising candidates for accident-tolerant fuel (ATF) claddings in third-generation light-water reactors (LWRs) and anticipated fourth-generation fission plants.[290] This Fig. 18 illustrates the stages from MAX-phase formation to MAX-phase tubes, which are utilized in fuel production for nuclear reactors, followed by steps of spent fuel storage, fuel reproduction, and fuel fabrication.[291] Traditional zirconium alloys, historically employed as cladding materials, have raised concerns regarding their performance in scenarios like Loss of Coolant Accidents (LOCAs). In response, MAX phases emerge as an appealing alternative or coating material due to their superior resistance to oxidation and corrosion. Coatings composed of dense, highly pure MAX phases can be applied at low temperatures, safeguarding the integrity of zircaloy substrates.

Moreover, in the realm of Generation IV reactor development, particularly in lead-fast reactor designs, MAX phases demonstrate favorable traits including radiation tolerance, corrosion resistance, mechanical stability, and compatibility with lead alloy coolants. These reactors, utilizing fast neutrons (>1 MeV) for fission reactions, enhance fuel efficiency, facilitating the use of depleted uranium and transmutation of long-lived nuclear waste. The demanding operational conditions of Generation IV reactors necessitate materials capable of

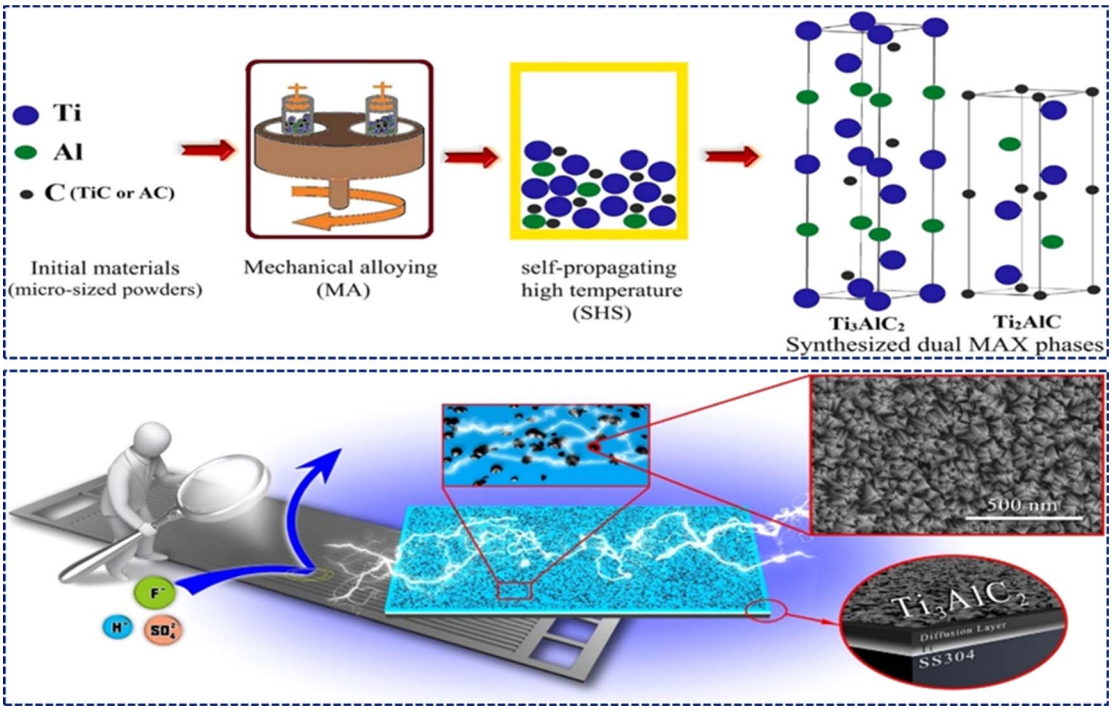

Fig. 17 Schematic representation illustrating the synthesis process of low-cost Ti_3AlC_2–Ti_2AlC dual MAX phase, highlighting the use of economical raw materials and innovative compositions for achieving high-electrical conductivity. (Reproduced from ref. 288 with permission from Elsevier, copyright 2023).[288] (Reproduced from ref. 289 with permission from Elsevier, copyright 2019). [289]

Open Access Article. Published on 27 August 2024. Downloaded on 11/30/2024 6:12:35 AM.
This article is licensed under a Creative Commons Attribution-NonCommercial 3.0 Unported Licence.

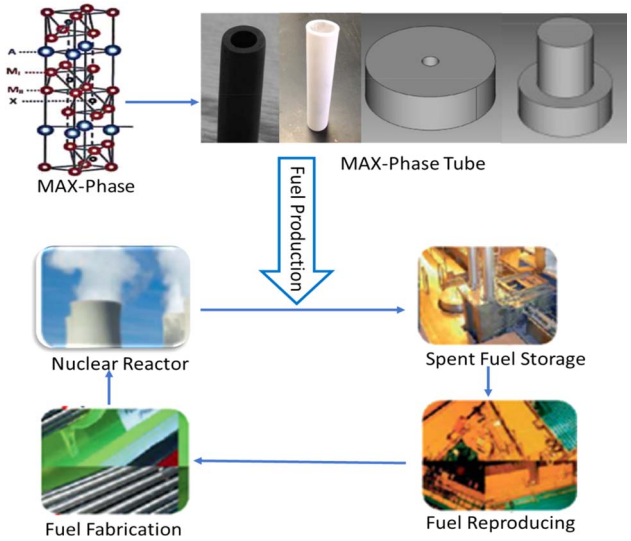

Fig. 18 Schematic representation of the fuel production process using MAX-phase materials. (Reproduced from ref. 291 with permission from Elsevier, copyright 2020).[291]

withstanding prolonged exposure to elevated temperatures, corrosive environments, and high neutron fluences. MAX phases, renowned for their high-temperature capabilities, damage tolerance, and resistance to radiation-induced amorphization, emerge as compelling options for nuclear applications. Extensive research validates the exceptional radiation damage tolerance of MAX phases like Ti_3AlC_2 and Ti_3SiC_2, which display resistance to amorphization up to 25 displacement per atom (dpa), with complete amorphization anticipated only beyond 100 dpa.[292] Additionally, MAX phases exhibit comparably low neutron activation, positioning them as competitive alternatives to conventional materials such as SiC and Alloy 617 to enhance safety and efficiency for next-generation reactor components.[293]

5.7 Intensified solar energy harvesting

MAX phases are highly promising for utilization within Intensified Solar Power (ISP) systems owing to their distinctive blend of thermal robustness, mechanical resilience, and resistance to corrosion. When incorporated into various ISP components like receiver tubes or heat storage materials, MAX phases can endure the extreme temperatures and challenging operational environments encountered during concentrated solar energy capture. Furthermore, their inherent spectral selectivity, as evidenced by reflectance spectra analyses, could bolster the effectiveness of solar energy absorption and thermal regulation within ISP setups. ISP systems facilitate the conversion of solar energy into electricity without emitting greenhouse gases and offer the advantage of thermal energy retention. These systems concentrate solar radiation onto a receiver *via* mirrors, and the resultant heat is conveyed by a heat transfer fluid (HTF) to a steam turbine for electricity generation.[294] Efficiency in energy conversion, typical of thermal processes, improves with higher temperatures and combined cycle configurations. ISP combined cycles ideally operate within the temperature range of 1000–1500 K, with heat transferred by HTFs like air, molten salts, minerals, or synthetic oils. Alternative nonoxide ceramics such as SiC and ZrB_2 have also been proposed for solar receivers due to their elevated degradation thresholds.[295–297] Particularly, porous SiC volumetric receivers have garnered attention due to heightened heat transfer per unit volume coupled with minimal pressure drops.[298] MAX phases demonstrate potential in two distinct sections of CSP systems: the solar receiver and the storage tank. An ideal solar receiver should possess exceptional oxidation resistance, along with attributes like high absorptance in the ultraviolet-visible-near infrared (UV-vis-NIR) spectrum and low thermal emission in the infrared (IR) spectrum.[299] The reflectance spectra of mirror-polished MAX phase samples reveal intrinsic spectral selectivity across the full range of wavelengths measured. While Ti_2AlC and Ti_3AlC_2 exhibit similar infrared spectra, Cr_2AlC displays a slightly lower reflectance and a blue shifted rise front. The corrosion resistance of Ti_3AlC_2 proves inferior, evidenced by significant degradation and complete disintegration after 672 hours of exposure, highlighting its susceptibility to corrosion in solar salt environments. Microscopic analysis suggests the absence of a continuous Al_2O_3 scale, emphasizing the material's vulnerability to corrosion shown in Fig. 19.[300] However, the extent of Ti_2AlC and Cr_2AlC's potential for CSP applications remains insufficiently researched. Despite both MAX phases exhibiting excellent resistance to high concentrated flux, Ti_2AlC displays higher light scattering due to surface oxidation. Their thermal performance varies within the range of 0.56–0.68 and 0.60–0.67, respectively, for the chosen flux levels. In terms of volumetric receivers with open and controlled porosity, MAX phase foams hold promise due to their minimal oxidation and exceptional thermal shock resilience compared to SiC, yet empirical testing remains pending. Moreover, they could serve as structural materials for storage tanks owing to their superb compatibility with molten solar salts. Recent studies by K. Van Loo *et al.* have evaluated the compatibility of various MAX phases, SiC grades, and reference metallic structural materials with a molten salt (40 wt% KNO_3 and 60 wt% $NaNO_3$) for 1000 hours at 600 °C, with Cr_2AlC exhibiting superior corrosion resistance attributable to the formation of a micrometric-thin, protective layer of Cr_7C_3.[301] Despite promising attributes, challenges such as corrosion resistance in solar salt environments remain to be addressed for widespread adoption of MAX phases in CSP applications. Nonetheless, ongoing research and development efforts are poised to unlock the full potential of MAX phases in advancing the sustainability and performance of ISP technology.

5.8 MXene formation building blocks

MAX phases serve as valuable precursors for MXenes, offering a robust platform for tailored material synthesis with diverse functionalities. By selectively etching the 'A' layers from MAX phases, MXenes with tunable surface chemistries and unique structural properties can be obtained. This process preserves the inherent mechanical strength and thermal stability of MAX

© 2024 The Author(s). Published by the Royal Society of Chemistry

Open Access Article. Published on 27 August 2024. Downloaded on 11/30/2024 6:12:35 AM.
This article is licensed under a Creative Commons Attribution-NonCommercial 3.0 Unported Licence.

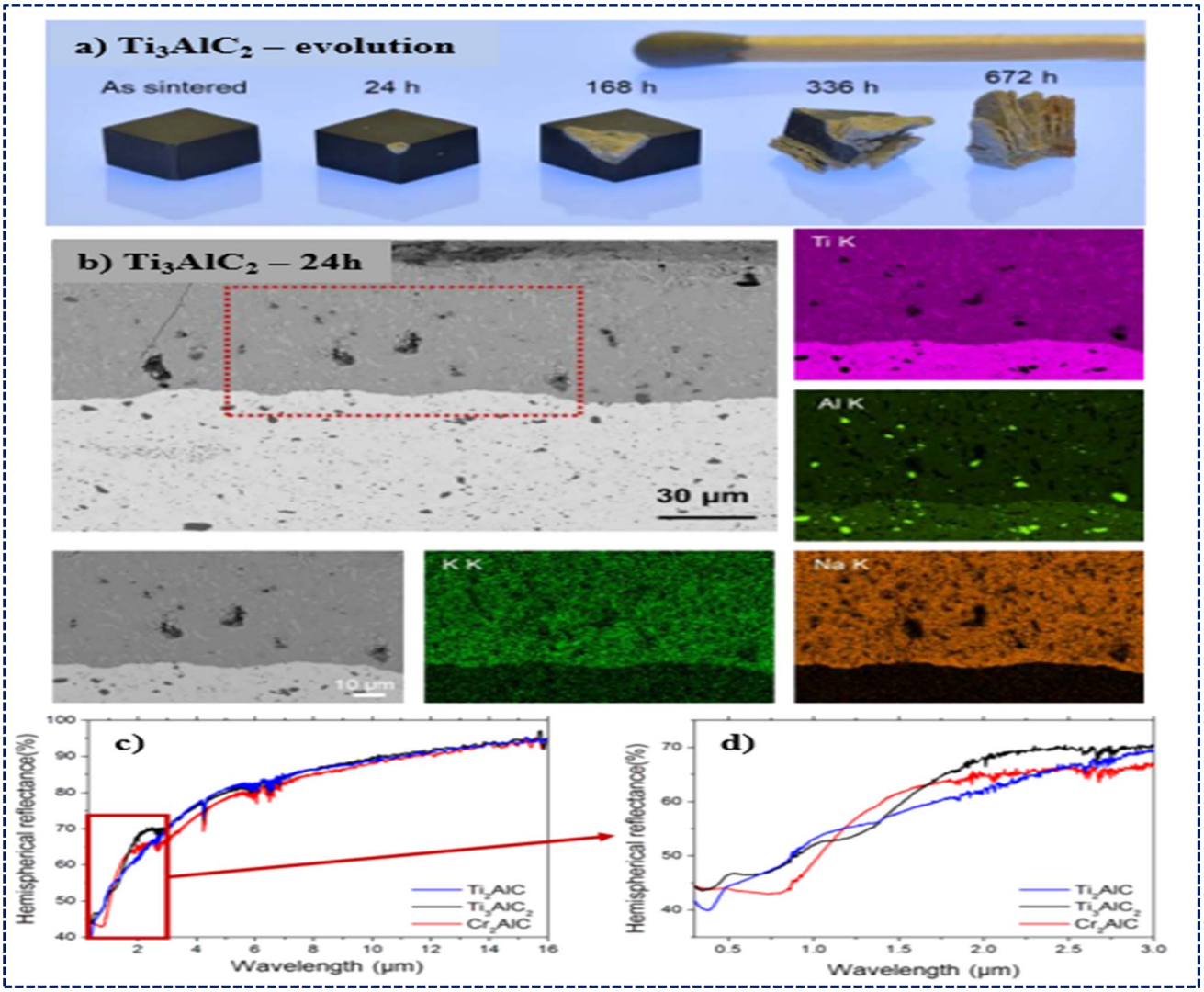

Fig. 19 (a) Images of samples before and after corrosion in solar salt at various intervals: as-sintered, and after 24, 168, 336, and 672 h. (b) Micrograph of corroded sample after 24 h with corresponding EDS elemental maps of the rectangular zone. (c) Hemispherical reflectance spectra of MAX samples in the 0.3–16 μm range, and (d) detail of the solar spectrum range. Reprinted with permission. (Reproduced from ref. 300 with permission from John Wiley and Sons, copyright 2017).[300]

phases while unlocking new opportunities for applications energy storage, hybrid-ion capacitors, Li/Na-ion batteries, water purification, photo- and electrocatalysis, as well as sensors.[302–304] Fig. 20 shown the various processes for MXene synthesis.[305] The advancement in MXene preparation techniques not only forms the foundation for investigating MXene surface terminations but also offers diverse avenues for tailoring MXene performance as functional materials. However, the use of F-containing solutions in MXene synthesis poses hazards, necessitating the exploration of nonhazardous synthesis routes.[282] In a recent breakthrough, Li *et al.* introduced a general Lewis acidic etching method, which circumvents the need for hazardous HF solutions. This method facilitates the etching of MAX phases through direct redox reactions between the A site element and the cation of the Lewis acid molten salt.[306] Consequently, various MXenes can be synthesized from unconventional MAX-phase precursors with A site elements such as Si, Zn, and Ga. A plethora of MXenes have already been synthesized from precursor MAX phases, including Ti_2C, V_2C, $(Ti_{0.5}, Nb_{0.5})_2C$, $(V_{0.5}Cr_{0.5})_3C_2$, Ti_3CN, Nb_4C_3, among others. The development of MAX phases plays a pivotal role in advancing MXene synthesis. For instance, the discovery of the first i-MAX phase $(Mo_{2/3}Sc_{1/3})_2AlC$ led to the synthesis of the first $Mo_{1.33}C$ MXene with ordered metal divacancies, exhibiting exceptional properties such as low resistivity (33.2 $\mu\Omega$ m^1) and high volumetric capacitance (1150 F cm^3).[307] The continual discovery of new MAX phases broadens the scope of potential MXene synthesis, offering prospects for further advancements in materials science. Furthermore, the ability to control the synthesis parameters allows for precise manipulation of MXene properties, such as surface chemistry, interlayer spacing, and electrical conductivity, enabling targeted design for specific applications.

Open Access Article. Published on 27 August 2024. Downloaded on 11/30/2024 6:12:35 AM.
This article is licensed under a Creative Commons Attribution-NonCommercial 3.0 Unported Licence.

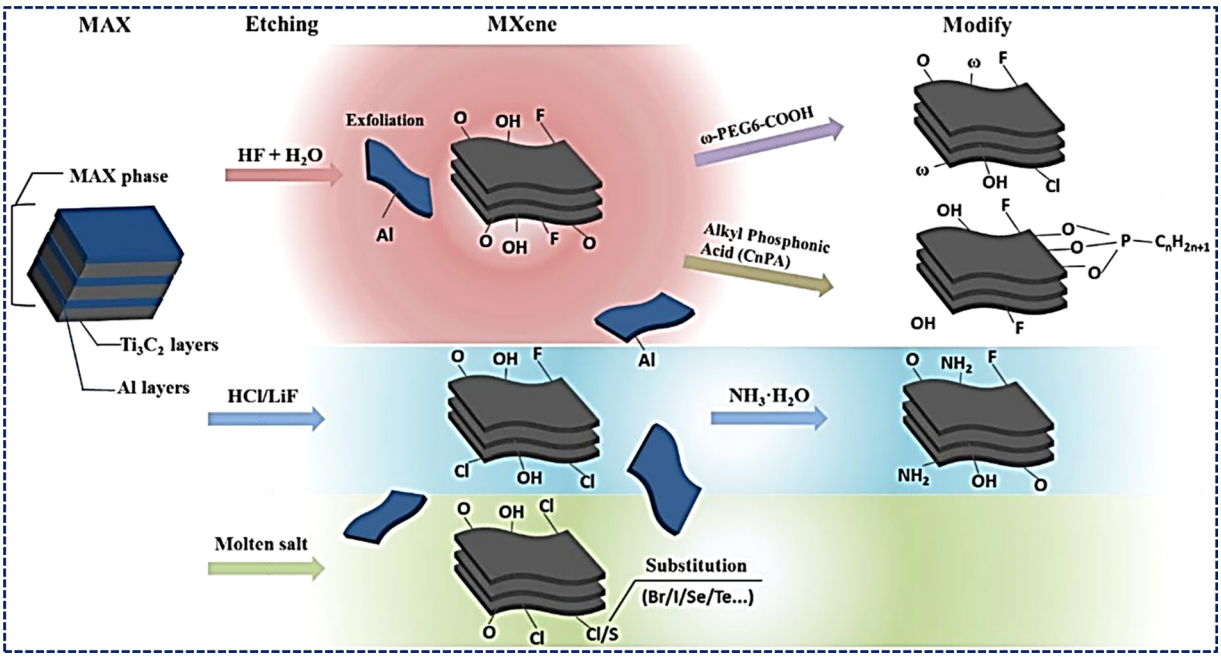

Fig. 20 The prevailing method for producing MXene currently. (Reproduced from ref. 305 with permission from MDPI AG, copyright 2022).[305]

5.9 Catalytic application

MAX phases, a class of ternary compounds with a unique layered structure, have garnered significant attention in recent years for their diverse range of applications, spanning from structural materials to electronic devices. However, their potential as catalysts remains relatively underexplored, despite the vast array of compositions and solid solutions that can occupy the "M", "A", and "X" sites within their crystal lattice. Notably, MAX phases possess the intriguing ability to function both as catalysts and supports in various catalytic processes. Types of MAX phases used in catalytic degradation reactions and processes based on C–H and C–O activation is shown in Fig. 21. For instance, research has demonstrated the effectiveness of Cr_2AlC powders as solid catalysts in catalytic wet peroxide oxidation (CWPO) processes aimed at reducing the formation of carbon monoxide (CO).[309] In such applications, the presence of Cr_2AlC significantly mitigates CO concentrations, with remarkable reductions observed compared to conventional activated carbon-Fe catalysts. Ti_3AlC_2, another prominent member of the MAX phase family, has exhibited promising capabilities in enhancing the reversible hydrogen storage properties of MgH_2 and facilitating the oxidative dehydrogenation of *n*-butane.[310,311] Moreover, Ti_3SiC_2, Ti_2AlC, and Ti_3AlC_2 have shown excellent chemo selectivity, boasting 100% selectivity for the hydrogenation of organic compounds even at low palladium content. Leveraging MAX phases as catalyst substrates further enhances their utility, as demonstrated by the coating of reticulated porous Ti_3AlC_2 with nanocrystalline CeO_2 for gas exhaust devices.[312,313] This innovation holds particular significance in addressing the challenge of hydrocarbon emissions during the cold start of modern car engines, where catalyst activity remains low. Preliminary electric heating of the system presents a potential solution, albeit with limitations on the use of conventional ceramic foams. MAX phases offer a compelling alternative in this regard due to their favorable electrical conductivity, thermal stability, and exceptional mechanical strength. The integration of MAX phases into catalytic systems not only promises enhanced performance but also underscores the versatility and untapped potential of these intriguing materials across diverse scientific and industrial domains. As research continues to unravel the myriad capabilities of MAX phases, their role as catalysts is poised to expand, driving innovation and advancement in catalysis-driven processes and technologies.

5.10 Biomedical applications

MAX phases, a family of layered ceramics, are increasingly garnering attention for their potential in biomedical applications. Their remarkable properties, including biocompatibility and osteo-conductivity, position them as promising contenders for biomedical implants and bone tissue engineering scaffolds. Unlike conventional metallic and ceramic biomaterials, MAX phases boast a distinctive combination of attributes, notably corrosion resistance, wear resistance, and biocompatibility, making them particularly suitable for biomedical purposes. Their inherent ability to integrate seamlessly with biological systems offers a pathway for enhanced healing and improved performance in various medical contexts.

For instance, the biocompatibility of MAX phases has been extensively studied, revealing minimal cytotoxicity and favorable cell adhesion properties, both of which are crucial for promoting tissue integration.[314] Similarly, investigations into the corrosion resistance of MAX phases under physiological conditions have underscored its importance in ensuring the

© 2024 The Author(s). Published by the Royal Society of Chemistry

Open Access Article. Published on 27 August 2024. Downloaded on 11/30/2024 6:12:35 AM.
This article is licensed under a Creative Commons Attribution-NonCommercial 3.0 Unported Licence.

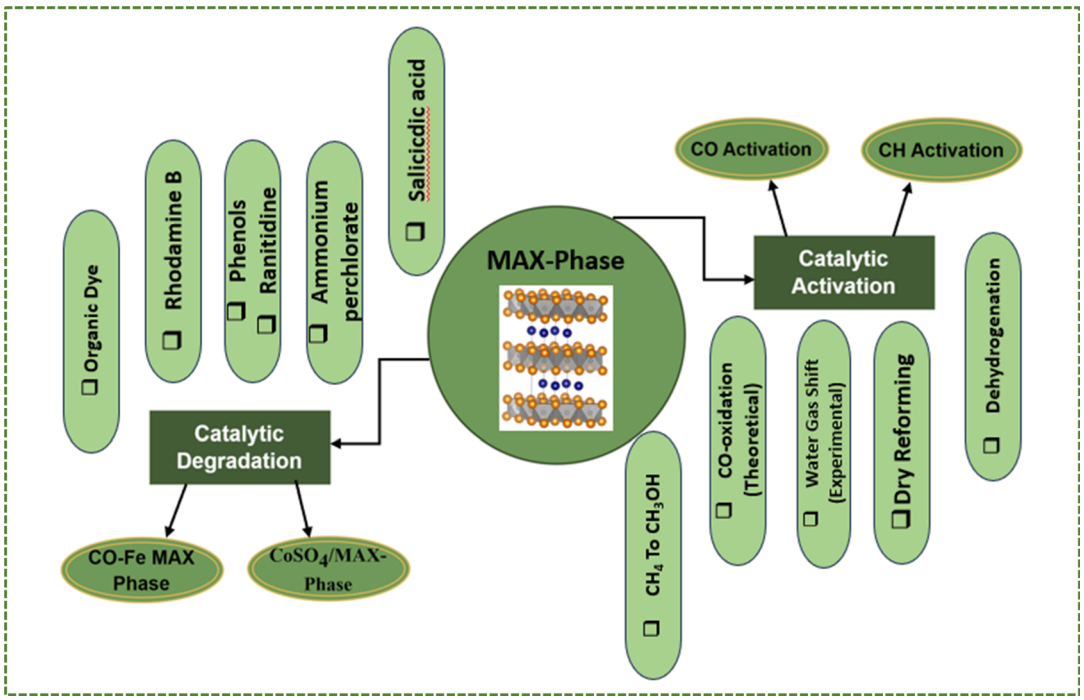

Fig. 21 Types of MAX phases used in catalytic degradation reactions and processes based on C–H and C–O activation. (Reproduced from ref. 308 with permission from The Royal society of Chemistry, copyright 2021).[308]

longevity and reliability of implants within the human body.[315] Furthermore, MAX phases exhibit an exceptional capacity to withstand harsh physiological environments, ensuring prolonged functionality and reduced risk of degradation within the human body. This robustness is essential for the longevity and effectiveness of implants, as they must endure the rigors of daily life while promoting tissue regeneration.[316] Moreover, MAX phases possess tailored mechanical properties that closely mimic those of natural bone, facilitating optimal load-bearing capabilities and minimizing the risk of implant failure. This similarity to bone structure not only enhances the compatibility of MAX phase implants but also promotes osseointegration, the process by which bone grows around the implant, ensuring long-term stability and functionality.[317] Additionally, the tunable nature of MAX phases allows for customization according to specific application requirements, offering versatility in design and performance. This adaptability opens avenues for the development of personalized biomedical implants tailored to individual patient needs, ultimately improving treatment outcomes and patient satisfaction. Furthermore, the use of MAX phases in bone tissue engineering scaffolds presents an innovative approach to regenerative medicine. By providing a supportive framework for cell growth and tissue regeneration, MAX phase scaffolds facilitate the repair of damaged or diseased bone tissue, offering a viable solution for conditions such as fractures, defects, and degenerative bone diseases.[318,319] Their porous structure and interconnected pore network enable efficient nutrient exchange and cell infiltration, fostering a conducive environment for tissue regeneration and integration. Moreover, MAX phase scaffolds can be engineered to degrade gradually over time, allowing for seamless replacement by newly formed bone tissue without the need for additional surgical interventions.[320] This biodegradability feature eliminates the risk of long-term implant retention and alleviates concerns associated with implant removal, offering a more patient-friendly approach to bone regeneration shown in Fig. 22. Overall, the biomedical applications of MAX phases hold tremendous promise for advancing the field of orthopedics and regenerative medicine, offering innovative solutions for improving patient outcomes and quality of life.[322] With ongoing research and development efforts, MAX phases are poised to play a pivotal role in shaping the future of biomedical implant technology and tissue engineering strategies.

5.11 Energy storage devices

MAX phases exhibit excellent electronic and ionic conductivity, owing to their metallic nature and inherent crystal structure. This combination of properties renders MAX phases highly promising candidates for next-generation battery technologies. One of the most compelling features of MAX phases is their ability to maintain structural integrity even after undergoing multiple intercalations and deintercalation cycles, a crucial requirement for long-term battery performance and durability. Additionally, their inherent stability against chemical and mechanical degradation further enhances their suitability for energy storage applications. Researchers are actively exploring the incorporation of MAX phases into electrode materials for lithium-ion batteries to exploit their exceptional ion accommodation capabilities and conductivity. By leveraging these

Open Access Article. Published on 27 August 2024. Downloaded on 11/30/2024 6:12:35 AM.
This article is licensed under a Creative Commons Attribution-NonCommercial 3.0 Unported Licence.

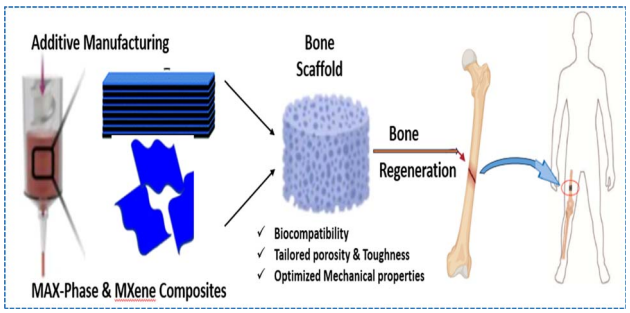

Fig. 22 Bio-medical applications for bone regeneration by MAX-phase composites. (Reproduced from ref. 321 with permission from Elsevier, copyright 2023).[321]

unique properties, MAX phases hold the potential to significantly enhance the energy storage capacity, efficiency, and lifespan of lithium-ion batteries, paving the way for the development of high-performance energy storage systems for diverse applications ranging from portable electronics to electric vehicles and grid-level energy storage.[323,324] Furthermore, the versatility of MAX phases extends beyond lithium-ion batteries, with investigations underway to explore their applicability in other types of energy storage devices such as supercapacitors and solid-state batteries.[325] Through continued research and development efforts, MAX phases are poised to play a pivotal role in advancing the landscape of energy storage technologies, driving innovation and sustainability in the quest for cleaner and more efficient energy solutions. MXene is developed from the MAX phase, which is being used as an energy-storing material, as shown in Fig. 23.

5.12 Refractory materials

MAX phases, characterized by their remarkable combination of high melting points and exceptional thermal stability, have emerged as valuable constituents in the fabrication of refractory materials tailored for demanding applications in high-temperature environments. Refractory materials play a critical role in industries where extreme heat conditions are prevalent, such as metallurgy, ceramics, and glass manufacturing. MAX phases, with their inherent resistance to thermal degradation and mechanical stress, offer a compelling solution to the challenges posed by such harsh operating conditions. These materials are adept at withstanding temperatures well above those tolerated by conventional refractory materials, making them ideal candidates for lining furnaces, crucibles, and other high-temperature equipment. MAX phases exhibit robust mechanical properties even at elevated temperatures, ensuring structural integrity and longevity in demanding industrial settings. Their ability to endure thermal cycling without undergoing significant degradation further enhances their suitability for refractory applications. Moreover, MAX phases demonstrate excellent resistance to chemical corrosion, a crucial attribute in environments where exposure to reactive substances is common. This resistance allows MAX phase-based refractory materials to maintain their performance and integrity over extended periods, minimizing downtime and maintenance costs.

Several studies in the literature underscore the suitability and advantages of MAX phase-based refractory materials for high-temperature applications. For example, research by Smith *et al.* highlighted the superior thermal stability of MAX phases compared to traditional refractory materials, showcasing their potential for enhancing furnace performance and prolonging service life.[326] Similarly, investigations by Johnson and colleagues elucidated the exceptional mechanical properties of MAX phase-based refractories, emphasizing their ability to withstand mechanical stresses under extreme heat conditions, thus reducing the risk of failure and downtime in industrial operations.[327]

Furthermore, the versatility of MAX phases enables the engineering of refractory materials with tailored properties to meet specific application requirements, including enhanced thermal conductivity, thermal shock resistance, and erosion resistance. As such, MAX phase-based refractory materials represent a promising avenue for improving the efficiency, reliability, and safety of high-temperature processes across various industries. Continued research and development efforts in this field are expected to unlock further potential in leveraging MAX phases to advance the performance and functionality of refractory materials, driving innovation and sustainability in high-temperature applications.

5.13 Sensor

The electrical and thermal properties of MAX phases make them promising materials for various sensor applications. Their

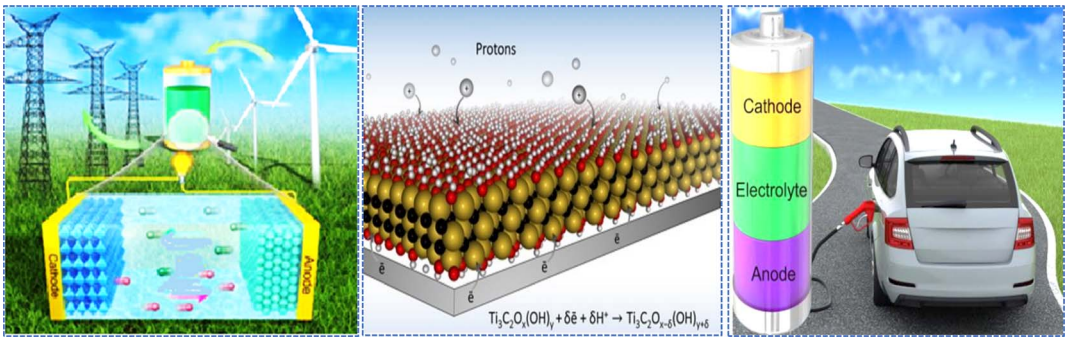

Fig. 23 Various energy storing application using MAX phases derivatives (MXene).

© 2024 The Author(s). Published by the Royal Society of Chemistry

Open Access Article. Published on 27 August 2024. Downloaded on 11/30/2024 6:12:35 AM.
This article is licensed under a Creative Commons Attribution-NonCommercial 3.0 Unported Licence.

ability to detect changes in temperature, pressure, strain, and gas concentrations can be utilized in sensors for industrial monitoring, environmental sensing, and healthcare diagnostics. The electrical and thermal properties inherent in MAX phases render them highly promising materials for a wide array of sensor applications. MAX phases exhibit intriguing electrical conductivity, which can range from metallic to semi-conducting behavior, depending on the specific composition and environmental conditions. This tunable conductivity makes them suitable for applications where precise electrical sensing is required, such as in strain sensors, temperature sensors, and gas sensors. Additionally, MAX phases possess excellent thermal stability and high thermal conductivity, attributes that are advantageous for sensing applications involving temperature monitoring and thermal imaging. Their ability to withstand extreme temperatures while maintaining structural integrity ensures reliable and accurate sensor performance even in harsh environments. This Fig. 24 illustrates the process of combining MAX-phases with a GCE to create a MAX-phase@GCE composite, which is then applied to improve the functionality of the resulting material as a sensor.[328]

Overall, the unique combination of electrical and thermal properties in MAX phases positions them as promising candidates for next-generation sensor technologies across various fields, including aerospace, automotive, healthcare, and environmental monitoring.

A straightforward and environmentally friendly approach was utilized to successfully create a $Ti_3Al_{0.5}Cu_{0.5}C_2$ MAX phase structure, leading to the development of a $Ti_3Al_{0.5}Cu_{0.5}C_2$-based glassy carbon electrode (GCE). Under optimized conditions, the $Ti_3Al_{0.5}Cu_{0.5}C_2$-based sensor showed good linearity within the range of 0.02–50.00 μmol L^{-1} for rutin analysis, achieving a low limit of detection (LOD) of 0.015 μmol L^{-1}. Moreover, the fabricated $Ti_3Al_{0.5}Cu_{0.5}C_2$ MAX phase was effectively utilized for the detection of trace levels of rutin in mandarin and kiwi samples, with validation conducted through high-performance liquid chromatography (HPLC), thus underscoring its potential for precise electrochemical analysis of small molecules in agricultural applications.[329]

5.14 Advanced nanocomposites

MAX phases are a versatile class of nanomaterials renowned for their unique blend of metallic and ceramic properties, making them highly coveted for applications in nanocomposites. Incorporating MAX phases into nanocomposites serves as a formidable reinforcement strategy, enhancing mechanical properties such as strength, stiffness, and fracture toughness. This is particularly advantageous for crafting lightweight yet resilient materials suited for structural needs across diverse industries. Furthermore, harnessing the exceptional thermal conductivity of MAX phases enables the engineering of nanocomposites with superior heat dissipation capabilities, crucial for applications where efficient thermal management is paramount, such as in electronics, aerospace, and automotive sectors. Moreover, the innate resistance to corrosion exhibited by MAX phases positions them as prime candidates for augmenting the durability of nanocomposite coatings, shielding substrates from degradation in harsh environments. Additionally, the distinctive combination of metallic and ceramic traits in MAX phases facilitates the development of nanocomposites with tailored electrical and electromagnetic properties, driving advancements in electronics, telecommunications, and sensor technologies.

Recent years have witnessed MAX phases emerging as focal points in global materials research, captivating scientists with their extraordinary properties. The surge in publications on MAX phases underscores the growing interest in these nanolaminate materials, which promise a plethora of applications. This comprehensive review aims to deepen our understanding of MAX phases while highlighting recent progress and developments in the field. Covering aspects from chemical composition to microstructure, including newly-discovered structural variants, the review provides insights into synthesis methods and explores the chemical and physical properties of MAX phases. Moreover, it surveys potential applications across diverse fields such as high-temperature and nuclear materials, as well as their role as precursors for producing 2D materials like MXenes.[330] Despite challenges in controlling MAX phase morphology at the nanoscale, recent advancements have led to the fabrication of nanostructured MAX phases, opening doors to exciting opportunities. For instance, the synthesis of nanostructured Ti–Al–C MAX phases has facilitated the production of nanosized multilayered MXenes with enhanced electrochemical properties, paving the way for advancements in energy storage technologies. Furthermore, the synergistic combination of MAX phases with other materials, as seen in nanocomposites, has resulted in improved thermal and mechanical properties, demonstrating their potential in various engineering applications.[331] This Fig. 25 shows the transformation of MAX-phase materials into various forms of advanced nanocomposites, including nanofibers, nanofillers, and nanoflakes. Moving forward, continued exploration of PANI-MAX phase nanocomposites presents avenues for novel applications, particularly in the realms of photocatalysis and solar energy. As

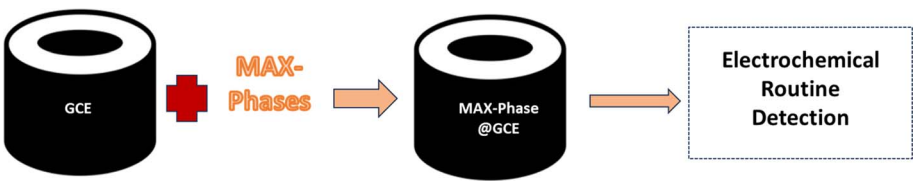

Fig. 24 Schematic of MAX-phase integration with Glassy Carbon Electrode (GCE) for enhanced performance as a sensor. (Reproduced from ref. 328 with permission from Elsevier, copyright 2022).[328]

Open Access Article. Published on 27 August 2024. Downloaded on 11/30/2024 6:12:35 AM.
This article is licensed under a Creative Commons Attribution-NonCommercial 3.0 Unported Licence.

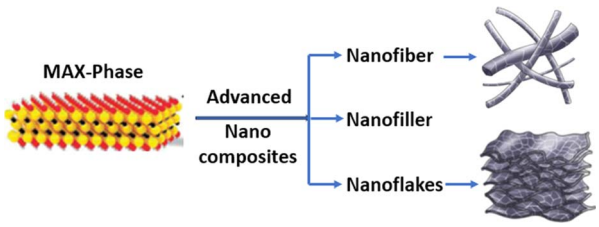

Fig. 25 Formation of advanced nanocomposites from MAX-phase materials.

research progresses, the integration of MAX phases into nanocomposites promises to drive innovation in materials science and engineering, ushering in a new era of advanced materials with tailored properties and functionalities.[332]

5.15 Functional materials

MAX phases, renowned for their diverse array of physical and chemical properties, have attracted attention as functional materials. Wang *et al.*[333] investigated the utilization of Ti_3AlC_2 as a catalyst to enhance the reversible hydrogen storage capabilities of MgH_2. The addition of 7 wt% Ti_3AlC_2 into MgH_2 significantly decreased the dehydrogenation onset temperature by 70 °C compared to pristine MgH_2, with a notable reduction in the apparent activation energy of the composite. The catalytic effectiveness of Ti_3AlC_2 was attributed to its capability to integrate hydrogen atoms into the interstitial sites of its Ti–Al layers.[334] Sun *et al.*[335] fabricated reticulated porous Ti_3AlC_2 for use as support material in gas exhaust catalyst devices, leveraging its attributes such as thermal stability, mechanical strength, erosion resistance, low heat capacity, thermal shock resistance, and electronic conductivity, thus enabling its application in electrically heated catalysts. Furthermore, Fashandi *et al.*[336] synthesized thin films of Ti_3AuC_2 and Ti_3IrC_2, which formed stable ohmic electrical contacts to SiC even after prolonged exposure to high temperatures in air. These MAX phases containing noble metals exhibit potential for stable electrical contacts in high-temperature power electronics or gas sensors. This Fig. 26 demonstrates the combination of MAX-phase materials, highlighting their use as functional materials to improve performance.

6. Summary and outlook

Recent advancements in MAX phase materials have significantly expanded our understanding of their complex structures, unique properties, and diverse applications. Through innovative synthesis techniques and precise control of composition and microstructure, researchers have unlocked new possibilities for tailoring MAX phase properties to meet the demands of various industries. MAX phases, characterized by their metallic conductivity, ceramic-like hardness, and polymer-like machinability, offer exceptional performance in high-temperature environments, corrosive conditions, and demanding mechanical applications. These materials exhibit remarkable stability, strength, and resistance to degradation, positioning them as key contenders for a wide range of applications, including aerospace, energy storage, electronics, and beyond. Looking ahead, the future of MAX phase materials appears promising, with continued research and development poised to unlock even greater potential for innovation and application. Emerging techniques such as additive manufacturing and nanoscale engineering offer new avenues for fine-tuning MAX phase properties and exploring novel applications in fields such as catalysis, biomedicine, and environmental remediation. Additionally, collaborative efforts between academia, industry, and government agencies will be crucial for advancing fundamental understanding, scaling up production, and accelerating the commercialization of MAX phase materials. By addressing remaining challenges such as processing scalability, cost-effectiveness, and environmental sustainability, MAX phase materials have the potential to revolutionize various industries and pave the way for the development of next-generation materials with unprecedented performance and functionality.

This review has provided a comprehensive review of MAX phases in terms of chemical compositions, microstructures, synthesis methods, properties, and novel applications. Tremendous progress on MAX phases has been made in terms of discovering more MAX phases, characterizing their microstructures and properties, and exploring their potential applications. Future directions for MAX phases include the ongoing search for new MAX phases, the need for thorough experimental investigations into their microstructures and properties, the

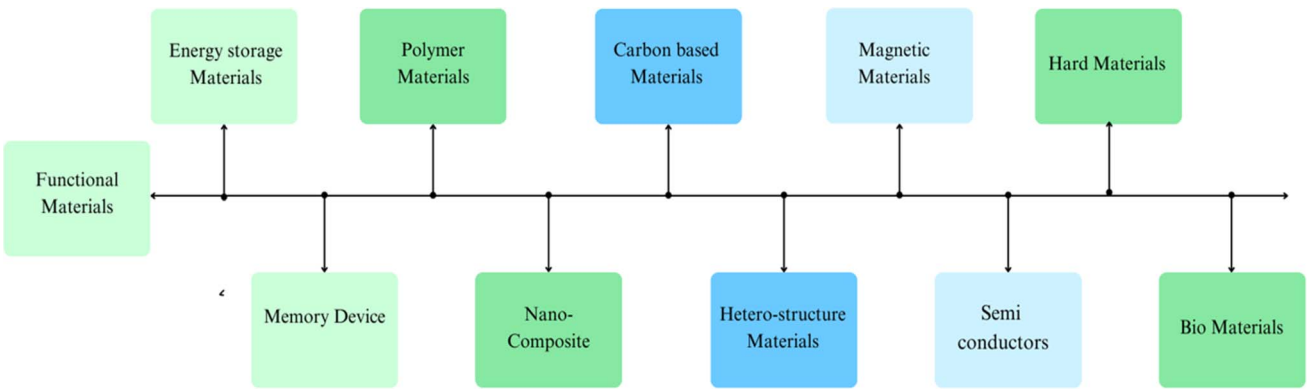

Fig. 26 Application of MAX-phase materials as functional materials.

© 2024 The Author(s). Published by the Royal Society of Chemistry

Open Access Article. Published on 27 August 2024. Downloaded on 11/30/2024 6:12:35 AM.
This article is licensed under a Creative Commons Attribution-NonCommercial 3.0 Unported Licence.

improvement of synthesis methods to achieve higher purity, and the characterization of a wide range of chemical and physical properties of newly developed MAX phases. Additionally, there is vast potential for the development of MAX phases as functional materials. The field continues to see rapid growth, with an increasing number of synthesized MAX phases reported each year, exemplifying a true revitalization of the field. Phase stability calculations are also proving useful for predicting new MAX phases for future syntheses, further advancing the field and opening up new opportunities for research and development. Recently, the progress of the new MAX phase synthesis has dramatically increased from earlier. Until now, researchers have discovered about 342 MAX phases, with the majority occurring after 2018. Challenges in MAX phase materials include intricate structural complexities, limited understanding of property correlations, and scalability hurdles for novel applications. Potential solutions involve advanced characterization techniques for structural elucidation, comprehensive property modeling frameworks, and innovative synthesis strategies optimized for industrial scalability. Integration of multidisciplinary approaches, collaboration between academia and industry, and continual research investment are vital for overcoming these challenges and unlocking the full potential of MAX phase Materials.

7. Future directions

Future directions in MAX phase materials study encompass exploring new synthesis routes to tailor properties, elucidating atomic-scale structural dynamics, integrating computational modeling for predictive design, advancing multi-functional applications, and enhancing sustainability through eco-friendly manufacturing processes. These efforts aim to unlock the full potential of MAX phase materials, which are known for their unique combination of metallic and ceramic properties, including high-temperature stability, electrical conductivity, and resistance to oxidation and corrosion.

Exploring new synthesis routes is essential for fine-tuning the properties of MAX phase materials to meet specific application requirements. Researchers are investigating various chemical and physical processes to develop more efficient and scalable methods for producing these materials. Understanding atomic-scale structural dynamics is crucial for optimizing performance. Advanced techniques like high-resolution electron microscopy and spectroscopy are employed to observe and manipulate the atomic arrangements and bonding characteristics within MAX phase materials.

The integration of computational modeling plays a pivotal role in the predictive design of MAX phase materials. By leveraging machine learning algorithms and high-throughput computational methods, scientists can simulate and predict the behavior of these materials under different conditions, thus accelerating the discovery of new compositions with desirable properties.

Advancing multi-functional applications is another significant focus area. MAX phase materials hold promise for a wide range of industries, including aerospace, energy, and electronics, due to their exceptional properties. Researchers are developing innovative ways to utilize these materials in various applications, such as thermal protection systems, electrical contacts, and energy storage devices.

Enhancing sustainability through eco-friendly manufacturing processes is a critical objective. Developing green synthesis methods and recycling strategies will reduce the environmental impact of producing and using MAX phase materials. Collaborative efforts between materials scientists, engineers, and industry partners are vital for driving innovation and ensuring the successful commercialization of next-generation MAX phase materials.

Emphasis on scalability, cost-effectiveness, and commercial viability will facilitate the widespread adoption of MAX phase materials in critical sectors. Continuous refinement of processing techniques and characterization methods will enable precise control over material properties, leading to breakthroughs in performance and functionality. Ultimately, pursuing these directions will expand the fundamental understanding of MAX phase materials and accelerate their transition from the laboratory to real-world applications.

Data availability

No primary research results, software or code have been included, and no new data were generated or analyzed as part of this review. All information cited within this review is derived from existing literature and publicly available sources.

Conflicts of interest

There are no conflicts to declare.

Acknowledgements

The authors would like to thank Department of Mechanical Engineering, Dhaka University of Engineering and Technology, Bangladesh and Bangladesh Army University of Engineering and Technology for providing all kinds of supports to conduct this research.

References

1 S. Venkateshalu and A. N. Grace, MXenes—A new class of 2D layered materials: Synthesis, properties, applications as supercapacitor electrode and beyond, *Appl. Mater. Today*, 2020, **18**, 100509.
2 C. Zhao, Y. Zhang, K. Nie, L. Yi, B. Li, Y. Yuan and Z. Liu, Recent advances in design and engineering of MXene-based heterostructures for sustainable energy conversion, *Appl. Mater. Today*, 2023, **32**, 101841.
3 A. G. Aleksanyan, S. K. Dolukhanyan, D. G. Mayilyan, G. N. Muradyan, O. P. Ter-Galstyan and N. L. Mnatsakanyan, Formation of Ti_2AlN_x MAX phase by "Hydride Cycle" and SHS methods, *Ceram. Int.*, 2023, **49**, 24229–24234.

Open Access Article. Published on 27 August 2024. Downloaded on 11/30/2024 6:12:35 AM.
This article is licensed under a Creative Commons Attribution-NonCommercial 3.0 Unported Licence.

4 S. Alam, M. A. Chowdhury, A. Shahid, R. Alam and A. Rahim, Synthesis of emerging two-dimensional (2D) materials–Advances, challenges and prospects, *FlatChem*, 2021, **30**, 100305.
5 M. W. Barsoum, The $M_{N+1}AX_N$ phases: A new class of solids: Thermodynamically stable nanolaminates, *Prog. Solid State Chem.*, 2000, **28**, 201–281.
6 D. Y. Kovalev, M. A. Luginina and A. E. Sytschev, Reaction synthesis of the Ti_2AlN MAX-phase, *Russ. J. Non-Ferrous Metals*, 2017, **58**, 303–307.
7 W. Jeitschko, H. Nowotny and F. Benesovsky, Ti_2AlN, eine stickstoffhaltige H-Phase, *Monatsh. Chem.*, 1963, **94**, 1198–1200.
8 H. Rohde and H. Kudielka, Strukturuntersuchungen an carbosulfiden von titan und zircon, *Z. Kristallogr.–Cryst. Mater.*, 1960, **114**, 447–456.
9 W. Jeitschko and H. Nowotny, Die kristallstruktur von Ti_3SiC_2—Ein neuer komplexcarbid-typ, *Monatsh. Chem.*, 1967, **98**, 329–337.
10 H. Wolfsgruber, H. Nowotny and F. Benesovsky, Die Kristallstruktur von Ti_3GeC_2: Kurze Mitteilung, *Monatsh. Chem.*, 1967, **98**, 2403–2405.
11 M. Dahlqvist, M. W. Barsoum and J. Rosen, MAX phases–Past, present, and future, *Mater. Today*, 2024, **72**, 1–24.
12 K. J. Baumler, O. S. Adamsa and R. E. Schaak, One-step topochemical transformation of MoAlB into metastable Mo_2AlB_2 using a metal chloride salt reaction, *Chem. Commun.*, 2023, **59**, 4814–4817.
13 M. W. Barsoum and T. El-Raghy, Synthesis and Characterization of a Remarkable Ceramic: Ti_3SiC_2, *J. Am. Ceram. Soc.*, 1996, **79**, 1953–1956.
14 M. Radovic and M. W. Barsoum, MAX phases: Bridging the gap between metals and ceramics, *Am. Ceram. Soc. Bull.*, 2013, **92**, 20–27.
15 M. Sokol, V. Natu, S. Kota and M. W. Barsoum, On the chemical diversity of the MAX phases, *Trends Chem.*, 2019, **1**, 210–223.
16 H. Shao, S. Luo, A. D. Mandine, K. Ge, Z. Lin, P. L. Taberna, Y. Gogotsi and P. Simon, Synthesis of MAX Phase Nanofibers and Nanoflakes and the Resulting MXenes, *Adv. Sci.*, 2023, **10**, 2205509.
17 M. A. Hadi, U. Monira, A. Chroneos, S. H. Naqib, A. K. M. A. Islam, N. Kelaidis and R. V. Vovk, Phase stability and physical properties of $(Zr_{1-x}Nb_x)_2AlC$ MAX phases, *J. Phys. Chem. Solids*, 2019, **132**, 38–47.
18 H. Fashandi, M. Dahlqvist, J. Lu, J. Palisaitis, S. I. Simak, I. A. Abrikosov, J. Rosen, L. Hultman, M. Andersson, A. L. loyd Spetz and P. Eklund, Synthesis of Ti_3AuC_2, $Ti_3Au_2C_2$ and Ti_3IrC_2 by noble metal substitution reaction in Ti_3SiC_2 for high-temperature-stable ohmic contacts to SiC, *Nat. Mater.*, 2017, **16**, 814–818.
19 J. Wang and Y. Zhou, Recent Progress in Theoretical Prediction, Preparation, and Characterization of Layered Ternary Transition-Metal Carbides, *Annu. Rev. Mater. Res.*, 2009, **9**, 415–443.
20 Z. Zhang, X. Duan, D. Jia, Y. Zhou and S. van der Zwaag, On the formation mechanisms and properties of MAX phases: A review, *J. Eur. Ceram.*, 2021, **41**, 3851–3878.
21 M. A. Pietzka and J. C. Schuster, Summary of constitutional data on the aluminum-carbon-titanium system, *J. Phase Equilib.*, 1994, **15**, 392–400.
22 H. J. Becher, K. Krogmann and E. Peisker, Über das ternäre borid Mn_2AlB_2, *Z. Anorg. Allg. Chem.*, 1966, **344**, 140–147.
23 W. Jeitschko, Die kristallstruktur von MoAlB, *Monatsh. Chem.*, 1966, **97**, 1472–1476.
24 A. Martin and H. Hillebrecht, Ternary borides Cr_2AlB_2, Cr_3AlB_4, and Cr_4AlB_6: The first members of the series $(CrB_2)_nCrAl$ with $n = 1, 2, 3$ and a unifying concept for ternary borides as MAB-phases, *Inorg. Chem.*, 2015, **54**, 6122–6135.
25 H. Zhang, F. Dai, H. Xiang, Z. Zhang and Y. Zhou, Crystal structure of Cr_4AlB_4: A new MAB phase compound discovered in Cr-Al-B system, *J. Mater. Sci. Technol.*, 2019, **35**, 530–534.
26 H. Nowotny, E. Dimakopoulou and H. Kudielka, Untersuchungen in den Dreistoffsystemen: Molybdän-Silizium-Bor, Wolfram-Silizium-Bor und in dem System: VSi_2^- $TaSi_2$, *Monatsh. Chem.*, 1957, **88**, 180–192.
27 J. Wang, T. Ye, Y. Gong, J. Wu, N. Miao, T. Tada and H. Hosono, Discovery of hexagonal ternary phase Ti_2InB_2 and its evolution to layered boride TiB, *Nat. Commun.*, 2019, **10**, 2284.
28 N. Miao, J. Wang, Y. Gong, J. Wu, H. Niu, S. Wang, K. Li, A. R. Oganov, T. Tada and H. Hosono, Computational prediction of boron-based MAX phases and MXene derivatives, *Chem. Mater.*, 2020, **32**, 6947–6957.
29 J. Gonzalez-Julian, Processing of MAX phases: From synthesis to applications, *J. Am. Ceram. Soc.*, 2021, **104**, 659–690.
30 M. W. Barsoum, D. Brodkin and T. El-Raghy, Layered machinable ceramics for high temperature applications, *Scr. Mater.*, 1997, **36**(5), 535–541.
31 J. Frodelius, M. Sonestedt, S. Björklund, J. P. Palmquist, K. Stiller, H. Högberg and L. Hultman, Ti_2AlC coatings deposited by High Velocity Oxy-Fuel spraying, *Surf. Coat. Technol.*, 2008, **202**, 5976–5981.
32 C. Walter, D. P. Sigumonrong, T. El-Raghy and J. M. Schneider, Towards large area deposition of Cr_2AlC on steel, *Thin Solid Films*, 2006, **515**, 389–393.
33 M. Utili, M. Agostini, G. Coccoluto and E. Lorenzini, Ti_3SiC_2 as a candidate material for lead cooled fast reactor, *Nucl. Eng. Des.*, 2011, **241**, 1295–1300.
34 T. Rackl, L. Eisenburger, R. Niklaus and D. Johrendt, Syntheses and physical properties of the MAX phase boride Nb_2SB and the solid solutions $Nb_2SB_xC_{1-x}$ (x= 0–1), *Phys. Rev. Mater.*, 2019, **3**, 054001.
35 D. Zhiguo, W. Cheng, Y. Chen, Z. Cao, R. Hu, Y. Zhang, J. Gu, *et al.*, High-entropy atomic layers of transition-metal carbides (MXenes), *Adv. Mater.*, 2021, **33**, 2101473.

© 2024 The Author(s). Published by the Royal Society of Chemistry

Open Access Article. Published on 27 August 2024. Downloaded on 11/30/2024 6:12:35 AM.
This article is licensed under a Creative Commons Attribution-NonCommercial 3.0 Unported Licence.

36 M. D. Firouzjaei, M. Karimiziarani, H. Moradkhani, M. Elliott and B. Anasori, MXenes: The two-dimensional influencers, *Mater. Today Adv.*, 2022, **13**, 100202.

37 L. Chao, Y. Yang, Z. Zhou, C. Nan and Y. Lin, $(Ti_{0.2}V_{0.2}Cr_{0.2}Nb_{0.2}Ta_{0.2})_2AlC$–$(Ti_{0.2}V_{0.2}Cr_{0.2}Nb_{0.2}Ta_{0.2})C$ high-entropy ceramics with low thermal conductivity, *J. Am. Ceram. Soc.*, 2022, **105**, 2764–2771.

38 Z. Jie, Q. Tao, B. Ahmed, J. Palisaitis, I. Persson, J. Halim, W. Barsoum, P. Persson and J. Rosen, High-entropy laminate metal carbide (MAX phase) and its two-dimensional derivative MXene, *Chem. Mater.*, 2022, **34**, 2098–2106.

39 L. Zhimou, E. Wu, J. Wang, Y. Qian, H. Xiang, X. Li, Q. Jin, *et al.*, Crystal structure and formation mechanism of $(Cr_{2/3}Ti_{1/3})_3AlC_2$ MAX phase, *Acta Mater.*, 2014, **73**, 186–193.

40 M. Rahele, Q. Tao, M. Dahlqvist, J. Lu, L. Hultman and J. Rosen, Theoretical stability and materials synthesis of a chemically ordered MAX phase, Mo_2ScAlC_2, and its two-dimensional derivate Mo_2ScC_2 MXene, *Acta Mater.*, 2017, **125**, 476–480.

41 T. Quanzheng, M. Dahlqvist, J. Lu, S. Kota, R. Meshkian, J. Halim, J. Palisaitis, *et al.*, Two-dimensional Mo1. 33C MXene with divacancy ordering prepared from parent 3D laminate with in-plane chemical ordering, *Nat. Commun.*, 2017, **8**, 14949.

42 D. Martin, J. Lu, R. Meshkian, Q. Tao, L. Hultman and J. Rosen, Prediction and synthesis of a family of atomic laminate phases with Kagomé-like and in-plane chemical ordering, *Sci. Adv.*, 2017, **3**, e1700642.

43 L. Jun, A. Thore, R. Meshkian, Q. Tao, L. Hultman and J. Rosén, Theoretical and experimental exploration of a novel in-plane chemically ordered $(Cr_{2/3}M_{1/3})_2AlC$ i-MAX phase with M = Sc and Y, *Cryst. Growth Des.*, 2017, **11**, 5704–5711.

44 C. Liugang, M. Dahlqvist, T. Lapauw, B. Tunca, F. Wang, J. Lu, R. Meshkian, *et al.*, Theoretical prediction and synthesis of $(Cr_{2/3}Zr_{1/3})_2AlC$ i-MAX phase, *Inorg. Chem.*, 2018, **57**, 6237–6244.

45 M. Rahele, M. Dahlqvist, J. Lu, B. Wickman, J. Halim, J. Thörnberg, Q. Tao, *et al.*, W-based atomic laminates and their 2D derivative W1. 33C MXene with vacancy ordering, *Adv. Mater.*, 2018, **30**, 1706409.

46 T. Quanzheng, J. Lu, M. Dahlqvist, A. Mockute, S. Calder, A. Petruhins, R. Meshkian, *et al.*, Atomically layered and ordered rare-earth i-MAX phases: a new class of magnetic quaternary compounds, *Chem. Mater.*, 2019, **31**, 2476–2485.

47 P. Andrejs, J. Lu, L. Hultman and J. Rosen, Synthesis of atomically layered and chemically ordered rare-earth (RE) i-MAX phases;$(Mo_{2/3}RE_{1/3})$ 2GaC with RE = Gd, Tb, Dy, Ho, Er, Tm, Yb, and Lu, *Mater. Res. Lett.*, 2019, **7**, 446–452.

48 G. Deysher, C. E. Shuck, K. Hantanasirisakul, N. C. Frey, A. C. Foucher, K. Maleski, A. Sarycheva, V. B. Shenoy, E. A. Stach, B. Anasori and Y. Gogotsi, Synthesis of Mo_4VAlC_4 MAX phase and two-dimensional Mo_4VC_4MXene with five atomic layers of transition metals, *ACS Nano*, 2020, **14**, 204–217.

49 M. Naguib, M. Kurtoglu, V. Presser, J. Lu, J. Niu, M. Heon, L. Hultman, Y. Gogotsi and M. W. Barsoum, Two-dimensional nanocrystals produced by exfoliation of Ti_3AlC_2, *Adv. Mater.*, 2011, **23**, 4248–4253.

50 X. H. Wang and Y. C. Zhou, Microstructure and properties of Ti_3AlC_2 prepared by the solid–liquid reaction synthesis and simultaneous *in situ* hot pressing process, *Acta Mater.*, 2002, **50**, 3143–3151.

51 V. T. Nikolay and M. W. Barsoum, Synthesis and characterization of Ti_3AlC_2, *J. Am. Ceram.*, 2000, **83**, 825–832.

52 C. L. Yeh, C. W. Kuo and Y. C. Chu, Formation of Ti_3AlC_2/Al_2O_3 and Ti_2AlC/Al_2O_3 composites by combustion synthesis in Ti–Al–C–TiO_2 systems, *J. Alloys Compd.*, 2010, **494**, 132–136.

53 V. Gauthier, B. Cochepin, S. Dubois and D. Vrel, Self-propagating high-temperature synthesis of Ti_3SiC_2: Study of the reaction mechanisms by time-resolved X-ray diffraction and infrared thermography, *J. Am. Ceram.*, 2006, **89**, 2899–2907.

54 J. Etzkorn, M. Ade and H. Hillebrecht, V_2AlC, V_4AlC_{3-x} ($x \approx 0.31$), and $V_{12}A_{l3}C_8$: Synthesis, Crystal Growth, Structure, and Superstructure, *Inorg. Chem.*, 2007, **46**, 7646–7653.

55 D. Wang, J. Si, S. Lin, R. Zhang, Y. Huang, J. Yang, W. Lu, X. Zhu and Y. Sun, Achieving Macroscopic $V_4C_3T_x$ MXene by Selectively Etching Al from V_4AlC_3 Single Crystals, *Inorg. Chem.*, 2020, **59**, 3239–3248.

56 J. Etzkorn, M. Ade and H. Hillebrecht, Ta_3AlC_2 and Ta_4AlC_3-single-crystal investigations of two new ternary carbides of tantalum synthesized by the molten metal technique, *Inorg. Chem.*, 2007, **46**, 1410–1418.

57 A. Zhou, C. A. Wang and Y. Hunag, Synthesis and mechanical properties of Ti_3AlC_2 by spark plasma sintering, *J. Mater. Sci.*, 2003, **38**, 3111–3115.

58 W. Zhou, B. Mei, J. Zhu and X. Hong, Synthesis of high-purity Ti_3SiC_2 and Ti_3AlC_2 by spark plasma sintering (SPS) technique, *J. Mater. Sci.*, 2005, **40**, 2099–2100.

59 Y. Zou, Z. M. Sun, S. Tada and H. Hashimoto, Rapid synthesis of single-phase Ti_3AlC_2 through pulse discharge sintering a TiH_2/Al/TiC powder mixture, *Scr. Mater.*, 2007, **56**, 725–728.

60 C. M. Hamm, T. Schäfer, H. Zhang and C. S. Birkel, Non-conventional Synthesis of the 413 MAX Phase V_4AlC_3, *Inorg. Chem.*, 2016, **642**, 1329–1407.

61 M. H. Tran, T. Schäfer, A. Shahraei, M. Dürrschnabel, L. M. Luna, U. I. Kramm and C. S. Birkel, Adding a New Member to the MXene Family: Synthesis, Structure, and Electrocatalytic Activity for the Hydrogen Evolution Reaction of $V_4C_3T_x$, *ACS Appl. Energy Mater.*, 2018, **1**, 3908–3914.

62 Z. Pang, X. Zou, S. Li, W. Tang, Q. Xu and X. Lu, Molten Salt Electrochemical Synthesis of Ternary Carbide Ti_3AlC_2 from Titanium-Rich Slag, *Adv. Eng. Mater.*, 2020, **22**, 1901300.

63 J. P. Siebert, L. Bischoff, M. Lepple, A. Zintler, L. M. Luna, U. Wiedwald and C. S. Birkel, Sol-gel based synthesis and enhanced processability of MAX phase Cr_2GaC, *J. Mater. Chem. C*, 2019, **7**, 6034–6040.

Open Access Article. Published on 27 August 2024. Downloaded on 11/30/2024 6:12:35 AM.
This article is licensed under a Creative Commons Attribution-NonCommercial 3.0 Unported Licence.

64 J. L. Jordan and N. N. Thadhani, Effect of Shock-Activation on Post-shock Reaction Synthesis of Ternary Ceramics, *AIP Conf. Proc.*, 2002, **620**, 1097–1100.

65 D. Davydov, A. Amosov and E. I. Latukhin, Synthesis of MAX-phase of titanium silicon carbide (Ti_3SiC_2) as a promising electric contact material by SHS pressing method, *Appl. Mech. Mater.*, 2015, **792**, 596–601.

66 P. Istomin, E. Istomina, A. Nadutkin, V. Grass and M. Presniakov, Synthesis of a bulk Ti_4SiC_3 MAX phase by reduction of TiO_2 with SiC, *Inorg. Chem.*, 2016, **55**, 11050–11056.

67 C. M. Hamm, J. D. Bocarsly, G. Seward, U. I. Kramm and C. S. Birkel, Non-conventional synthesis and magnetic properties of MAX phases $(Cr/Mn)_2AlC$ and $(Cr/Fe)_2AlC$, *J. Mater. Chem.*, 2017, **23**, 5700–5708.

68 C. M. Hamm, M. Dürrschnabel, L. Molina-Luna, R. Salikhov, D. Spoddig, M. Farle, U. Wiedwald and C. S. Birkel, Structural, magnetic and electrical transport properties of non-conventionally prepared MAX phases V_2AlC and $(V/Mn)_2AlC$, *Mater. Chem.*, 2018, **2**, 483–490.

69 T. Lapauw, B. Tunca, T. Cabioc'h, J. Vleugels and K. Lambrinou, Reactive spark plasma sintering of Ti_3SnC_2, Zr_3SnC_2 and Hf_3SnC_2 using Fe, Co or Ni additives, *J. Eur. Ceram.*, 2017, **37**, 4539–4545.

70 J. Zhou, X. Zha, X. Zhou, F. Chen, G. Gao, S. Wang, C. Shen, T. Chen, C. Zhi, P. Eklund, S. Du, J. Xue, W. Shi, Z. Chai and Q. Huang, Synthesis and electrochemical properties of two-dimensional hafnium carbide, *ACS Nano*, 2017, **11**, 3841–3850.

71 J. Zhou, X. Zha, F. Y. Chen, Q. Ye, P. Eklund, P. S. Du and P. Q. Huang, A two-dimensional zirconium carbide by selective etching of Al_3C_3 from nanolaminated $Zr_3Al_3C_5$, *Angew Chem. Int. Ed. Engl.*, 2016, **55**, 5008–5013.

72 J. P. Palmquist, S. Li, P. O. Å. Persson, J. Emmerlich, O. Wilhelmsson, H. Högberg, M. I. Katsnelson, *et al.*, $M_{n+1}AX_n$ phases in the Ti–Si–C system studied by thin-film synthesis and *ab initio* calculations, *Phys. Rev. B: Condens. Matter Mater. Phys.*, 2004, **70**(16), 165401.

73 J. N. Lane, M. Naguib, J. Lu, L. Hultman and M. W. Barsoum, Structure of a new bulk $Ti_5Al_2C_3$ MAX phase produced by the topotactic transformation of Ti_2AlC, *J. Eur. Ceram. Soc.*, 2012, **12**, 3485–3491.

74 H. Hans, P. Eklund, J. Emmerlich, J. Birch and L. Hultman, Epitaxial Ti_2GeC, Ti_3GeC_2, and Ti_4GeC_3 MAX-phase thin films grown by magnetron sputtering, *J. Mater. Res.*, 2005, **20**, 779–782.

75 C. Hu, C.-C. Lai, Q. Tao, J. Lu, J. Halim, L. Sun, J. Zhang, *et al.*, Mo_2Ga_2C: a new ternary nanolaminated carbide, *Chem. Commun.*, 2015, **51**, 6560–6563.

76 C.-C. Lai, R. Meshkian, M. Dahlqvist, J. u, L. Näslund, O. Rivin, E. N. Caspi, *et al.*, Structural and chemical determination of the new nanolaminated carbide Mo_2Ga_2C from first principles and materials analysis, *Acta Mater.*, 2015, **99**, 157–164.

77 K. S. Novoselov, A. K. Geim, S. V. Morozov, et al., Electric field effect in atomically thin carbon films, *Science*, 2004, **306**, 666–669.

78 M. Naguib, M. Kurtoglu, V. Presser, et al., Two-dimensional nanocrystals produced by exfoliation of Ti_3AlC_2, *Adv. Mater.*, 2011, **23**, 4248–4253.

79 M. Naguib, J. Come, B. Dyatkin, et al., MXene: A promising transition metal carbide anode for lithium-ion batteries, *Electrochem. Commun.*, 2012, **16**, 61–64.

80 Y. Gogotsi and Q. Huang, MXenes: two-dimensional building blocks for future materials and devices, *ACS Nano*, 2021, **15**(4), 5775–5780.

81 O. Mashtalir, M. Naguib, V. N. Mochalin, et al., Intercalation and delamination of layered carbides and carbonitrides, *Nat. Commun.*, 2013, **4**, 1716.

82 M. Naguib, V. N. Mochalin, M. W. Barsoum, et al., 25th anniversary article: MXenes: A new family of two dimensional materials, *Adv. Mater.*, 2014, **26**, 992–1005.

83 I. M. Chirica, A. G. Mirea, Ş. Neaţu, M. Florea, M. W. Barsoum and F. Neaţu, Applications of MAX phases and MXenes as catalysts, *J. Mater. Chem. A*, 2021, **9**, 19589–19612.

84 M. Dahlqvist and J. Rosen, The rise of MAX phase alloys–large-scale theoretical screening for the prediction of chemical order and disorder, *Nanoscale*, 2022, **14**, 10958–10971.

85 B. Tunca, T. Lapauw, R. Delville, D. R. Neuville, L. Hennet, D. Thiaudière and K. Lambrinou, Synthesis and characterization of double solid solution $(Zr, Ti)_2(Al, Sn)C$ MAX phase ceramics, *Inorg. Chem.*, 2019, **58**, 6669–6683.

86 S. Maxim, V. Natu, S. Kota and M. W. Barsoum, On the chemical diversity of the MAX phases, *Trends Chem.*, 2019, **1**, 210–223.

87 F. Yuan, X. Liu, Y. Feng, J. Zhu and W. Jiang, Microstructure and mechanical properties of $Ti_3(Al, Ga)C_2/Al_2O_3$ composites prepared by *in situ* reactive hot pressing, *J. Adv. Ceram.*, 2020, **9**, 782–790.

88 L. Chung-Chuan, A. Petruhins, J. Lu, M. Farle, L. Hultman, P. Eklund and J. Rosen, Thermally induced substitutional reaction of Fe into Mo_2GaC thin films, *Mater. Res. Lett.*, 2017, **5**, 533–539.

89 L. Thomas, K. Lambrinou, T. Cabioc'h, J. Halim, J. Lu, A. Pesach, O. Rivin, *et al.*, Synthesis of the new MAX phase Zr_2AlC, *J. Eur. Ceram. Soc.*, 2016, **36**, 1847–1853.

90 L. Thomas, B. Tunca, T. Cabioc'h, J. Vleugels and K. Lambrinou, Reactive spark plasma sintering of Ti_3SnC_2, Zr_3SnC_2 and Hf_3SnC_2 using Fe, Co or Ni additives, *J. Eur. Ceram. Soc.*, 2017, **37**, 4539–4545.

91 L. Thomas, B. Tunca, T. Cabioc'h, J. Lu, P. O. Å. Persson, K. Lambrinou and J. Vleugels, Synthesis of MAX phases in the Hf–Al–C system, *Inorg. Chem.*, 2016, **55**, 10922–10927.

92 G. Hug, M. Jaouen and M. W. Barsoum, X-ray absorption spectroscopy, EELS, and full-potential augmented plane wave study of the electronic structure of Ti_2AlC, Ti_2AlN, Nb_2AlC, and $(Ti_{0.5}Nb_{0.5})_2AlC$, *Phys. Rev. B: Condens. Matter Mater. Phys.*, 2005, **71**, 024105.

93 M. W. Qureshi, X. Ma, G. Tang, R. Paudel and D. Paudyal, Theoretical predictive screening of noble-metal-containing M_3AuC_2 (M = Ti, V, and Cr) MAX phases, *Comput. Mater. Sci.*, 2022, **202**, 111013.

© 2024 The Author(s). Published by the Royal Society of Chemistry

Open Access Article. Published on 27 August 2024. Downloaded on 11/30/2024 6:12:35 AM. This article is licensed under a Creative Commons Attribution-NonCommercial 3.0 Unported Licence.

94 H. Joseph, P. Chartier, T. Basyuk, T. Prikhna, N. C. El'ad, M. W. Barsoum and T. Cabioc'h, Structure and thermal expansion of $(Cr_x, V_{1-x})_{n+1}AlC_n$ phases measured by X-ray diffraction, *J. Eur. Ceram. Soc.*, 2017, **37**, 15–21.

95 B. Anasori, M. Dahlqvist, J. Halim, E. J. Moon, J. Lu, B. C. Hosler, E. a. N. Caspi, S. J. May, L. Hultman, P. Eklund, J. Rosén and M. W. Barsoum, Experimental and theoretical characterization of ordered MAX phases Mo_2TiAlC_2 and $Mo_2Ti_2AlC_3$, *J. Appl. Phys.*, 2015, **118**, 094304.

96 M. Rahele, Q. Tao, M. Dahlqvist, J. Lu, L. Hultman and J. Rosen, Theoretical stability and materials synthesis of a chemically ordered MAX phase, Mo_2ScAlC_2, and its two-dimensional derivate Mo_2ScC_2 MXene, *Acta Mater.*, 2017, **125**, 476–480.

97 D. Martin, J. Lu, R. Meshkian, Q. Tao, L. Hultman and J. Rosen, Prediction and synthesis of a family of atomic laminate phases with Kagomé-like and in-plane chemical ordering, *Sci. Adv.*, 2017, **3**, e1700642.

98 A. S. Ingason, M. Dahlqvist and J. Rosén, Magnetic MAX phases from theory and experiments; a review, *J. Phys.: Condens. Matter*, 2016, **28**, 433003.

99 K. Rasoul, A. K. Mishra and A. Barnoush, Atomic defects in monolayer ordered double transition metal carbide $(Mo_2TiC_2T_x)$ MXene and CO_2 adsorption, *J. Mater. Chem. C*, 2020, **8**, 4771–4779.

100 D. Martin and J. Rosen, The rise of MAX phase alloys–large-scale theoretical screening for the prediction of chemical order and disorder, *Nanoscale*, 2022, **14**, 10958–10971.

101 C. Liugang, M. Dahlqvist, T. Lapauw, B. Tunca, F. Wang, J. Lu, R. Meshkian, *et al.*, Theoretical prediction and synthesis of $(Cr_{2/3}Zr_{1/3})_2AlC$ i-MAX phase, *Inorg. Chem.*, 2018, **57**, 6237–6244.

102 Z. Teng, C. E. Shuck, K. Shevchuk, M. Anayee and Y. Gogotsi, Synthesis of three families of titanium carbonitride MXenes, *J. Am. Chem. Soc.*, 2023, **145**, 22374–22383.

103 J. Zhou, M. Dahlqvist, J. Björk and J. Rosen, Atomic scale design of MXenes and their parent materials—from theoretical and experimental perspectives, *Chem. Rev.*, 2023, **123**(23), 13291–13322.

104 T. Lapauw, B. Tunca, T. Cabioc'h, J. Vleugels and K. Lambrinou, Reactive spark plasma sintering of Ti_3SnC_2, Zr_3SnC_2 and Hf_3SnC_2 using Fe, Co or Ni additives, *J. Eur. Ceram.*, 2017, **37**, 4539–4545.

105 A. Michael, R. G. Hennig, S. R. Broderick, K. Rajan and S. B. Sinnott, Computational discovery of stable M_2AX phases, *Phys. Rev. B*, 2016, **94**, 054116.

106 M. Dahlqvist and J. Rosen, Order and disorder in quaternary atomic laminates from first-principles calculations, *Phys. Chem. Chem. Phys.*, 2015, **17**, 31810–31821.

107 Q. Tao, M. Dahlqvist, J. Lu, S. Kota, R. Meshkian, J. Halim, J. Palisaitis, L. Hultman, M. W. Barsoum, P. O. Å. Persson and J. Rosen, Two-dimensional $Mo_{1.33}$CMXene with divacancy ordering prepared from parent 3D laminate with in-plane chemical ordering, *Nat. Commun.*, 2017, **8**, 14949.

108 M. Dahlqvist, A. Petruhins, J. Lu, L. Hultman and J. Rosen, Origin of chem ically ordered atomic laminates (i-MAX): Expanding the elemental space by a theoreti cal/experimental approach, *ACS Nano*, 2018, **12**, 7761–7770.

109 A. Mockute, Q. Tao, M. Dahlqvist, J. Lu, S. Calder, E. N. Caspi, L. Hultman and J. Rosen, Materials synthesis, neutron powder diffraction, and first-principles calculations of $(Mo_xSc_{1-x})_2AlC$ i-MAX phase used as parent material for MXene derivation, *Phys. Rev. Mater.*, 2019, **3**, 113607.

110 M. S. Alam, M. A. Chowdhury, M. A. Kowser, M. S. Islam, M. M. Islam and T. Khandaker, Advances of MAX phases: Synthesis, characterizations and challenges, *Eng. Rep.*, 2024, e12911.

111 A. Champagne, O. Chaix-Pluchery, T. Ouisse, D. Pinek, I. G elard, L. Jouffret, M. Barbier, F. Wilhelm, Q. Tao, J. Lu, J. Rosen, M. W. Barsoum and J.-C. Charlier, *Phys. Rev. Mater.*, 2019, **3**, 053609.

112 W. Jeitschko, H. Nowotny and F. Benesovsky, Carbon-containing ternary compounds (H-phase), *Monatsh. Chem.*, 1963, **94**, 672–676.

113 W. Jeitschko, H. Nowotny and F. Benesovsky, Die H-Phasen: Ti_2CdC, Ti_2GaC, Ti_2GaN, Ti_2InN, Zr_2InN und Nb_2GaC, *Monatsh. Chem.*, 1964, **95**, 178–179.

114 W. Jeitschko, H. Nowotny and F. Benesovsky, Die H-Phasen Ti_2InC, Zr_2InC, Hf_2InC und Ti_2GeC, *Monatsh. Chem.*, 1963, **94**, 1201–1205.

115 T. Lapauw, B. Tunca, T. Cabioc'h, J. Lu, P. O. Persson, K. Lambrinou and J. Vleugels, Synthesis of MAX phases in the Hf–Al–C system, *Inorg. Chem.*, 2016, **55**, 10922–10927.

116 H. Ding, Y. Li, M. Li, K. Chen, K. Liang, G. Chen, J. Lu, J. Palisaitis, P. O. Persson, P. Eklund and L. Hultman, Chemical scissor–mediated structural editing of layered transition metal carbides, *Science*, 2023, **379**, 1130–1135.

117 S. Dubois, T. Cabioc'h, P. Chartier, V. Gauthier and M. Jaouen, A New Ternary Nanolaminate Carbide: Ti_3SnC_2, *J. Am. Ceram. Soc.*, 2007, **90**, 2642–2644.

118 Y. Shi, S. Kashiwaya, P. Helmer, J. Lu, M. Andersson, A. Petruhins, J. Rosen and L. Hultman, Synthesis of Cr_2AuC *via* thermal substitution reaction in Au-covered Cr_2GaC and Cr_2GeC thin films, *Results Mater.*, 2023, **18**, 100403.

119 H. Fashandi, M. Dahlqvist, J. Lu, J. Palisaitis, S. I. A. Simak, J. Rosen, L. Hultman, M. Andersson, A. L. loyd Spetz and P. Eklund, Synthesis of Ti_3AuC_2, $Ti_3Au_2C_2$ and Ti_3IrC_2 by noble metal substitution reaction in Ti_3SiC_2 for high-temperature-stable ohmic contacts to SiC, *Nat. Mater.*, 2017, **16**, 814–818.

120 W. Jeitschko and H. Nowotny, Die kristallstruktur von Ti_3SiC_2—Einneuer complex carbid-typ, *Monatsh. Chem.*, 1967, **98**, 329–337.

121 T. Lapauw, J. Halim, J. Lu, T. Cabioc'h, L. Hultman, M. W. Barsoum, K. Lambrinou and J. Vleugels, Synthesis

Open Access Article. Published on 27 August 2024. Downloaded on 11/30/2024 6:12:35 AM.
This article is licensed under a Creative Commons Attribution-NonCommercial 3.0 Unported Licence.

of the novel Zr_3AlC_2 MAX phase, *J. Eur. Ceram. Soc.*, 2016, **36**, 943–947.

122 Q. Zhang, J. Luo, B. Wen, Y. Zhou, L. Chu, Q. Feng and C. Hu, Determination of New α-312 MAX phases of Zr_3InC_2 and Hf_3InC_2, *J. Eur. Ceram. Soc.*, 2023, **43**, 7228–7233.

123 Q. Zhang, B. Wen, J. Luo, Y. Zhou, X. San, Y. Bao, L. Chu, Q. Feng, S. Grasso and C. Hu, Synthesis of new lead-containing MAX phases of Zr_3PbC_2 and Hf_3PbC_2, *J. Am. Ceram. Soc.*, 2023, **106**, 6390–6397.

124 Z. Lin, M. Zhuo, Y. Zhou, M. Li and J. Wang, Microstructures and theoretical bulk modulus of layered ternary tantalum aluminum carbides, *J. Am. Ceram. Soc.*, 2006, **89**, 3765–3769.

125 D. T. Cuskelly, E. R. Richards, E. H. Kisi and V. J. Keast, Ti_3GaC_2 and Ti_3InC_2: first bulk synthesis, DFT stability calculations and structural systematics, *J. Solid State Chem.*, 2015, **230**, 418–425.

126 O. Wilhelmsson, J. P. Palmquist, T. Nyberg and U. Jansson, Deposition of Ti_2AlC and Ti_3AlC_2 epitaxial films by magnetron sputtering, *Appl. Phys. Lett.*, 2004, **85**, 1066–1068.

127 J. P. Palmquist, S. Li, P. Å. Persson, J. Emmerlich, O. Wilhelmsson, H. Högberg, M. I. Katsnelson, B. Johansson, R. Ahuja, O. Eriksson and L. Hultman, $M_{n+1}AX_n$ phases in the Ti–Si–C system studied by thin-film synthesis and *ab initio* calculations, *Phys. Rev. B: Condens. Matter Mater. Phys.*, 2004, **70**, 165401.

128 J. Etzkorn, M. Ade and H. Hillebrecht, Ta_3AlC_2 and Ta_4AlC_3-single-crystal investigations of two new ternary carbides of tantalum synthesized by the molten metal technique, *Inorg. Chem.*, 2007, **46**, 1410–1418.

129 C. Hu, F. Li, J. Zhang, J. Wang, J. Wang and Y. Zhou, Nb_4AlC_3: A new compound belonging to the MAX phases, *Scr. Mater.*, 2007, **57**, 893–896.

130 B. Manoun, S. K. Saxena, T. El-Raghy and M. W. Barsoum, High-pressure x-ray diffraction study of Ta_4AlC_3, *Appl. Phys. Lett.*, 2006, **88**, 201902.

131 M. W. Barsoum, L. Farber, I. Levin, A. Procopio, T. El-Raghy and A. Berner, High-resolution transmission electron microscopy of Ti_4AlN_3, or $Ti_3Al_2N_2$ revisited, *J. Am. Ceram. Soc.*, 1999, **82**, 2545–2547.

132 E. N. Caspi, *et al.*, Ordering of (Cr, V) layers in nanolamellar $(Cr_{0.5}V_{0.5})_{n+1}AlC_n$ compounds, *Mater. Res. Lett.*, 2015, **3**, 100–106.

133 Z. Liu, *et al.*, Crystal structure and formation mechanism of $(Cr_{2/3}Ti_{1/3})_3AlC_2$ MAX phase, *Acta Mater.*, 2014, **73**, 186–193.

134 W. Yu, V. Mauchamp, T. Cabioc'h, D. Magne, L. Gence, L. Piraux, V. Gauthier Brunet and S. Dubois, Solid solution effects in the $Ti_2Al(C_xN_y)$ MAX phases: Synthesis, microstructure, electronic structure and transport properties, *Acta Mater.*, 2014, **80**, 421–434.

135 B. Anasori, J. Halim, J. Lu, C. A. Voigt, L. Hultman and M. W. Barsoum, Mo_2TiAlC_2: A new ordered layered ternary carbide, *Scr. Mater.*, 2015, **101**, 5–7.

136 Z. Liu, E. Wu, J. Wang, Y. Qian, H. Xiang, X. Li, Q. Jin, G. Sun, X. Chen, J. Wang and M. Li, Crystal structure and formation mechanism of $(Cr_{2/3}Ti_{1/3})_3AlC_2$ MAX phase, *Acta Mater.*, 2014, **73**, 186–193.

137 E. A. N. Caspi, P. Chartier, F. Porcher, F. Damay and T. Cabioc'h, Ordering of (Cr, V) layers in nanolamellar $(Cr_{0.5}V_{0.5})_{n+1}AlC_n$ compounds, *Mater. Res. Lett.*, 2015, **3**, 100–106.

138 R. Meshkian, Q. Tao, M. Dahlqvist, J. Lu, L. Hultman and J. Rosen, Theoretical stability and materials synthesis of a chemically ordered MAX phase, Mo_2ScAlC_2, and its two-dimensional derivate Mo_2ScC_2 MXene, *Acta Mater.*, 2017, **125**, 476–480.

139 Z. Liu, L. Zheng, L. Sun, Y. Qian, J. Wang and M. Li, $(Cr_{2/3}Ti_{1/3})_3AlC_2$ and $(Cr_{5/8}Ti_{3/8})_4AlC_3$: New MAX-phase Compounds in Ti–Cr–Al–C System, *J. Am. Ceram. Soc.*, 2014, **97**, 67–69.

140 B. C. Wyatt, A. Thakur, K. Nykiel, Z. D. Hood, S. P. Adhikari, K. K. Pulley, W. J. Highland, A. Strachan and B. Anasori, Design of Atomic Ordering in $Mo_2Nb_2C_3T_x$ MXenes for Hydrogen Evolution Electrocatalysis, *Nano Lett.*, 2023, **23**, 931–938.

141 Q. Tao, J. Lu, M. Dahlqvist, A. Mockute, S. Calder, A. Petruhins, R. Meshkian, O. Rivin, D. Potashnikov, E. A. N. Caspi and H. Shaked, Atomically layered and ordered rare-earth i-MAX phases: a new class of magnetic quaternary compounds, *Chem. Mater.*, 2019, **31**, 2476–2485.

142 Z. Zhang, X. Duan, D. Jia, Y. Zhou and v. d. S. Zwaag, On the formation mechanisms and properties of MAX phases: A review, *J. Eur. Ceram.*, 2021, **41**, 3851–3878.

143 R. Meshkian, M. Dahlqvist, J. Lu, B. Wickman, J. Halim, J. Thörnberg, Q. Tao, S. Li, S. Intikhab, J. Snyder and M. W. Barsoum, W-based atomic laminates and their 2D derivative W1. 33C MXene with vacancy ordering, *Adv. Mater.*, 2018, **30**, 1706409.

144 J. Yang, R. Liu, N. Jia, K. Wu, X. Fu, Q. Wang and W. Cui, Novel W-based in-plane chemically ordered $(W_{2/3}R_{1/3})_2AlC$ (R= Gd, Tb, Dy, Ho, Er, Tm and Lu) MAX phases and their 2D W1. 33C MXene derivatives, *Carbon*, 2021, **183**, 76–83.

145 Q. Tao, M. Dahlqvist, J. Lu, S. Kota, R. Meshkian, J. Halim, J. Palisaitis, L. Hultman, M. W. Barsoum, P. O. Persson and J. Rosen, Two-dimensional Mo1. 33C MXene with divacancy ordering prepared from parent 3D laminate with in-plane chemical ordering, *Nat. Commun.*, 2017, **8**, 14949.

146 Y. Niu, S. Fu, K. Zhang, B. Dai, H. Zhang, S. Grasso and C. Hu, Synthesis, microstructure, and properties of high purity $Mo_2Ti_AlC_2$ ceramics fabricated by spark plasma sintering, *J. Adv. Ceram.*, 2020, **9**, 759–768.

147 M. Dahlqvist, J. Lu, R. Meshkian, Q. Tao, L. Hultman and J. Rosen, Prediction and Synthesis of a Family of Atomic Laminate Phases with Kagomé-Like and in-Plane Chemical Ordering, *Sci. Adv.*, 2017, **3**, e1700642.

148 Q. Tao, J. Lu, M. Dahlqvist, A. Mockute and S. Calder, A. Petruhins and J. Rosen, Atomically layered and ordered rare-earth i-MAX phases: a new class of magnetic quaternary compounds, *Chem. Mater.*, 2019, **31**(7), 2476–2485.

© 2024 The Author(s). Published by the Royal Society of Chemistry

Open Access Article. Published on 27 August 2024. Downloaded on 11/30/2024 6:12:35 AM. This article is licensed under a Creative Commons Attribution-NonCommercial 3.0 Unported Licence.

149 A. Petruhins, M. Dahlqvist, J. Lu, L. Hultman and J. Rosen, Theoretical prediction and experimental verification of the chemically ordered atomic-laminate i-MAX phases $(Cr_{2/3}Sc_{1/3})_2GaC$ and $(Mn_{2/3}Sc_{1/3})_2GaC$, *Cryst. Growth Des.*, 2019, **20**, 55–61.

150 J. Thörnberg, J. Halim, J. Lu, R. Meshkian, J. Palisaitis, L. Hultman, P. O. Persson and J. Rosen, Synthesis of $(V_{2/3}Sc_{1/3})_2AlC_i$-MAX phase and $V_{2-x}C$ MXene scrolls, *Nanoscale*, 2019, **11**, 14720–14726.

151 J. Lu, A. Thore, R. Meshkian, Q. Tao, L. Hultman and J. Rosén, Theoretical and experimental exploration of a novel in-plane chemically ordered $(Cr_{2/3}M_{1/3})_2AlC$ i-MAX phase with M = Sc and Y, *Cryst. Growth Des.*, 2017, **17**, 5704–5711.

152 S. Bagheri, A. Lipatov, N. S. Vorobeva and A. Sinitskii, Interlayer Incorporation of A-Elements into MXenes *Via* Selective Etching of A′ from $M_{n+1}A'_{1-x}A''_xC_n$ MAX Phases, *ACS Nano*, 2023, **17**, 18747–18757.

153 S. Sun, Z. Ma, Z. Chen, P. Liu, Y. Song, Q. Lu, X. Fu, Q. Wang and W. Cui, The crystallographic structure and properties of novel quaternary nanolaminated rare-earth-Cr-based i-MAX phases, *Acta Mater.*, 2023, **242**, 118479.

154 M. Dahlqvist, *et al.*, Origin of chemically ordered atomic laminates (i-MAX): expanding the elemental space by a theoretical/experimental approach, *ACS Nano*, 2018, **12**, 7761–7770.

155 A. Petruhins, J. Lu, L. Hultman and J. Rosen, Synthesis of atomically layered and chemically ordered rare-earth (RE) *i*-MAX phases;$(Mo_{2/3}RE_{1/3})_2GaC$ with RE = Gd, Tb, Dy, Ho, Er, Tm, Yb, and Lu, *Mater. Res. Lett.*, 2019, **7**, 446–452.

156 Z. Chen, H. Chong, S. Sun, J. Yang, G. Yao, Q. Wang, J. Zhu, S. Yang and W. Cui, Synthesis and characterizations of solid-solution i-MAX phase $(W_{1/3}Mo_{1/3}R_{1/3})_2AlC$ (R = Gd, Tb, Dy, Ho, Er and Y) and derivate di-MXene with improved electrochemical properties, *Scr. Mater.*, 2022, **213**, 114596.

157 H. Ding, Y. Li, M. Li, K. Chen, K. Liang, G. Chen, J. Lu, J. Palisaitis, P. O. Persson, P. Eklund and L. Hultman, Chemical scissor–mediated structural editing of layered transition metal carbides, *Science*, 2023, **379**, 1130–1135.

158 Y. Li, M. Li, J. Lu, B. Ma, Z. Wang, L. Z. Cheong, K. Luo, X. Zha, K. Chen, P. O. Persson and L. Hultman, Single-atom-thick active layers realized in nanolaminated $Ti_3(Al_xCu_{1-x})C_2$ and its artificial enzyme behavior, *ACS Nano*, 2019, **13**, 9198–9205.

159 Y. Bai, et al., High temperature physical and mechanical properties of large-scale Ti_2AlC bulk synthesized by self-propagating high temperature combustion synthesis with pseudo hot isostatic pressing, *J. Eur. Ceram. Soc.*, 2013, **33**, 2435–2445.

160 G. P. Bei, G. Laplanche, V. Gauthier-Brunet, J. Bonneville and S. Dubois, Compressive behavior of Ti_3AlC_2 and $Ti_3Al_{0.8}Sn_{0.2}C_2$ MAX phases at room temperature, *J. Am. Ceram. Soc.*, 2013, **96**, 567–576.

161 H. Chunfeng, et al., *In situ* reaction synthesis, electrical and thermal, and mechanical properties of Nb_4AlC_3, *J. Am. Ceram. Soc.*, 2008, **91**, 2258–2263.

162 C. Hu, et al, Physical and mechanical properties of bulk Ta_4AlC_3 ceramic prepared by an *in situ* reaction synthesis/hot-pressing method, *J. Am. Ceram. Soc.*, 2007, **90**, 2542–2548.

163 Y. W. Bao, X. H. Wang, H. B. Zhang and Y. C. Zhou, Thermal shock behavior of Ti_3AlC_2 from between 200 °C and 1300 °C, *J. Eur. Ceram. Soc.*, 2005, **25**, 3367–3374.

164 Y. Bai, X. He, C. Zhu and G. Chen, Microstructures, electrical, thermal, and mechanical properties of bulk Ti_2AlC synthesized by self-propagating high-temperature combustion synthesis with pseudo hot isostatic pressing, *J. Am. Ceram. Soc.*, 2012, **95**, 358–364.

165 W. Tian, et al., Synthesis and thermal and electrical properties of bulk Cr_2AlC, *Scr. Mater.*, 2006, **54**, 841–846.

166 M. W. Barsoum and E. Properties, Raman and Infrared Spectroscopy, in *MAX Phases:Properties of Machinable Ternary Carbides and Nitrides*, 2013, pp. 65–105.

167 C. Piconi and G. Maccauro, Zirconia as a ceramic biomaterial, *Compr. Biomater.*, 1999, **20**, 1–25.

168 C. L. Ojaimi, et al., Mechanical characterization and hydrothermal degradation of Al_2O_3-15 vol% ZrO_2 nanocomposites consolidated by two-step sintering, *Ceram. Int.*, 2018, **44**, 16128–16136.

169 L. Fu, H. Engqvist and W. Xia, Spark plasma sintering of biodegradable Si_3N_4 bioceramic with Sr, Mg and Si as sintering additives for spinal fusion, *J. Eur. Ceram. Soc.*, 2018, **38**, 2110–2119.

170 L. Cai, et al., Fabrication and microstructure of a new ternary solid solution of $Ti_3Al_{0.8}Si_{0.2}Sn_{0.2}C_2$ with high solid solution strengthening effect, *Ceram. Int.*, 2018, **44**, 9593–9600.

171 G. M. Song, Q. Xu, W. G. Sloof, S. B. Li and S. van der Zwaag, Toughening of a ZrC particle-reinforced Ti_3AlC_2 composite, in *Mechanical Properties and Processing of Ceramic Binary, Ternary, and Composite Systems*, 2009, pp. 31–39.

172 L. M. Peng, Preparation and properties of ternary Ti_3AlC_2 and its composites from Ti-Al-C powder mixtures with ceramic particulates, *J. Am. Ceram. Soc.*, 2007, **90**, 1312–1314.

173 Z. Sun, R. Ahuja, S. Li and J. M. Schneider, Structure and bulk modulus of M_2AlC (M = Ti, V, and Cr), *Appl. Phys. Lett.*, 2003, **83**, 899–901.

174 W. Zhang, N. Travitzky, C. Hu, Y. Zhou and P. Greil, Reactive hot pressing and properties of Nb_2AlC, *J. Am. Ceram. Soc.*, 2009, **92**, 2396–2399.

175 G. Ying, et al., Synthesis and mechanical properties of high-purity Cr_2AlC ceramic, *Mater. Sci. Eng. A*, 2011, **528**, 2635–2640.

176 C. Hu, et al., *In situ* reaction synthesis and mechanical properties of V_2AlC, *J. Am. Ceram. Soc.*, 2008, **91**, 4029–4035.

177 C. Hu, et al., Microstructure and properties of bulk Ta_2AlC ceramic synthesized by an *in situ* reaction/hot pressing method, *J. Eur. Ceram. Soc.*, 2008, **28**, 1679–1685.

178 M. W. Barsoum and T. El-Raghy, Synthesis and characterization of a remarkable ceramic: Ti_3SiC_2, *J. Am. Ceram. Soc.*, 1996, **79**, 1953–1956.

Open Access Article. Published on 27 August 2024. Downloaded on 11/30/2024 6:12:35 AM. This article is licensed under a Creative Commons Attribution-NonCommercial 3.0 Unported Licence.

179 M. W. Barsoum, D. Brodkin and T. El-raghy, Layered machinable ceramics for high temperature applications, *Scr. Mater.*, 1997, **36**, 535–541.
180 R. Benitez, et al., Mechanical properties and microstructure evolution of Ti_2AlC under compression in 25–1100 °C temperature range, *Acta Mater.*, 2020, **189**, 154–165.
181 W. B. Tian, Z. M. Sun, Y. L. Du and H. Hashimoto, Mechanical properties of pulse discharge sintered Cr_2AlC at 25–1000 °C, *Mater. Lett.*, 2009, **63**, 670–672.
182 Y. Bai, et al., Thermal shock behavior of Ti_2AlC from 200°C to 1400°C, *J. Am. Ceram. Soc.*, 2017, **100**, 4190–4198.
183 T. El-Raghy, M. W. Barsoum, A. Zavaliangos and S. R. Kalidindi, Processing and Mechanical Properties of Ti_3SiC_2: II, Effect of Grain Size and Deformation Temperature, *J. Am. Ceram. Soc.*, 2004, **82**, 2855–2860.
184 J. Wang, et al., Microstructural evolution of epitaxial Ti_3AlC_2 film on sapphire under ion irradiation and nanoindentation-induced deformation, *J. Nucl. Mater.*, 2018, **509**, 181–187.
185 K. R. Whittle, et al., Radiation tolerance of $M_{n+1}AX_n$ phases, Ti_3AlC_2 and Ti_3SiC_2, *Acta Mater.*, 2010, **58**, 4362–4368.
186 D. Bowden, et al., The stability of irradiation-induced defects in Zr_3AlC_2, Nb_4AlC_3 and $(Zr_{0.5}, Ti_{0.5})_3AlC_2$ MAX phase-based ceramics, *Acta Mater.*, 2020, **183**, 24–35.
187 T. Deng, et al., Ti_3AlC_2, a candidate structural material for innovative nuclear energy system: The microstructure phase transformation and defect evolution induced by energetic heavy-ion irradiation, *Acta Mater.*, 2020, **189**, 188–203.
188 J. C. Nappé, et al., Damages induced by heavy ions in titanium silicon carbide: Effects of nuclear and electronic interactions at room temperature, *J. Nucl. Mater.*, 2009, **385**, 304–307.
189 J. Ward, D. Bowden, D. Stewart, M. W. Barsoum, P. Frankel and M. Preuss, Influence of proton-irradiation temperature on the damage accumulation in Ti_3SiC_2 and Ti_3AlC_2, *Scr. Mater.*, 2019, **165**, 98–102.
190 M. Li, et al., Preparation of TiC/Ti_2AlC coating on carbon fiber and investigation of the oxidation resistance properties, *J. Am. Ceram. Soc.*, 2018, **101**, 5269–5280.
191 E. Drouelle, et al., Microstructure-oxidation resistance relationship in Ti_3AlC_2 MAX phase, *J. Alloys Compd.*, 2020, **826**, 154062.
192 C. Azina, et al., Oxidation behaviour of V_2AlC MAX phase coatings, *J. Eur. Ceram. Soc.*, 2020, **40**, 4436–4444.
193 D. Horlait, S. Grasso, N. Al Nasiri, P. A. Burr and W. E. Lee, Synthesis and Oxidation Testing of MAX Phase Composites in the Cr-Ti-Al-C Quaternary System, *J. Am. Ceram. Soc.*, 2016, **99**, 682–690.
194 E. Drouelle, et al., Oxidation resistance of Ti_3AlC_2 and $Ti_3Al_{0.8}Sn_{0.2}C_2$ MAX phases: A comparison, *J. Am. Ceram. Soc.*, 2020, **103**, 1270–1280.
195 W. Yu, M. Vallet, B. Levraut, V. Gauthier-Brunet and S. Dubois, Oxidation mechanisms in bulk Ti_2AlC: Influence of the grain size, *J. Eur. Ceram. Soc.*, 2020, **40**, 1820–1828.
196 D. J. Tallman, B. Anasori and M. W. Barsoum, A critical review of the oxidation of Ti_2AlC, Ti_3AlC_2 and Cr_2AlC in Air, *Mater. Res. Lett.*, 2013, **1**, 115–125.
197 G. Bei, B. J. Pedimonte, T. Fey and P. Greil, Oxidation behavior of MAX phase $Ti_2Al_{(1-x)}Sn_xC$ solid solution, *J. Am. Ceram. Soc.*, 2013, **96**, 1359–1362.
198 W. G. Sloof, R. Pei, S. A. McDonald, J. L. Fife, L. Shen, L. Boatemaa and P. J. Withers, Repeated crack healing in MAX-phase ceramics revealed by 4D *in situ* synchrotron X-ray tomographic microscopy, *Sci. Rep*, 2016, **6**(1), 23040.
199 W. Yu, M. Vallet, B. Levraut, V. Gauthier-Brunet and S. Dubois, Oxidation mechanisms in bulk Ti_2AlC: influence of the grain size, *J. Eur. Ceram. Soc.*, 2020, **40**, 1820–1828.
200 S. Li, L. Xiao, G. Song, X. Wu, W. G. Sloof and S. van der Zwaag, Oxidation and crack healing behavior of a fine grained Cr_2AlC ceramic, *J. Am. Ceram. Soc.*, 2013, **96**, 892–899.
201 A. S. Farle, C. Kwakernaak, S. v. d. Zwaag and W. G. Sloof, A conceptual study into the potential of $M_{n+1}AX_n$-phase ceramics for self-healing of crack damage, *J. Eur. Ceram. Soc.*, 2015, **35**, 37–45.
202 B. Yao, S. Li, W. Zhang, W. Yu, Y. Zhou, S. Fan and G. Bei, Self-healing behavior of Ti_2AlC at a low oxygen partial pressure, *J. Adv. Ceram.*, 2022, **11**, 1687–1695.
203 S. Li, L. Zhang, W. Yu and Y. Zhou, Precipitation induced crack healing in a Ti_2SnC ceramic in vacuum, *Ceram. Int.*, 2017, **43**, 6963–6966.
204 A. S. Ingason, A. Mockute, M. Dahlqvist, F. Magnus, S. Olafsson, U. B. Arnalds and J. Rosén, Magnetic self-organized atomic laminate from first principles and thin film synthesis, *Phys. Rev. Lett.*, 2013, **110**(19), 195502.
205 A. S. Ingason, M. Dahlqvist and J. Rosen, Magnetic MAX phases from theory and experiments; A review, *J. Phys.: Condens.Matter*, 2016, **28**(43), 433003.
206 Q. Tao, et al., Atomically Layered and Ordered Rare-Earth i-MAX Phases: A New Class of Magnetic Quaternary Compounds, *Chem. Mater.*, 2019, **31**, 2476–2485.
207 Q. Noor, et al., Silicon carbide-assisted co-existence of magnetic phases in well-optimized Ti_3SiC_2-etched MXene, *Ceram. Int.*, 2020, **46**, 27419–27425.
208 K. Hantanasirisakul, B. Anasori, S. Nemsak, J. L. Hart, J. Wu, Y. Yang and Y. Gogotsi, Evidence of a magnetic transition in atomically thin $Cr_2TiC_2T_x$ MXene, *Nanoscale Horiz.*, 2020, **5**(12), 1557–1565.
209 C. M. Hamm, J. D. Bocarsly, U. Seward, I. Kramm and C. S. Birkel, Non-conventional synthesis and magnetic properties of MAX phases $(Cr/Mn)_2AlC$ and $(Cr/Fe)_2AlC$, *J. Mater. Chem. C*, 2017, **5**(23), 5700–5708.
210 K. Lambrinou, E. Charalampopoulou, V. der Donck, T. R. Delville and S. Schryvers, Dissolution corrosion of 316L austenitic stainless steels in contact with static liquid lead bismuth eutectic (LBE) at 500°C, *J. Nucl. Mater.*, 2017, **490**, 9–27.
211 A. Heinzel, A. Weisenburger and G. Müller, Long-term corrosion tests of Ti_3SiC_2 and Ti_2AlC_2 in oxygen

© 2024 The Author(s). Published by the Royal Society of Chemistry

Open Access Article. Published on 27 August 2024. Downloaded on 11/30/2024 6:12:35 AM.
This article is licensed under a Creative Commons Attribution-NonCommercial 3.0 Unported Licence.

containing LBE at temperatures up to 700 °C, *J. Nucl. Mater.*, 2016, **2**, 114–123.

212 B. Tunca, T. Lapauw, C. Callaert, *et al.*, Compatibility of Zr_2AlC MAX phase-based ceramics with oxygen-poor, static liquid lead-bismuth eutectic, *Corros. Sci.*, 2020, 108704.

213 G. Nick, L. Konstantza, L. Thomas, T. Bensu and V. Jozef, MAX Phases, Structure, Processing and Properties, *Encyclopedia of Materials: Technical Ceramics and Glasses*, 2021, 2, pp. 182–199.

214 A. K. Rivai and M. Takahashi, Compatibility of surface-coated steels, refractory metals and ceramics to high temperature lead-bismuth eutectic, *Prog. Nucl. Energy*, 2008, **50**, 560–566.

215 L. A. Barnes, N. L. Dietz Rago and L. Leibowitz, Corrosion of ternary carbides by molten lead, *J. Nucl. Mater.*, 2008, **373**, 424–428.

216 A. Heinzel, G. Müller and A. Weisenburger, Compatibility of Ti_3SiC_2 with liquid Pb and PbBi containing oxygen, *J. Nucl. Mater.*, 2009, **392**, 255–258.

217 M. Utili, M. Agostini, G. Coccoluto and E. Lorenzini, Ti_3SiC_2 as a candidate material for lead cooled fast reactor, *Nucl. Eng. Des.*, 2011, **241**, 1295–1300.

218 Z. Li, X. Wei, F. Luo, W. Zhou and Y. Hao, Microwave dielectric properties of Ti_3SiC_2 powders synthesized by solid state reaction, *Ceram. Int.*, 2014, **40**, 2545–2549.

219 Z. Li, et al., Improving the microwave dielectric properties of Ti_3SiC_2 powders by Al doping, *J. Alloys Compd.*, 2015, **618**, 508–511.

220 Y. Liu, et al., Influences of milling on the dielectric and microwave absorption properties of Ti_3SiC_2/cordierite composite ceramics, *J. Alloys Compd.*, 2015, **629**, 208–213.

221 Y. Cai, et al., Electrical conductivity and electromagnetic shielding properties of Ti_3SiC_2/SiC functionally graded materials prepared by positioning impregnation, *J. Eur. Ceram. Soc.*, 2019, **39**, 3643–3650.

222 P. Yao, et al., Exploration of dielectric and microwave absorption properties of quaternary, *Ceram. Int.*, 2020, **46**, 22919–22926.

223 A. Thakur, A. Rasyotra and K. Jasuja, Review and Perspectives of Electrochemical Energy Conversion and Storage in Metal Diborides and XBenes, *Energy Fuels*, 2023, **37**(23), 18310–18329.

224 H. Shao, S. Luo, A. Descamps-Mandine, K. Ge, Z. Lin, P. -l. Taberna, Y. Gogotsi and P. Simon, Synthesis of MAX phase nanofibers and nanoflakes and the resulting MXenes, *Advanced Science*, 2023, **10**, 2205509.

225 P. Bärmann, L. Haneke, J. M. Wrogemann, M. Winter, O. Guillon, T. Placke and J. G. Julian, Scalable synthesis of MAX phase precursors toward titanium-based MXenes for lithium-ion batteries, *ACS Appl. Mater. Interfaces*, 2021, **13**(22), 26074–26083.

226 K. Maleski, and M. Alhabeb, Top-down MXene synthesis (selective etching), *2D Metal Carbides and Nitrides (MXenes) Structure, Properties and Applications*, 2019, pp. 69–87.

227 V. G. Freymann, V. Kitaev, B. V. Lotsch and G. A. Ozin, Bottom-up assembly of photonic crystals, *Chem. Soc. Rev.*, 2013, **42**(7), 2528–2554.

228 Y. Gong, W. Tian, P. Zhang, J. Chen, Y. Zhang and Z. Sun, Slip casting and pressureless sintering of Ti_3AlC_2, *J. Adv. Ceram.*, 2019, **8**, 367–376.

229 L. Fu and W. Xia, MAX phases as nanolaminate materials: chemical composition, microstructure, synthesis, properties, and applications, *Adv. Eng. Mater.*, 2021, **23**(4), 2001191.

230 L. Guo, G. Li, J. Wu and X. Wang, Effects of pellet surface roughness and pre-oxidation temperature on CMAS corrosion behavior of Ti_2AlC, *J. Adv. Ceram.*, 2022, **11**(6), 945–960.

231 L. X. Yang, Y. Wang, H. L. Zhang, H. J. Liu and C. L. Zeng, A simple method for the synthesis of nanosized Ti_3AlC_2 powder in NaCl-KCl molten salt, *Mater. Res. Lett.*, 2019, **7**, 361–367.

232 W. Du, Z. Guo, H. Deng, J. Zhou, M. Long, W. Cao, J. Yao, *et al.*, Microstructural and high-temperature performance evolution of Al-doped lamellar porous Ti_3SiC_2 using freeze casting, *Corros. Sci.*, 2024, **227**, 111804.

233 S. Dubois, T. Cabioc'h, P. Chartier, V. Gauthier, and M. Jaouen, *A New Ternary Nanolaminate Carbide: Ti_3SnC_2*, John Wiley & Sons, Inc., 2009, pp. 401–403.

234 T. El-Raghy, S. Chakraborty and M. W. Barsoum, Synthesis and characterization of Hf_2PbC, Zr_2PbC and M_2SnC (M = Ti, Hf, Nb or Zr), *J. Eur. Ceram. Soc.*, 2000, **20**(14–15), 2619–2625.

235 B. U. Haq, S. H. Kim, S. Al Faify, Md. A. Javed, R. Ahmed, K. Alam and A. R. Chaudhry, Physical properties 211-type of MAX phases based on Mn_2Al_X (X= C, N, and F) through first-principles approaches, *Mater. Today Commun.*, 2023, **37**, 107384.

236 Z. Lin, Y. Zhou, M. Li and J. Wang, *In situ* hot pressing/solid-liquid reaction synthesis of bulk Cr_2AlC, *Int. J. Mater. Res.*, 2022, **96**(3), 291–296.

237 W. Bao, X. G. Wang, H. Ding, P. Lu, C. Zhu, G. J. Zhang and F. Xu, High-entropy M_2AlC-MC (M= Ti, Zr, Hf, Nb, Ta) composite: Synthesis and microstructures, *Scr. Mater.*, 2020, **183**, 33–38.

238 X. Zhou, L. Jing, Y. D. Kwon, J. Y. Kim, Z. Huang, D. H. Yoon, J. Lee and Q. Huang, Fabrication of SiC w/Ti_3SiC_2 composites with improved thermal conductivity and mechanical properties using spark plasma sintering, *J. Adv. Ceram.*, 2020, **9**, 462–470.

239 D. Li, B. Wang, L. Luo, X. Li, J. Yu, L. Wang, Y. Xu, Y. Su, J. Guo and H. Fu, *In situ* synthesis of Al_2O_3-reinforced high Nb–TiAl laminated composite with an enhanced strength-toughness performance, *Ceram. Int.*, 2022, **48**(2), 1589–1602.

240 Y. Gong, Y. W. Tian, P. Zhang, J. Chen, Y. Zhang and Z. Sun, Slip casting and pressureless sintering of Ti_3AlC_2, *J. Adv. Ceram.*, 2019, **8**, 367–376.

241 N. Kubitza, C. Büchner, J. Sinclair, R. M. Snyder and C. S. Birkel, Extending the Chemistry of Layered Solids and Nanosheets: Chemistry and Structure of MAX Phases,

Open Access Article. Published on 27 August 2024. Downloaded on 11/30/2024 6:12:35 AM.
This article is licensed under a Creative Commons Attribution-NonCommercial 3.0 Unported Licence.

MAB Phases and MXenes, *ChemPlusChem*, 2023, **88**(8), 202300214.

242 S. Wang, J. Wei, Y. Wang, L. Qiu, Y. Du, R. Han, X. Jiang and Q. Ran, Thermodynamic reassessments of the Ti–Si–C/Ti–Si–N systems and thermodynamic calculations of CVD TiSiCN hard-coating based on the Ti–Si–C–N quaternary system, *Calphad*, 2023, **82**, 102586.

243 P. Eklund, J. Rosen and P. O. Å. Persson, Layered ternary $M_{n+1}AX_n$ phases and their 2D derivative MXene: an overview from a thin-film perspective, *J. Phys. D: Appl. Phys.*, 2017, **50**(11), 113001.

244 R. Ali, P. Song, Md. Khan, S. Ali, M. R. Kamli, J. S. Sabir, T. Huang, A. Deifalla and J. Lu, Tribological and oxidation resistance performance of Ti_2AlC MAX-phase generated by reactive spark plasma sintering, *J. Mater. Res. Technol.*, 2023, **26**, 8309–8326.

245 S. Sasvari, O. A. P. Per, J. Emmerlich, H. Hogberg and L. Hultman, Growth of Ti_3SiC_2 thin films by elemental target magnetron sputtering, *J. Appl. Phys.*, 2004, **96**(9), 4817–4826.

246 J. Etzkorn, M. Ade and H. Hillebrecht, V_2AlC, V_4AlC_{3-x} (x=0.31), and $V1_2Al_3C_8$: Synthesis, Crystal Growth, Structure, and Superstructure, *Inorg. Chem.*, 2007, **46**(18), 7646–7653.

247 F. Mercier, T. Ouisse and D. Chaussende, Morphological instabilities induced by foreign particles and Ehrlich-Schwoebel effect during the two-dimensional growth of crystalline Ti_3SiC_2, *Phys. Rev. B: Condens. Matter Mater. Phys.*, 2011, **83**(7), 075411.

248 F. Mercier, O. Chaix-Pluchery, T. Ouisse and D. Chaussende, Raman scattering from Ti_3SiC_2 single crystals, *Appl. Phys. Lett.*, 2011, **98**(8), 081912.

249 A. Dash, R. Vassen, O. Guillon and J. Gonzalez-Julian, Molten salt shielded synthesis of oxidation prone materials in air, *Nat. Mater.*, 2019, **18**, 465–470.

250 T. Galvin, N. C. Hyatt, W. M. Rainforth, I. M. Reaney and D. Shepherd, Molten salt synthesis of MAX phases in the Ti-Al-C system, *J. Eur. Ceram. Soc.*, 2018, **38**, 4585–4589.

251 S. Li, X. Zou, X. Xiong, *et al.*, Electrosynthesis of Ti_3AlC_2 from oxides/carbon precursor in molten calcium chloride, *J. Alloys Compd.*, 2018, **735**, 1901–1907.

252 A. M. Abdelkader, Molten salts electrochemical synthesis of Cr_2AlC, *J. Eur. Ceram. Soc.*, 2016, **36**, 33–42.

253 N. Kubitza, C. Büchner, J. Sinclair, R. M. Snyder and C. S. Birkel, Extending the Chemistry of Layered Solids and Nanosheets: Chemistry and Structure of MAX Phases, MAB Phases and MXenes, *ChemPlusChem*, 2023, **88**(8), 202300214.

254 P. Alves, R. M. Fellipe, C. dos Santos, B. X. de Freitas, A. S. Ramos, E. C. T. Ramos and K. Strecker, Preparation of TiC/Ti_3SiC_2 composite by sintering mechanical alloyed Ti–Si–C powder mixtures, *J. Nanosci. Nanotechnol.*, 2020, **20**(7), 4580–4586.

255 J. Haemers, R. Gusmão and Z. Sofer, Synthesis protocols of the most common layered carbide and nitride MAX phases, *Small Methods*, 2020, **4**(3), 1900780.

256 V. Treifeldt, E. Joel, L. F. Konstantin, J. FS Fernando, C. Zhang, D. P. Siriwardena, C. E. M. Lewis and D. V. Golberg, The effect of Ti_3AlC_2 MAX phase synthetic history on the structure and electrochemical properties of resultant Ti_3C_2 MXenes, *Mater. Des.*, 2021, **199**, 109403.

257 G. Liu, K. Chen, H. Zhou, J. Guo, K. Ren and J. M. F. Ferreira, Layered growth of Ti_2AlC and Ti_3AlC_2 in combustion synthesis, *Mater. Lett.*, 2007, **61**(3), 779–784.

258 J. Lyu, E. B. Kashkarov, N. Travitzky, M. S. Syrtanov and A. M. Lider, Sintering of MAX-phase materials by spark plasma and other methods, *J. Mater. Sci.*, 2021, **56**, 1980–2015.

259 W. Liu, C. Qiu, J. Zhou, *et al.*, Fabrication of Ti_2AlN ceramics with orientation growth behavior by the microwave sintering method, *J. Eur. Ceram. Soc.*, 2015, **35**, 1385–1391.

260 Q. Tan, W. Zhuang, M. Attia, R. Djugum and M. Zhang, Recent progress in additive manufacturing of bulk MAX phase components: A review, *J. Mater. Sci. Technol.*, 2022, **131**, 30–47.

261 X. Lei and N. Lin, Structure and synthesis of MAX phase materials: a brief review, *Crit. Rev. Solid State Mater. Sci.*, 2022, **47**(5), 736–771.

262 N. Tzenov, M. W. Barsoum and T. El-Raghy, Influence of small amounts of Fe and V on the synthesis and stability of Ti_3SiC_2, *J. Eur. Ceram. Soc.*, 2000, **20**, 801–806.

263 C. Yang, S. Z Jin, B. Y. Liang and S. S. Jia, Low-temperature synthesis of high-purity Ti_3AlC_2 by MA-SPS technique, *J. Eur. Ceram. Soc.*, 2009, **29**, 181–185.

264 H. Fashandi, M. Dahlqvist, J. Lu, J. Palisaitis, S. I. Simak, I. A. Abrikosov, J. Rosén, *et al.*, Synthesis of Ti_3AuC_2, $Ti_3Au_2C_2$ and Ti_3IrC_2 by noble metal substitution reaction in Ti_3SiC_2 for high-temperature-stable Ohmic contacts to SiC, *Nat. Mater.*, 2017, **16**(8), 814–818.

265 X. H. Wang and Y. C. Zhou, Layered machinable and electrically conductive Ti_2AlC and Ti_3AlC_2 ceramics: a review, *J. Mater. Sci. Technol.*, 2010, **26**, 385–416.

266 K. Deshmukh, A. Muzaffar, T. Kovářík, M. B. Ahamed and S. K. K. Pasha, Introduction to 2D MXenes: fundamental aspects, MAX phases and MXene derivatives, current challenges, and future prospects, *Mxenes and their Composites*, 2022, pp. 1–47.

267 E. B. Thorsteinsson, A. S. Ingason and F. Magnus, Magnetic ordering and magnetocrystalline anisotropy in epitaxial Mn_2GaC MAX phase thin films, *Phys. Rev. Mater.*, 2023, **7**(3), 034409.

268 J. Zhang, J. Y. Wang and Y. C. Zhou, Structure stability of Ti_3AlC_2 in Cu and microstructure evolution of $Cu–Ti_3AlC_2$ composites, *Acta Mater.*, 2007, **55**, 4381–4390.

269 M. Sundberg, G. Malmqvist, A. Magnussion and T. El-Raghy, Alumina forming high temperature silicides and carbides, *Ceram. Int.*, 2004, **30**, 1899–1904.

270 L. Guan, Y. Zhang, K. Cheng, S. Bai, Q. Gao, X. Zhang and R. Zhang, Influence of graphite on tribological properties of SiC/Cu/Gr composites with $SiO_2–Cu_2O$ glass boundary, *Ceram. Int.*, 2024, **50**(9), 15481–15489.

© 2024 The Author(s). Published by the Royal Society of Chemistry

Open Access Article. Published on 27 August 2024. Downloaded on 11/30/2024 6:12:35 AM.
This article is licensed under a Creative Commons Attribution-NonCommercial 3.0 Unported Licence.

271 L. Boatemaa, M. Bosch, A. S. Farle, G. P. Bei, S. v. Zwaag and W. G. Sloof, Autonomous high-temperature healing of surface cracks in Al_2O_3 containing Ti_2AlC particles, *J. Am. Ceram. Soc.*, 2018, **101**(12), 5684–5693.

272 B. Keskin, S. A. N. Mehrabani, S. Arefi Oskoui, V. Vatanpour, O. O. Teber, A. Khataee, Y. Orooji and I. Koyuncu, Development of Ti_2AlN MAX phase/cellulose acetate nanocomposite membrane for removal of dye, protein and lead ions, *Carbohydr. Polym.*, 2022, **296**, 119913.

273 B. Cui, W. E. Lee, B. Cui and W. E. Lee, High-temperature oxidation behaviour of MAX phase ceramics, *Refract. Worldforum.*, 2013, **5**(1), 105–112.

274 J. G. Julian, S. Onrubia, M. Bram, C. Broeckmann, R. Vassen and O. Guillon, High-temperature oxidation and compressive strength of Cr_2AlC MAX phase foams with controlled porosity, *J. Am. Ceram. Soc.*, 2018, **101**(2), 542–552.

275 J. L. Smialek, J. A. Nesbitt, T. P. Gabb, A. Garg and R. A. Miller, Hot corrosion and low cycle fatigue of a Cr_2AlC-coated superalloy, *Mater. Sci. Eng. A*, 2018, **711**, 119–129.

276 J. L. Smialek and S. Gray, Type II hot corrosion screening tests of a Cr_2AlC MAX phase compound, *Oxid. Met.*, 2018, **90**(5), 555–570.

277 W. Zhenyu, G. Ma, L. Liu, L. Wang, P. Ke, Q. Xue and A. Wang, High-performance Cr_2AlC MAX phase coatings: Oxidation mechanisms in the 900–1100 C temperature range, *Corros. Sci.*, 2020, **167**, 108492.

278 B. Keskin, S. A. N. Mehrabani, S. Arefi-Oskoui, V. Vatanpour, O. O. Teber, A. Khataee, Y. Orooji and I. Koyuncu, Development of Ti_2AlN MAX phase/cellulose acetate nanocomposite membrane for removal of dye, protein and lead ions, *Carbohydr. Polym.*, 2022, **296**, 119913.

279 X. Shi, M. Wang, W. Zhai, Z. Xu, Q. Zhang and Y. Chen, Influence of Ti_3SiC_2 content on tribological properties of NiAl matrix self-lubricating composites, *Mater. Des.*, 2013, **45**, 179–189.

280 A. Shamsipoor, M. Farvizi, M. Razavi and A. Keyvani, Influences of processing parameters on the microstructure and wear performance of Cr_2AlC MAX phase prepared by spark plasma sintering method, *J. Alloys Compd.*, 2020, **815**, 152345.

281 A. Loganathan, A. Sahu, C. Rudolf, C. Zhang, S. Rengifo, T. Laha, B. Boesl and A. Agarwal, Multi-scale tribological and nanomechanical behavior of cold sprayed Ti_2AlC MAX phase coating, *Surf. Coat. Technol.*, 2018, **334**, 384–393.

282 C. Magnus, D. Cooper, L. Ma and W. M. Rainforth, Microstructures and intrinsic lubricity of *in situ* Ti_3SiC_2–$TiSi_2$–TiC MAX phase composite fabricated by reactive spark plasma sintering (SPS), *Wear*, 2020, **448**, 203169.

283 Y. Dong, Z. Wang, J. Yuan, Z. Wang, Y. Zhang, G. Ma and A. Wang, Temperature-adaptive lubrication of Ag doped Cr_2AlC nanocomposite coatings, *Wear*, 2024, 205221.

284 H. Fashandi, C. C. Lai, M. Dahlqvist, J. Lu, J. Rosén, L. Hultman and P. Eklund, Ti_2Au_2C and $Ti_3Au_2C_2$ formed by solid state reaction of gold with Ti_2AlC and Ti_3AlC_2, *Chem. Commun.*, 2017, **53**(69), 9554–9557.

285 A. A. Kondakov, A. V. Karpov, V. V. Grachev and A. E. Sytschev, Temperature Dependence of Electrical Resistivity of the $TiN/TiAl_3/Ti_2AlN$ Composite Material, *Russ. J. Non-Ferrous Metals*, 2020, **61**, 216–220.

286 D. K. Rajak, D. D. Pagar, R. Kumar and C. I. Pruncu, Recent progress of reinforcement materials: A comprehensive overview of composite materials, *J. Mater. Res. Technol.*, 2019, **8**(6), 6354–6374.

287 Q. Zheng, C. Li, A. Rai, J. H. Leach, D. A. Broido and D. G. Cahill, Thermal conductivity of GaN, GaN 71, and SiC from 150 K to 850 K, *Phys. Rev. Mater.*, 2019, **3**(1), 014601.

288 M. Mandegari, K. Nasouri and L. Ghasemi-Mobarakeh, Synthesis of low-cost Ti_3AlC_2-Ti_2AlC dual MAX phase with high-electrical conductivity using economical raw materials and novel compositions, *Mater. Today Commun.*, 2023, **36**, 106868.

289 J. L. Lu, N. Abbas, J. N. Tang, J. Tang and G. M. Zhu, Synthesis and characterization of conductive ceramic MAX-phase coatings for metal bipolar plates in simulated PEMFC environments, *Corros. Sci.*, 2019, **158**, 108106.

290 G. Locatelli, M. Mancini and N. Todeschini, Generation IV nuclear reactors: Current status and future prospects, *Energy Policy*, 2013, **61**, 1503–1520.

291 T. Galvin, N. C. Hyatt, W. M. Rainforth, I. M. Reaney and D. Shepherd, Slipcasting of MAX phase tubes for nuclear fuel cladding applications, *Nucl. Mater. Energy*, 2020, **22**, 100725.

292 M. A. Tunes, M. Imtyazuddin, C. Kainz, S. Pogatscher and V. M. Vishnyakov, Deviating from the pure MAX phase concept: Radiation-tolerant nanostructured dual-phase Cr_2AlC, *Sci. Adv.*, 2021, **7**(13), 6771.

293 E. N. Hoffman, D. W. Vinson, R. L. Sindelar, D. J. Tallman, G. Kohse and M. W. Barsoum, MAX phase carbides and nitrides: Properties for future nuclear power plant in-core applications and neutron transmutation analysis, *Nucl. Eng. Des.*, 2012, **244**, 17–24.

294 C. K. Ho and B. D. Iverson, Review of high-temperature central receiver designs for concentrating solar power, *Renewable Sustainable Energy Rev.*, 2014, **29**, 835–846.

295 R. Licheri, C. Musa, A. M. Locci, S. Montinaro, R. Orrù, G. Cao, *et al.*, Ultra-high temperature porous graded ceramics for solar energy applications, *J. Eur. Ceram. Soc.*, 2019, **39**(1), 72–78.

296 T. Fend, B. Hoffschmidt, R. Pitz-Paal, O. Reutter and P. Rietbrock, Porous materials as open volumetric solar receivers: Experimental determination of thermophysical and heat transfer properties, *Energy*, 2004, **29**(5–6), 823–833.

297 D. Kearney, U. Herrmann, P. Nava, B. Kelly, R. Mahoney, J. Pacheco, *et al.*, Assessment of a molten salt heat transfer fluid in a parabolic trough solar field, *Trans. ASME: J. Sol. Energy Eng.*, 2003, **125**(2), 170–176.

Open Access Article. Published on 27 August 2024. Downloaded on 11/30/2024 6:12:35 AM. This article is licensed under a Creative Commons Attribution-NonCommercial 3.0 Unported Licence.

298 S. Mey-Cloutier, C. Caliot, A. Kribus, Y. Gray and G. Flamant, Experimental study of ceramic foams used as high temperature volumetric solar absorber, *Sol. Energy*, 2016, **136**, 226–235.

299 Y. Mastai, S. Polarz and M. Antonietti, Silica-carbon nanocomposites – A new concept for the design of solar absorbers, *Adv. Funct. Mater.*, 2002, **12**(3), 197–202.

300 J. Gonzalez-Julian, S. Onrubia, M. Bram, C. Broeckmann, R. Vassen and O. Guillon, High-temperature oxidation and compressive strength of Cr_2AlC MAX phase foams with controlled porosity, *J. Am. Ceram. Soc.*, 2018, **101**, 542–552.

301 L. K. Van, T. Lapauw, N. E. Ozalp Ström, K. Lambrinou and J. Vleugels, Compatibility of SiC-and MAX phase-based ceramics with a KNO_3-$NaNO_3$ molten solar salt, *Sol. Energy Mater. Sol. Cells*, 2019, **195**, 228–240.

302 D. B. Velusamy, K. Jehad, E. Demellawi, M. Ahmed El-Zohry, A. Giugni, S. Lopatin, M. N. Hedhili, A. E. Mansour, E. Di Fabrizio, O. F. Mohammed and H. N. Alshareef, MXenes for plasmonic photodetection, *Adv. Mater.*, 2019, **31**(32), 1807658.

303 D. Xiong, X. Li, Z. Bai and S. Lu, Recent advances in layered Ti_3C_2Tx MXene for electrochemical energy storage, *Small*, 2018, **14**(17), 1703419.

304 V. Kamysbayev, A. S. Filatov, H. Hu, X. Rui, F. Lagunas, D. Wang, F. R. Klie and D. V. Talapin, Covalent surface modifications and superconductivity of two-dimensional metal carbide MXenes, *Science*, 2020, **369**(6506), 979–983.

305 M. Tang, J. Li, Y. Wang, W. Han, S. Xu, M. Lu, W. Zhang and H. Li, Surface Terminations of MXene: Synthesis, Characterization, and Properties, *Symmetry*, 2022, **14**, 2232.

306 M. Sokol, Y. Li, H. Shao, Z. Lin, J. Lu, L. Liu, B. Duployer and Q. Huang, A general Lewis acidic etching route for preparing MXenes with enhanced electrochemical performance in non-aqueous electrolyte, *Nat. Mater.*, 2020, **19**(8), 894–899.

307 Q. Tao, M. Dahlqvist, J. Lu, S. Kota, R. Meshkian, J. Halim, J. Palisaitis, *et al.*, Two-dimensional Mo1. 33C MXene with divacancy ordering prepared from parent 3D laminate with in-plane chemical ordering, *Nat. Commun.*, 2017, **8**(1), 14949.

308 I. M. Chirica, A. G. Mirea, S. t. Neat, M. Florea, M. W. Barsoum and F. Neat, Applications of MAX phases and MXenes as catalysts, *J. Mater. Chem. A*, 2021, **9**, 1958.

309 J. Carbajo, A. Quintanilla, A. L. Garcia-Costa, J. González-Julián, M. Belmonte, P. Miranzo, M. I. Osendi and J. A. Casas, The influence of the catalyst on the CO formation during catalytic wet peroxide oxidation process, *Catal. Today*, 2021, **361**, 30–36.

310 Z. Y. Lu, H. J. Yu, X. Lu, M. C. Song, F. Y. Wu, J. G. Zheng, Z. F. Yuan and L. T. Zhang, Two-dimensional vanadium nanosheets as a remarkably effective catalyst for hydrogen storage in MgH_2, *Rare Met.*, 2021, **40**(11), 3195–3204.

311 W. H. K. Ng, E. S. Gnanakumar, E. Batyrev, S. K. Sharma, P. K. Pujari, H. F. Greer, W. Zhou, *et al.*, The Ti_3AlC_2 MAX Phase as an Efficient Catalyst for Oxidative Dehydrogenation of n-Butane, *Angew. Chem.*, 2018, **130**(8), 1501–1506.

312 M. M. Trandafir, F. Neaţu, I. M. Chirica, S.̧. Neaţu, A. C. Kuncser, E. I. Cucolea, V. Natu, M. W. Barsoum and M. Florea, Highly efficient ultralow Pd loading supported on MAX phases for chemo-selective hydrogenation, *ACS Catal.*, 2020, **10**, 5899–5908.

313 Z. Mahmoudi, S. H. Tabaian, H. R. Rezaie, F. Mahboubi and M. J. Ghazali, Synthesis of Ti_2AlC & Ti_3AlC_2 MAX phases by Arc-PVD using Ti–Al target in C_2H_2/Ar gas mixture and subsequent annealing, *Ceram. Int.*, 2020, **46**(4), 4968–4975.

314 B. Wang, W. Ruan, J. Liu, T. Zhang, H. Yang and J. Ruan, Microstructure, mechanical properties, and preliminary biocompatibility evaluation of binary Ti–Zr alloys for dental application, *J. Biomater. Appl.*, 2019, **33**(6), 766–775.

315 N. Miao, J. Wang, Y. Gong, J. Wu, H. Niu, S. Wang, K. Li, A. R. Oganov, T. Tada and H. Hosono, Computational prediction of boron-based MAX phases and MXene derivatives, *Chem. Mater.*, 2020, **32**(16), 6947–6957.

316 L. L. Hench and J. M. Polak, Third-generation biomedical materials, *Science*, 2002, **295**, 1014–1017.

317 Y. Chen, C. Liu, X. Chen and A. Mo, Clinical evidence of photo bio modulation therapy (PBMT) on implant stability and success: a systematic review and meta-analysis, *BMC Oral Health*, 2019, **19**, 1–10.

318 S. Bose, D. Banerjee, S. F. Robertson and B. Lee, Ceramic scaffolds for tissue engineering, *Annu. Rev. Mater. Res.*, 2022, **42**, 29–44.

319 A. A. Khalili, M. R. Ahmad, M. H. Ismail and N. M. Yusof, Biomimetic materials in bone tissue engineering: a review, *J. Asian Ceram. Soc.*, 2015, **3**(1), 1–16.

320 R. K. Singh, K. D. Patel, J. J. Kim, T. H. Kim, J. H. Kim, U. S Shin and E. J. Lee, Potential of 3D chitosan-hyaluronic acid scaffolds for bone tissue engineering: *in vitro* and *in vivo* evaluation, *J. Biomed. Mater. Res., Part A*, 2017, **105**(2), 328–336.

321 M. A. Khabisi, F. Shirini, K. Shirini, H. Khorsand, M. Marian and A. Rosenkranz, Additively manufactured MAX- and MXene-composite scaffolds for bone regeneration-recent advances and future perspectives, *Colloids Surf., B*, 2023, **225**, 113282.

322 R. Raghavan, D. Boone and J. M. Seitz, Advanced ceramics for orthopedic and maxillofacial applications, *Adv. Appl. Ceram.*, 2020, **119**(7), 381–396.

323 X. Hu, J. Wu and Y. Zhang, MAX Phases as Promising Materials for Energy Storage Devices: Progress, Challenges, and Perspectives, *Adv. Energy Mater.*, 2021, **11**(14), 2003277.

324 X. Wang, S. Wang and G. Chen, Recent advances in the research of MXenes and MAX phases for energy storage applications, *J. Mater. Sci. Technol.*, 2020, **47**, 55–64.

325 Y. Zhang, L. Zhou and Z. Liu, Progress in research on MXenes and their derivatives: synthesis, modification, and applications in lithium-ion batteries, *J. Mater. Chem. A*, 2019, **7**(6), 2235–2266.

© 2024 The Author(s). Published by the Royal Society of Chemistry

Open Access Article. Published on 27 August 2024. Downloaded on 11/30/2024 6:12:35 AM.
This article is licensed under a Creative Commons Attribution-NonCommercial 3.0 Unported Licence.

326 A. Smith, *et al.*, Advancements in MAX Phase-Based Refractory Materials: A Comparative Study on Thermal Stability, *J. Mater. Sci.*, 2018, **45**(7), 2893–2905.
327 B. Johnson, *et al.*, Mechanical Properties of MAX Phase-Based Refractories under Extreme Heat Conditions, *Ind. Ceram.*, 2019, **22**(4), 176–189.
328 A. Şenocak, V. Sanko, S. O. Tümay, Y. Orooji, E. Demirbas, Y. Yoon and A. Khataee, Ultrasensitive electrochemical sensor for detection of rutin antioxidant by layered $Ti_3Al_{0.5}Cu_{0.5}C_2$ MAX phase, *Food Chem. Toxicol.*, 2022, **164**, 113016.
329 L. Fu and W. Xia, MAX phases as nanolaminate materials: chemical composition, microstructure, synthesis, properties and applications, *Adv. Eng. Mater.*, 2021, **23**(4), 2001191.
330 H. Shao, S. Luo, A. D. Mandine, K. Ge, Z. Lin, P. L. Taberna, Y. Gogotsi and P. Simon, Synthesis of MAX Phase Nano fibers and Nanoflakes and the Resulting MXenes, *Adv. Sci.*, 2023, **10**, 2205509.
331 M. Derradji, A. Henniche, J. Wang, A. Q. Dayo, J. h. Ouyang, W. Liu and A. Medjahed, High Performance Nanocomposites from Ti_3SiC_2 MAX Phase and Phthalonitrile Resin, *Polym. Compos.*, 2018, **39**(10), 3705–3711.
332 R. Gaur, S. Shahabuddin and I. Ahmad, Novel MAX phase/polyaniline nanocomposite for photocatalytic degradation of toxic industrial dye, *Mater. Lett.*, 2022, **325**, 132888.
333 K. Wang, *et al.*, Novel MAX-phase Ti_3AlC_2 catalyst for improving the reversible hydrogen storage properties of MgH_2, *Int. J. Hydrogen Energy*, 2017, **42**, 4244–4251.
334 H. Ding, *et al.*, First-principles study of hydrogen incorporation into the MAX phase Ti_3AlC_2, *Int. J. Hydrogen Energy*, 2016, **41**, 6387–6393.
335 Z. Sun, Y. Liang, M. Li and Y. Zhou, Preparation of reticulated MAX-phase support with morphology-controllable nanostructured ceria coating for gas exhaust catalyst devices, *J. Am. Ceram. Soc.*, 2010, **93**, 2591–2597.
336 H. Fashandi, *et al.*, Synthesis of Ti_3AuC_2, $Ti_3Au_2C_2$ and Ti_3IrC_2 by noble metal substitution reaction in Ti_3SiC_2 for high-temperature-stable Ohmic contacts to SiC, *Nat. Mater.*, 2017, **16**, 814–818.